U.S. DEPARTMENT OF COMMERCE
ENVIRONMENTAL SCIENCE SERVICES ADMINISTRATION
INSTITUTES FOR ENVIRONMENTAL RESEARCH

Institutes for Environmental Research Technical Memorandum -NSSL 33

ON THE CONTINUITY OF WATER SUBSTANCE

Edwin Kessler

NATIONAL SEVERE STORMS LABORATORY
TECHNICAL MEMORANDUM NO. 33

BOULDER, COLORADO
APRIL 1967

FOREWORD

Four papers are presented here.

In the first, principles of continuity are applied with simple models of airflows and microphysical processes. Associations among the distributions of water substance, the microphysical processes, and the air motion are described.

The second short note discusses the gravitational separation of raindrops of different sizes.

The third paper presents an interpretation of radar weather data, based on the theory discussed in the first paper.

The last is a reprint of a paper first published in the Monthly Weather Review. This is included for readers who may wish to have convenient access to background for the first paper and to discussion of some related topics not given elsewhere.

TABLE OF CONTENTS

	Page
List of Figures	vii
List of Tables	xi
List of Symbols Frequently Used	xii
MODEL CIRCULATIONS WITH MICROPHYSICAL PROCESSES	
Abstract	1
1. Introduction	3
2. Basic Equations	3
A. A Continuity Equation for Precipitation	3
B. A Continuity Equation for Cloud and Vapor	4
C. A System of Continuity Equations for Vapor, Cloud, and Precipitation Including Cloud-Precipitation Interactions	6
3. The Steady-State Precipitation Rate from a Saturated, Horizontally Uniform Updraft Column	8
4. The Steady-State Vertical Profile of Cloud in the Compressible Atmosphere	12
5. Example Steady-State Vertical Profiles of Interacting Precipitation and Cloud in an Incompressible Atmosphere	14
6. Models of Microphysical Parameters	20
A. The Condensation and Evaporation of Cloud	20
B. The Conversion of Cloud	22
C. The Drop Size Distribution in Precipitation	22
D. The Fall Speed of Precipitation	23
E. The Rainfall Rate	23
F. The Radar Reflectivity Factor of Precipitation	24
G. Collection of Cloud by Rain	25
H. Evaporation of Rain	26
I. Summary	28
7. A Model of the Onset of Precipitation	30
8. Numerical Determination of Vertical Profiles of Cloud and Precipitation	33
A. Relationships between Microphysical Parameters and the Onset of Precipitation	33

Page

B. Relationships between Microphysical Parameters and Steady-State Profiles of Cloud and Precipitation 39

C. The Amount of Cloud which Coexists with Precipitation in the Steady State 42

D. Roles of Updraft Strength and Duration in Model Cloud and Precipitation Development 44

(1) Specified vertical displacement of the air at a very rapid rate 44

(2) Various updraft speeds and durations 47

E. Development of Cloud and Precipitation in an Initially Unsaturated Updraft Column 49

9. A Two-Dimensional Rectilinear Circulation Cell Model 50

A. The Model Circulation 50

B. Water Budget Parameters Independent of Circulation Intensity and Microphysical Processes 51

(1) Total water 51

(2) Maximum condensable water 53

(3) Circulation-condensable water 53

(4) Condensed water 56

C. Water Distributions in Weak and Strong Circulations Initially Saturated and Unsaturated 56

D. Effect of the Shape Parameter N_O on the Water Distribution in the Model Circulation Cell 64

E. Discussion of Budget Parameters in the Model Two-Dimensional Circulation 64

10. Some Implications of the Model and Suggestions for Future Work 69

A. Interpretation of Radar Weather Data 69

B. Implications of Microphysical Parameters for Weather Modification and Global Climate 73

(1) Weather modification 73

(2) Global climate 76

C. Other Suggestions for Further Study 76

11. Appendices 77

A. The Difference between the Horizontal Speed of Raindrops and the Horizontal Wind Speed 77

B. Method for Numerical Solution 78

Page

(1) Model updraft columns 78

(2) Two-dimensional model circulations 79

Acknowledgment 80

References 81

SORTING OF RAINDROPS BY GRAVITY 87

Abstract 87

1. Introduction 87

2. Example Case 87

References 91

DISTRIBUTION WITH HEIGHT OF THE RADAR ECHO COVERAGE AND ITS METEOROLOGICAL SIGNIFICANCE 93

Abstract 93

1. Introduction 93

2. Empirical Data 94

3. Conclusions 96

References 98

ELEMENTARY THEORY OF ASSOCIATIONS BETWEEN ATMOSPHERIC MOTIONS AND DISTRIBUTIONS OF WATER CONTENT (Reprinted from Monthly Weather Review) 99

Abstract 99

1. Introduction 99

2. The Distribution of M Along Verticals Where There Is No Horizontal Advection 101

A. V + w Everywhere Less than Zero (Motion of Condensate Everywhere Downward) 101

(1) Steady-state solutions 101

(2) Time-dependent solutions 104

B. V + w Somewhere Greater than Zero (Motion of Condensate Somewhere Upward) 104

3. The Steady-State Precipitation Rate from a Saturated, Horizontally Uniform Updraft Column 104

4. Assumptions Implicit in the Relationship N(V + w) = Constant 106

5. Two-Dimensional Solutions 109

		Page
	A. Instantaneous Evaporation of Condensate in Subsaturated Air	109
	B. No Evaporation of Condensate in Subsaturated Air	111
6.	The Kinematic Bases of Generators	116
7.	The Stalactite Problem	120
8.	Conclusions	124
	Acknowledgments	124
	References	125

LIST OF FIGURES

MODEL CIRCULATIONS WITH MICROPHYSICAL PROCESSES

Figure	Description	Page
1	Role of horizontal divergence in the precipitation process.	10
2	Steady-state vertical profiles of cloud in a model tropical atmosphere.	13
3	Steady-state vertical profiles of cloud and precipitation for extrema of microphysical processes.	16
4	Condensation rate in model saturated updrafts.	20
5	Graphical representation of microphysical parameters.	29
6	Precipitation onset in relation to accretion and cloud autoconversion.	32
7	Decrease of cloud water accompanying precipitation development in a uniform model cloud.	33
8	Precipitation transients in relation to the magnitude of the cloud conversion threshold parameter.	34
9	Precipitation transients in relation to height variations of the cloud conversion threshold.	34
10	Cloud and precipitation profiles at different times, where precipitation forms first in the cloud base.	35
11	Cloud and precipitation profiles where precipitation forms first in the middle of the cloud.	35
12	Cloud and precipitation profiles where precipitation forms first in the top of the cloud.	36
13	Precipitation onset in relation to the cloud conversion rate.	38
14	Precipitation onset in relation to the collection efficiency.	38
15	Precipitation onset in relation to the drop size distribution parameter.	38
16	Steady-state profiles of cloud and precipitation in relation to the cloud conversion threshold.	40
17	Steady-state profiles in relation to the cloud conversion rate	40
18	Steady-state profiles in relation to the collection efficiency.	40
19	Steady-state profiles in relation to the drop size distribution	40

20	Numerical model of a cloud profile where advection and autoconversion are zero.	44
21	Cloud profiles where vertical displacement of air occurs without autoconversion.	46
22	Precipitation rate at the ground vs time, following rapid vertical displacement of air.	46
23	Total rainfall at the ground in a model with rapid vertical displacement of air.	46
24	Rainfall rate vs time for various rates of small vertical displacement of air.	47
25	Rainfall rate vs time for various rates of large vertical displacement of air.	48
26a,b	Vertical profiles of cloud and precipitation, for a model atmosphere initially unsaturated.	49
27	Streamlines of a two-dimensional model wind field.	51
28	Advection of a line or plane initially horizontal in the model wind field.	51
29	Distribution of circulation-condensable water in a saturated model atmosphere.	54
30a	Distribution of saturation deficit in a model atmosphere.	54
30b	Distribution of circulation-condensable water in the unsaturated model.	54
31	Water condensed vs time in two model atmospheres.	57
32	Example computer printout of water distributions.	58
33	Example computer printout of budget parameters.	59
34	Water distributions in a two-dimensional, initially saturated atmosphere with a weak circulation.	60
35	Water budget parameters for the case shown in Figure 34.	60
36	Water distributions in an initially saturated atmosphere with a strong circulation.	61
37	Budget parameters for the case shown in Figure 36.	61
38	Water distributions in an initially unsaturated atmosphere with a weak circulation.	62
39	Budget parameters for the case shown in Figure 38.	62
40	Water distributions in an initially unsaturated atmosphere with a strong circulation.	63
41	Budget parameters associated with Figure 40.	63

42	Water distributions in an initially saturated model where the raindrops are unusually small and numerous.	65
43	Budget parameters for the case shown in Figure 42.	65
44	Precipitation concentration in a weak updraft model, in relation to height and time.	70
45	Precipitation concentration in a strong updraft model, in relation to height and time.	71
46	Time averaged water content as a function of height in weak and strong circulations.	72
47	Vertical profile of precipitation vs time in a weak updraft model.	73
48	Vertical profile of precipitation vs time in a strong updraft model.	74

SORTING OF RAINDROPS BY GRAVITY

1	Initial conditions of the problem.	88
2	Times of onset and termination of various drop sizes at the ground.	89
3	Contribution to the rainfall rate by drops of different sizes.	89
4	Composition of rain at the ground as a function of time.	90
5	Geometry of the stretching factor.	91

DISTRIBUTION WITH HEIGHT OF THE RADAR ECHO COVERAGE AND ITS METEOROLOGICAL SIGNIFICANCE

1	Model circulation.	93
2	Average precipitation content at different heights in weak and strong circulations.	94
3	Height profiles of average echo coverage in weak and strong model circulations	94
4a	Surface weather chart, 1200 CST, 3 April 1964.	95
4b	500-mb. chart, 1800 CST, 3 April 1964.	95
5a	Surface weather chart, 1200 CST, 15 Nov. 1964.	95
5b	500-mb. chart, 1800 CST, 1800 CST, 15 Nov. 1964.	95
6	Soundings at Tinker AFB, Oklahoma on 3 April and 15 Nov. 1964.	96
7	Echo coverage vs height and time, and distribution of echo intensity vs time, 3-4 April 1964.	97
8	Echo coverage vs height and time, and distribution of echo intensity vs time, 15 Nov. 1964.	98

ELEMENTARY THEORY OF ASSOCIATIONS BETWEEN ATMOSPHERIC MOTIONS AND DISTRIBUTIONS OF WATER CONTENT

1	Vertical profiles of precipitation and saturation deficit in updrafts and downdrafts, respectively.	102
2	Steady-state vertical profiles of water content in a model snowstorm where the fall speed increases following descent of snow particles.	102
3	Streamlines of a model wind field.	110
4	Distributions of water substance in weak circulations for a case of instantaneous evaporation of condensate in subsaturated air, and for a case without evaporation.	112
5	Distributions of water substance in strong circulations.	113
6	Streamlines of precipitation and vapor, and the shifting boundary between saturated and unsaturated air.	114
7	Steady-state solutions and time vs height along precipitation streamlines.	114
8	Time-height record produced by a vertically pointing K-band radar.	117
9	Model precipitation generators and their trails.	119
10	Parameters of generator and their trails.	119
11	Descent of precipitation through a convective cell.	120
12	Model stalactite length in relation to the ratio between the precipitation fall speed and the updraft speed.	121
13	The time required for precipitation to descend through unsaturated vertical drafts.	123

LIST OF TABLES

MODEL CIRCULATIONS WITH MICROPHYSICAL PROCESSES

Table	Description	Page
1	Cloud and precipitation distributions in idealized one-dimensional cases.	17
2	Mathematical models of microphysical parameters.	28
3	Budget parameters independent of microphysical processes in saturated and unsaturated model atmospheres.	55
4	Comprehensive lists of water budget data.	66-67

ELEMENTARY THEORY OF ASSOCIATIONS BETWEEN ATMOSPHERIC MOTIONS AND DISTRIBUTIONS OF WATER CONTENT

Table	Description	Page
1	Atmospheric parameters of a model snowstorm.	103

LIST OF SYMBOLS FREQUENTLY USED

a	cloud conversion threshold
A	used in $G = A + Bz$; see G below; $(A > 0)$
B	used in $G = A + Bz$; see G below; $(B < 0)$
D	drop diameter
$\mathbb{D}$	air displacement parameter $= w_{max}t/H$
$\mathcal{D}$	discriminant of a quadratic equation
E	efficiency with which raindrops capture cloud drops
G	condensation generating function; $G = -\rho\frac{\partial Q_s'}{\partial z}$
h	space increment in a finite difference problem; from page 87 to 93, height of a precipitation column when precipitation starts at the ground.
H	height of the top of an updraft column; from page 87 to 93, the height of the base of a precipitation packet
H'	a reference height
k	time increment in a finite difference problem
k_1	cloud autoconversion coefficient
k_2	usually, the accretion coefficient 6.96×10^{-4}; on p.43 and in Section 7, however, $k_2 = 6.96 \times 10^{-4}EN_o^{.125}$
k_3	evaporation coefficient $= 1.93 \times 10^{-6}$
K	an approximation to $\frac{\partial \ln \rho}{\partial z}$; after p. 99, $K = V/w_{max}$
m	cloud density + vapor density - saturation vapor density
m'	cloud mixing ratio + vapor mixing ratio - saturation vapor mixing ratio
M	a positive quantity defining the precipitation content, gm. m^{-3}; in a cloud free model (pp. 99 ff) $M < 0$ measures the saturation deficit.
M'	precipitation mixing ratio, dimensionless

M^*	$M + m$, where $m = 0$ when $M^* > 0$ and $M = 0$ when $M^* < 0$
m	all the water substance except precipitation
N_o	intercept of the drop size distribution function with the axis $D = 0$
N_t	total number of raindrops in unit volume
q	vapor density - saturation vapor density
Q	water vapor density
Q'	water vapor mixing ratio
Q_s	saturation water vapor density
Q_s'	saturation water vapor mixing ratio
R	precipitation rate
R_o	precipitation rate beneath an updraft column or at the ground
t	time
T_1	problem time when the air circulation stops
T_2	problem time when computations end
u	windspeed in the horizontal or x-direction; when v also appears u is the west wind
U	horizontal velocity of a raindrop, usually assumed to be the same as u
v	the south wind, i.e., the wind speed in the y-direction
V	terminal fall speed of raindrops, often taken as V_o
V_o	terminal fall speed of the raindrop whose diameter divides the distribution of drops into parts with equal water contents.
w	the wind in the vertical or z-direction
w_{max}	the maximum air speed in the z-direction
x,y,z	Cartesian coordinates associated with u, v, and w
Z	radar reflectivity factor of precipitation $= \Sigma ND^6$

∂, δ differential operators

Γ the gamma function

λ slope of the drop size distribution function

ρ air density

ρ_ℓ density of liquid water = 10^6 gm. m.$^{-3}$

The meter-gram-second system of units is used except where explicitly noted otherwise.

MODEL CIRCULATIONS WITH MICROPHYSICAL PROCESSES[1]

ABSTRACT

A kinematic model of the atmosphere illustrates relationships among distributions of air motion, precipitation, cloud and vapor, and microphysical processes. Continuity equations are derived and discussed, and applied to a variety of sample situations.

The steady precipitation rate beneath a saturated, horizontally uniform updraft column is generally different from the condensation rate there; the magnitude of the difference is regulated by the horizontal divergence of moisture, itself determined by various microphysical parameters and the updraft. The steady-state vertical profile of cloud density in a precipitation-free column exhibits a maximum whose height increases with the height of the condensation level; this is shown to imply that cirrus cloudiness might sometimes increase locally with descending velocities in the real atmosphere, even without horizontal advection of cloud. Vertical profiles of coexisting cloud and precipitation are presented for model microphysical parameters and processes, including the autoconversion of cloud to precipitation, the drop size distribution and fall speed of precipitation, the rainfall rate, the accretion of cloud by rain, and the evaporation of rain.

A model of the onset of precipitation from infinite uniform cloud is presented. This illustrates the dependence of an onset-time parameter on the strength of cloud autoconversion and accretion processes, and on the ratio of these processes. The role of the microphysical parameters in regulating the development of precipitation and cloud in model updrafts is illustrated by numerical solutions of equations which define time-dependent and steady solutions along the height-axis. For example, the steady-state cloud amount which coexists with precipitation is shown to be only weakly dependent on the shape of the drop-size distribution in precipitation, the updraft speed, and the condensation function; it is moderately dependent, however, on the height of the updraft column, and on the efficiency with which rain collects cloud. Generally, in the kinematic framework of this study, the shapes of vertical profiles of precipitation and cloud water contents and the amounts of condensate aloft are sensitive to the magnitude and distribution of microphysical processes. However, the accumulation of precipitation and its steady-state rate are strongly dependent only on the condensation function and the updrafts.

---

[1] This paper organizes and extends work done while the author was at the Travelers Research Center and favored with the support of Contract DA 36-039 SC 89099 between TRC and the U. S. Army Electronic Research and Development Laboratory (see [21]).

The precipitation rate and accumulation at the ground beneath an updraft core, in relation to updraft strength and duration, are examined. In those cases where the updraft speed is greater than the fall speed of precipitation, there is, for defined displacement, only a weak relationship between the speed of updrafts and the precipitation rate. The accumulated precipitation may fairly measure the vertical displacement of air, but it seems probable that the rainfall rate in showers only occasionally corresponds to the vertical velocity of air.

Some implications of the one-dimensional models for radar observations are discussed, and probable cause is shown for the height of first echoes to increase with updraft speed.

Distributions of water substance in two-dimensional circulation models 6 km. deep are considered. Defined parameters of the water budget include the total water, maximum condensable water, circulation condensable water, condensed water, cloud and vapor, and precipitation aloft and accumulated at the ground. Cloud is relatively dense shortly after condensation starts, then thins in response to its efficient accretion by precipitation. When the circulation is strong, precipitation accumulates aloft until model overturning is complete, then falls out suddenly. About 30% of total water or 82% of condensed water is precipitated from an initially saturated circulation where the maximum updraft is 2.5 m./sec.; with maximum updrafts 10 m./sec., the precentages decline to 27 and 72. The percentage of total water which condenses increases in deeper circulations, and the percentage of condensed water which precipitates declines in drier atmospheres. In the model, the circulation depth, intensity, and duration, and the initial water content, rather than microphysical parameters such as the distribution of raindrop sizes, are the principal regulators of precipitation amounts.

The height profile of the horizontal average of precipitation content in the model two-dimensional circulation cells, has a maximum aloft during most of problem time and in averaged problem time. The maximum aloft is more prominent in stronger circulations. The height profiles of condensed water are a measure of the intensity of convection, and probably influence the measurement of rainfall by radar.

The microphysical parameters for precipitation production have a role secondary to that of the updrafts in the kinematic models treated in this paper. However, microphysical effects maybe more important in the real world, since the updrafts there are regulated by dynamical factors which are influenced by microphysical processes. Problems of weather modification and global climate are considered in the light of this study.

Suggestions for further study include more realistic modelling of real atmospheric circulations and hydrometeor families with different fall speeds in air, and development of a theory which relates transport of moisture, heat, and momentum in the atmosphere, with statistical properties of radar echoes. Eventually, we should produce a model dynamical system which incorporates continuity principles for water substance in all its forms.

1. INTRODUCTION

The distributions of cloud and precipitation are closely related to the distributions of water vapor and wind, and to the microphysical processes which cause cloud particles to unite as larger elements of precipitation. This paper presents a model of these relationships, and should provide a view of the stormy atmosphere which is interesting to professional meteorologists, and, indeed, to anyone who ponders the intricate interweaving flows of water and air.

The approach is kinematic, and it may provide better understanding of some observations on natural coexisting distributions of water and air. The improved description of natural circulations from observations by radar, radiosonde, and other means should better enable us to evaluate the circulations as transporters and organizers of energy, mass, and momentum, and may lead to improved models of nature which include dynamical effects.

Part of the background of the present study is the work of Wexler and Atlas [47] who modeled microphysical processes to investigate the balance between cloud water which shares the motion of air, and widespread precipitation which falls relative to the air. They derived vertical profiles of cloud and precipitation for steady cases where horizontal advection is absent and where the updraft speed is small compared to the fall speed of most of the precipitation particles. Subsequently, Kessler [18, 19, 20] used more general continuity equations to study precipitation distributions in wind fields where saturated updrafts produce precipitation without an intervening cloud stage. ([20] is reproduced within these covers, starting on p. 99.)

The present study incorporates model microphysical processes into the continuity equations and suggests how the processes and air motions, acting together, regulate the vapor, cloud, and precipitation distributions.

2. BASIC EQUATIONS

A. A Continuity Equation for Precipitation

The precipitation content of the air is M, always positive or zero. Assume that M shares the horizontal motion of the air: this assumption is examined carefully in Appendix A. Let the downward velocity of M relative to the air at any one height and time be represented by V, a negative quantity; if the precipitation content at a point is distributed over particles of different sizes and fall speeds, V at that point is then a kind of average. With these assumptions, a development practically identical to that given by Haurwitz [14], for example, gives the following continuity equation for M:

$$\frac{\partial M}{\partial t} = -\left\{\frac{\partial}{\partial x}(Mu) + \frac{\partial}{\partial y}(Mv) + \frac{\partial}{\partial z}\left[M(V+w)\right]\right\} , \qquad (1)$$

where u and v are the winds in the x- and y- (horizontal) directions and w is the wind in the z- (vertical) direction. This equation governs the distribution of precipitation already formed but makes no allowance for its creation. Creation is considered in Section 2C.

Assume that the air motions are well enough defined by the continuity equation

$$\frac{\partial u}{\partial x} + \frac{\partial v}{\partial y} + \frac{\partial w}{\partial z} = -w\frac{\partial \ln \rho}{\partial z} , \qquad (2)$$

where ρ is the air density. Equation (2) applies strictly when the air density is locally steady and horizontally uniform. Substitute Eq. (2) into Eq. (1) to obtain:

$$\frac{\partial M}{\partial t} = -u\frac{\partial M}{\partial x} - v\frac{\partial M}{\partial y} - (V+w)\frac{\partial M}{\partial z} - M\left[\frac{\partial V}{\partial z} - w\frac{\partial \ln \rho}{\partial z}\right] \qquad (3)$$

The derivatives of the wind appearing in Eq. (1) are absent from Eq. (3), having been replaced by the last term in density which accounts for the compressibility of the atmosphere. This term is itself comparatively small, except when $(V + w) \doteqdot 0$, as discussed in Section 7a of [18].

B. A Continuity Equation for Cloud and Vapor

A tendency to supersaturation in the atmosphere is almost wholly offset by the condensation of many tiny cloud particles which closely follow both horizontal and vertical air motions; also, cloud particles evaporate in a matter of seconds when the relative humidity is more than a few percent below saturation [29, 42].

These properties of cloud have suggested a quantity m, defined as the cloud density minus the saturation vapor density plus the actual vapor density. If, when m is positive, the actual vapor density is taken as the saturation vapor density, then m is the amount of cloud. When m is negative, and the cloud content is zero, m is the amount of moisture required to saturate the air. We have

$$m = \text{cloud density} + \text{vapor density} - \text{saturation vapor density}$$
$$= \mathcal{M} - Q_S \quad , \tag{4}$$

where Q_S is the saturation vapor density, and $\mathcal{M}$ is the content of all water substance except precipitation.

A continuity equation for m is derived by first considering that for $\mathcal{M}$. This has the same form as Eq. (3), except for the absence of terms containing V:

$$\frac{\partial \mathcal{M}}{\partial t} = -u \frac{\partial \mathcal{M}}{\partial x} - v \frac{\partial \mathcal{M}}{\partial y} - w \frac{\partial \mathcal{M}}{\partial z} + \mathcal{M} w \frac{\partial \ln \rho}{\partial z} \quad . \tag{5}$$

Substitute for $\mathcal{M}$ in (5) from (4) to obtain

$$\frac{\partial (m+Q_s)}{\partial t} = -u \frac{\partial (m+Q_s)}{\partial x} - v \frac{\partial (m+Q_s)}{\partial y} - w \frac{\partial (m+Q_s)}{\partial z} + (m+Q_s) w \frac{\partial \ln \rho}{\partial z} . \tag{6}$$

Assume that the saturation vapor density of the air is locally steady and horizontally uniform, i.e., that

$$\frac{\partial Q_S}{\partial t} = \frac{\partial Q_S}{\partial x} = \frac{\partial Q_S}{\partial y} = 0 \ .$$

Although this is rarely strictly true, it is usual for the local change and horizontal variation of Q_S to be quite small compared with its vertical variation. Then

$$\frac{\partial m}{\partial t} = -u \frac{\partial m}{\partial x} - v \frac{\partial m}{\partial y} - w \frac{\partial m}{\partial z} + m w \frac{\partial \ln \rho}{\partial z} + w \left[Q_s \frac{\partial \ln \rho}{\partial z} - \frac{\partial Q_s}{\partial z} \right] . \tag{7}$$

Equation (7) is significantly unlike Eq. (3). Equation (7) does not contain terms in the fall speed of m, since m is assumed in this model to share the motion of the air in all respects. And since the saturation deficit of cloud content changes when the air is displaced vertically, Eq. (7) contains terms in the saturation vapor density Q_S which account for these changes. The sum of the terms in Q_S in (7) we call the generating function G; a first approximation to G in the real troposphere is a linear function of height, and its magnitude in the lower tropical troposphere is about 3×10^{-3} gm. m.$^{-4}$

C. A System of Continuity Equations for Vapor, Cloud, and Precipitation including Cloud-Precipitation Interactions

A modification of Eqs. (3) and (7) to model the bulk effects of interactions among the three-dimensional cloud and precipitation particles as well as their distribution by wind, is based on elementary considerations of precipitation physics. The first product of rising motion is cloud. Coalescence of cloud particles to form precipitation seems favored by the presence of a broad spectrum of cloud particle sizes, e.g., by the presence of large hygroscopic salt nuclei in the subsaturated atmosphere. Selective growth of tiny ice particles to precipitation size may also occur when liquid and ice phases coexist at subfreezing temperatures. Both of these processes are represented by a term called "autoconversion of cloud."

Once precipitation particles are formed, their fall speed carries them through the population of cloud particles and facilitates the growth of precipitation by collection of cloud. This process is represented by a term whose magnitude must increase with the content of cloud and precipitation; this term called "collection of cloud" contributes to development of precipitation and equal depletion of cloud.

The third process of particular interest is evaporation. The terms in Q_s in Eq. (7) and our concept of m provides for evaporation of cloud in saturated downdrafts at just the rate which maintains saturation. The evaporation of precipitation in unsaturated (cloud free) air must be represented by another term.

Equations (3) and (7) are now rewritten with the addition of terms representing the transfer of water substance from cloud to precipitation and from precipitation to vapor:

$$\frac{\partial M}{\partial t} = -u\frac{\partial M}{\partial x} - v\frac{\partial M}{\partial y} - (V+w)\frac{\partial M}{\partial z} - M\frac{\partial V}{\partial z} + Mw\frac{\partial \ln \rho}{\partial z} \qquad (8)$$

+ autoconversion of cloud + collec. of cld. - evap. of precip.

$$\frac{\partial m}{\partial t} = -u\frac{\partial m}{\partial x} - v\frac{\partial m}{\partial y} - w\frac{\partial m}{\partial z} + mw\frac{\partial \ln \rho}{\partial z} + wG \qquad (9)$$

- autoconversion of cloud - collec. of cld. + evap. of precip.

In Eq. (9) $G = Q_s(\partial \ln\rho/\partial z) - \partial Q_s/\partial z = -\rho(\partial Q_s'/\partial z)$, where Q_s is the saturation vapor density, and Q_s' is the saturation mixing ratio. The autoconversion and collection terms in (8) and (9) are non-zero only when $m > 0$, i.e., when there is cloud. And, as noted above, the evaporation term is non-zero only when $m < 0$, i.e., when the air is not saturated with vapor. The microphysical terms are treated numerically and Eqs. (8) and (9) presented in their complete forms in Section 6 below.

It is interesting at this point to consider how Eqs. (8) and (9) can be related to the continuity equation which describes a cloud-free precipitation process and which was the basis of earlier work [16, 17, 18]. The addition of Eqs. (8) and (9) yields

$$\frac{\partial(M+m)}{\partial t} = -u\frac{\partial(M+m)}{\partial x} - v\frac{\partial(M+m)}{\partial y} - w\frac{\partial(M+m)}{\partial z} - \frac{\partial}{\partial z}(MV) + (M+m)\,w\frac{\partial \ln\rho}{\partial z} + wG \,. \tag{10}$$

Let $M + m$ be denoted by a new variable M^*. If $m = 0$ when $M^* > 0$ and $M, V = 0$ when $M^* < 0$, Eq. (10) can be written

$$\frac{\partial M^*}{\partial t} = -u\frac{\partial M^*}{\partial x} - v\frac{\partial M^*}{\partial y} - w\frac{\partial M^*}{\partial z} - \frac{\partial}{\partial z}M^*V + M^*w\frac{\partial \ln\rho}{\partial z} + wG \,. \tag{11}$$

$$m = 0 \text{ when } M^* > 0$$

$$M,V = 0 \text{ when } M^* < 0$$

Eq. (11) is the basis for the earlier model. When negative, M^* is the saturation deficit which follows the motion of the air; when positive, M^* is the precipitation content which falls at speed V relative to the air. Equation (11) models a system wherein cloud does not exist because condensate appears instantly as precipitation.

Equations (8) and (9) are reformulated to refer to mixing ratio units, designated as primed quantities, by substitution of $\rho m'$ wherever m appears, $\rho M'$ wherever M appears, and $\rho Q_s'$ whereever Q_s appears. After simplification, there is obtained

$$\frac{\partial M'}{\partial t} = -u\frac{\partial M'}{\partial x} - v\frac{\partial M'}{\partial y} - (w+V)\frac{\partial M'}{\partial z} - M'\left[\frac{\partial V}{\partial z} + V\frac{\partial \ln\rho}{\partial z}\right] \tag{8'}$$

$$- \text{cld. cnvrsn.} - \text{cld. collection} + \text{evap. of precipitation.}$$

$$\frac{\partial m'}{\partial t} = - u\frac{\partial m'}{\partial x} - v\frac{\partial m'}{\partial y} - w\frac{\partial m'}{\partial z} - w\,\frac{\partial Q_s'}{\partial z} \tag{9'}$$

- cld. cnvrsn. - cld. collection + evap. of precipitation.

The absence of the density term in (9') is due to the conservative nature of the mixing ratios of water vapor and cloud following the motion of air parcels. Although (9') is therefore slightly simpler than Eq. (9), the equations in density units are used here because the parameters of weather radar, visual appearance of clouds, and some physical processes are more easily understood in such terms.

3. THE STEADY-STATE PRECIPITATION RATE FROM A SATURATED, HORIZONTALLY UNIFORM UPDRAFT COLUMN

Bannon's work [4] is an example of the early studies which relate steady precipitation rate to updrafts through the assumption that the precipitation rate equals the vertically integrated rate of condensation. In the cloud-free model of Kessler [18], however, analysis of steady precipitation without horizontal advection leads to the conclusion that the steady precipitation rate beneath an updraft column and the condensation rate within it, tend toward equality as the fall speed of precipitation becomes much greater than the speed of updrafts. In the particular ideal case where all of the precipitation particles fall relative to the air at a speed only slightly larger than the maximum updraft, the steady precipitation rate at the ground is substantially greater than the rate of condensation in the vertical column above. The excess of precipitation over condensation in such cases is explained in terms of the distribution of horizontal divergence which must accompany vertical currents. Horizontal convergence in the lower part of the updraft concentrates precipitation at the base of the updraft column at the expense of the amounts away from the center of the column. This is clearly shown in two-dimensional rectilinear models [19, 20] and by the visual appearance of thunderstorms, for example.

Eqs. (8) and (9) provide means for extending the earlier analysis to a model in which both cloud and precipitation occur. At a shower core, or in an area of widespread uniform precipitation, the horizontal advection terms in (8) and (9) vanish and the sum of the equations is

$$\frac{\partial (M + m)}{\partial t} = - w\frac{\partial (M + m)}{\partial z} - \frac{\partial}{\partial z} MV + wG + (M + m)w\frac{\partial \ln\rho}{\partial z} \tag{12}$$

Consider the vertical integral of Eq. (12) in a saturated updraft column when the distributions are locally steady:

$$0 = -\int_0^H w \frac{\partial (M+m)}{\partial z} dz - \int_0^H \frac{\partial}{\partial z}(MV)\, dz + \int_0^H wG\, dz + \int_0^H (M+m) \frac{\partial \ln \rho}{\partial z} dz \quad . \qquad (13)$$

The limits of integration are from the base ($z = 0$) to the top, ($z = H$) of the updraft column. The vertical air velocity w is zero at and outside these limits. At the top of the updraft column, the boundary condition $M(H) = 0$ is also imposed, meaning that no precipitation enters the updraft column from above it.

The second integral on the right is seen immediately to be equal to $(MV)_{z=H} - (MV)_{z=0}$. Since $M = 0$ at $z = H$, as explained above, the first of these terms is zero; the second is just the precipitation rate R_0 at the base of the updraft (in general, $R = -M(V + w)$; however, the limits of the updraft column are defined so that $w = 0$ at $z = 0$). R_0 may be the precipitation rate at the ground without loss of generality, since the updraft is always zero there. The third integral on the right is the rate at which condensate is produced by updrafts in a vertical column of unit cross section.

The first integral in Eq. (13) is studied by integration by parts. Note that

$$-w \frac{\partial (M+m)}{\partial z} = -\frac{\partial}{\partial z} w(M+m) + (M+m) \frac{\partial w}{\partial z} \quad . \qquad (14)$$

The integral from $z = 0$ to $z = H$ of the first term on the right of Eq. (14) vanishes because w is zero at the base and at the top of the updraft column. The divergence of the vertical wind in the second term on the right can be replaced by its equivalent in the equation of continuity for air, Eq. (2). Substitution from Eq. (2) into Eqs. (14) and (13), with the other simplifications noted above, and rearrangement of terms, gives

$$R_0 = \int_0^H wG\, dz - \int_0^H (M+m)\left(\frac{\partial u}{\partial x} + \frac{\partial v}{\partial y}\right) dz \quad . \qquad (15)$$

Eq. (15) is a reminder that the horizontal divergence of the wind is implicit even in the one-dimensional forms of Eqs. (8) and (9). The last term may be positive, negative or zero; it depends on the distribution and intensity of microphysical processes affecting the interactions between cloud and precipitation and on the magnitude and distribution of the ratio of precipitation fall speed to the updraft. Because horizontal convergence characterizes the lower part of an updraft column, and horizontal divergence the upper part, precipitation rates in excess of the condensation rate are favored by relatively large values of (m + M) below the level where the horizontal divergence is zero.

In an incompressible model atmosphere the terms in $\partial \ln \rho / \partial z$ are absent from both Eq. (2) and (13). Procedures like those described above then lead to the same Eq. (15). Although Eq. (15) is the same in a compressible model atmosphere as in an incompressible one, evaluation of its terms gives slightly different results in the two cases, since the profiles of m and M vary with considerations of compressibility when other parameters are equal.

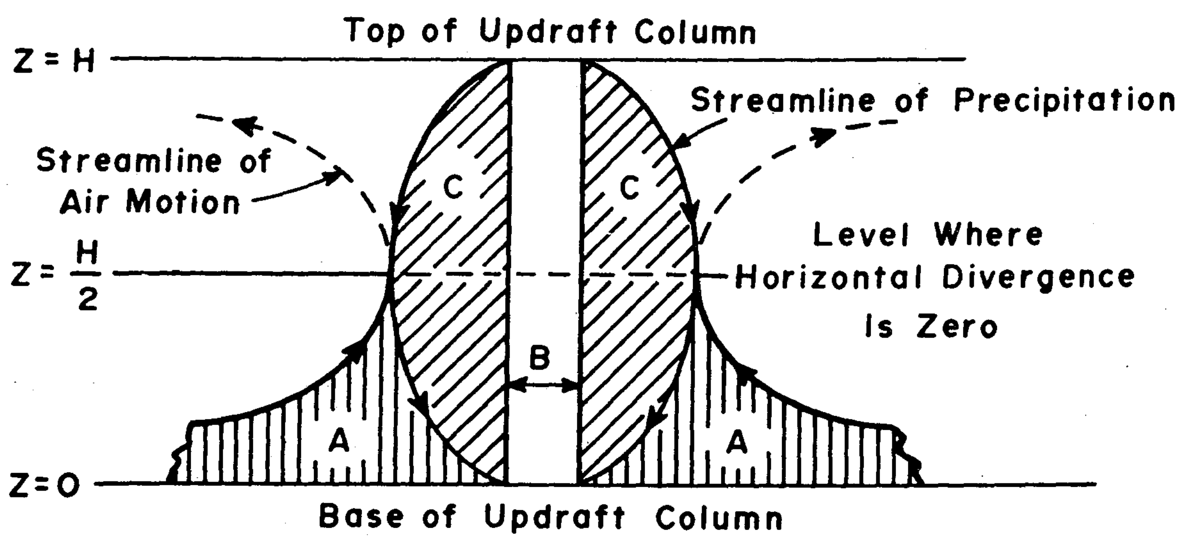

Figure 1. - Illustrating Eq. (15). Horizontal divergence at high altitudes accompanies rising air motion and spreads precipitation packets horizontally as they descend in the area marked B and C. Below the level of nondivergence, packets contract horizontally in the convergent wind field. Precipitation at the ground in B is due to condensation in a volume larger than that directly overhead, by an amount indicated by the diagonal shading. When cloud is collected by precipitation at the level of nondivergence but not below that height, the region contributing moisture to the precipitation at B is further increased as indicated by the vertically shaded area A. (See text, pp. 11 and 12.)

The mechanism exposed by Eq. (15) is illustrated by figure 1, a vertical cross section through a horizontally uniform distribution of vertical velocity. Consider the rainfall at the base of the cross section marked B. Precipitation particles descending from the top of the updraft column are spread by horizontal divergence, then contracted by convergence. In a cloud-free incompressible atmosphere, with the updraft symmetric about its midheight and the fall speed of precipitation constant relative to air, for example, the region contributing to precipitation at the ground exceeds that vertically overhead by an amount represented by the diagonally shaded area in the figure. Thus, the steady precipitation rate must exceed the vertically integrated condensation rate in this case. (See also [18], p. 634.) Equation (15) gives the same result: since $m = 0$ in the cloud-free model atmosphere and M increases downward, the contribution of the third term in Eq.(15) is clearly positive.

Since in nature the magnitude of V usually increases following the descent of M, and particularly increases when snow melts to form fast-falling rain, the term $M(\partial V/\partial Z)$ in Eq. (8) tends to diminish M as it descends. Then the contribution of the divergence term in Eq. (15) is less than would be measured in the ideal case of constant fall speed illustrated by figure 1. When melting occurs at the level of nondivergence, the effect of fall speed changes is maximized and the precipitation rate at the ground at updraft centers may be a little less than that condensed overhead. (See Section 7b, p. 635 in [17], and Section 4 below.) In any event, excesses or deficiencies of precipitation over condensation rates at an updraft center are balanced at places removed from the center.

Consideration of Eq. (15) and figure 1 reveals the cloud-precipitation interactions which maximize the steady precipitation rate at updraft centers. If cloud is present above the level of nondivergence, some of it is carried by horizontal divergence outside the diagonally shaded region contributing to precipitation at the ground in Section B. Therefore, precipitation at the earth's surface within Section B is larger if, above the level of nondivergence, the condensation process results in immediate augmentation of precipitation without a cloud phase. Below the level of non-divergence, the positive contribution of the third term in (15) is clearly maximized by simultaneously maximizing both m and M. Suppose that the cloud content m does have at each height below the level of non-divergence its maximum possible value, viz., that defined by ascent of saturated air from the surface with retention of all cloud; this condition is shown also to be associated with the greatest possible content of precipitation M. Since we have postulated that precipitation grows directly from the vapor without a cloud phase above the level of nondivergence, all of the cloud ascending from below the level of nondivergence must be collected at that level by the descending precipitation.

Everywhere below that level, the content of M reflects the contribution of all the condensation in the whole depth of the updraft column. In this limiting case, discontinuities of m and M exist at the level of nondivergence and the region contributing to precipitation at the ground is augmented by the area marked A in figure 1. (See discussion of Cases 4 and 5 in Section 5 below.) When, as postulated in this special case, collection of cloud by precipitation is zero within region A, all cloud condensing there is borne inward by horizontal convergence and upward by ascending motion to the collection level from which it returns to the ground in Section B. The augmentation of precipitation at the updraft center is again at the expense of amounts away from the center.

4. THE STEADY-STATE VERTICAL PROFILE OF CLOUD IN THE COMPRESSIBLE ATMOSPHERE

A steady distribution of cloud content is established in a rising saturated air column when the cloud is not mixed with dry surroundings or depleted by change to precipitation and descent to the ground. At each height where the cloud content is steady, air has risen all the way from the condensation level. The steady-state cloud content at each point of the profile is then the maximum that can exist for the given condensation level.

In the steady case without cloud conversion or horizontal advection, Eq. (9) becomes

$$\frac{\partial m}{\partial z} - m\,\frac{\partial \ln \rho}{\partial z} - G = 0 \quad . \tag{16}$$

Since w does not appear in Eq. (16), the steady-state solution is independent of the shape of the vertical velocity distribution. Reasonable approximations to the real atmosphere are $G = A + Bz$ ($0 \geq z \geq -A/B$) and $\partial \ln\rho/\partial z = K$, a constant. The constants B and K are negative, and A is positive. Then the solution of Eq. (16) is

$$m = e^{K(z-z_c)}\left[\frac{1}{K}\left(A + Bz_c + \frac{B}{K}\right)\right] - \frac{1}{K}\left[A + Bz + \frac{B}{K}\right] \qquad \left(0 \leq z \leq -\frac{A}{B}\right) \quad , \tag{17}$$

where z_c is the condensation level where the cloud content is zero.

It is important to note that Eq. (17) has a maximum. Its location is found by setting $\partial m/\partial z = 0$ in Eq. (16) and substituting this solution for the left side of (17). Then

$$z\,(m = max) = z_c + \frac{1}{K}\ln\frac{B}{AK + Bz_cK + B} \tag{18}$$

The height where m is a maximum I call the compensation level, because there the tendency of the generating function to increase the amount of cloud is offset by the decreasing density of ascending air. Above this level of compensation, cloud density decreases with ascent and increases with descent of air.

Above the level $z = -A/B$, the generating function is very small. In this region, Eq. (17) can be extended by use of the relationship

$$m(z) = m\left(-\frac{A}{B}\right) e^{K\left(z + \frac{A}{B}\right)} \tag{19}$$

which is similar to that for the other atmospheric constituents not bound by the particular laws applicable to water substance.

Although Eqs. (16) through (19) are suitable for certain theoretical analyses[2], it is desirable to estimate more closely the steady profiles of m in the real atmosphere. Since no relatively simple formula has been found to approximate the natural generating function at high levels (low temperatures) with the desired accuracy, accurate cloud profiles have been computed with the aid of the Smithsonian Meteorological Tables, Tables 71, 78, and 108 [12]. The results for an atmosphere of constant wet-bulb potential temperature 295° are shown in figure 2. The height scale can be displaced upward to represent conditions approximately in potentially cooler atmospheres.

Since cloud amounts in excess of about 1 gm/m^3 are almost invariably associated with precipitation and are, therefore, only transient,

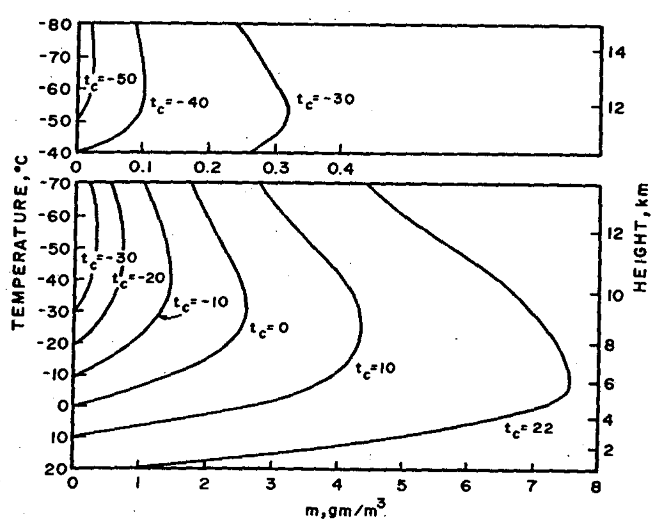

Figure 2. - Steady-state vertical profiles of cloud in a model tropical atmosphere with condensation level temperatures t_c.

[2] Eqs. (17) and (18) are graphed in Report No. 2 of [21].

most of the profiles shown in figure 2 have principally academic interest. However, this analysis suggests that the associations between high clouds and vertical currents may be rather complicated. In discussing this we note that equality of local and individual spatial derivatives is a feature of the steady state. Therefore, the derivative $\partial m/\partial z$ in (16) can as well be dm/dz, and the study applied to the change of cloud content following the vertical displacement of cloudy air parcels. In the region 10-14 km. where cirrus clouds often occur, cloud densities as small as .03 gm. m.$^{-3}$ are associated with anamalous behaviour, i.e., decreasing cloud density with ascending motion and conversely. Although individual cloud particles must grow in ascending saturated air at any level, such growth at heights above the height of compensation is more than offset by the increasing distance that separates particles as the air containing them expands; the converse holds for descent of cloud between levels above the height of compensation. Thus, descending motion of air in a widespread cloud layer at levels above the height of compensation, might be associated with local increases of both cloud layer thickness and density, instead of the opposite usually assumed. The anvil or plume at some distance from an active thunderstorm, or the cirrostratus layer well in advance of a developing winter cyclone would be appropriate places to search for this phenomenon. Accurate measurements of water content and temperature in dense tropical cirrus would also be of special interest in connection with the application of this theory to problems concerning the development and persistence of high cloud. In this connection, it is important to extend the present work to consider effects of microphysical processes; a start in this direction is discussed in the following sections.

5. EXAMPLE STEADY-STATE VERTICAL PROFILES OF INTERACTING PRECIPITATION AND CLOUD IN AN INCOMPRESSIBLE ATMOSPHERE

The discussion of the previous sections is here extended by presentation of exact vertical profiles of cloud and precipitation content that accompany idealized distributions of the microphysical processes, condensation function, and updrafts in an incompressible atmosphere. These cases suggest how extreme modification of cloud-precipitation interactions might affect the distributions of cloud and precipitation, including the areal distribution of the precipitation rate at the ground. For each set of microphysical parameters, the profiles presented below apply to particular distributions of other atmospheric parameters; however, these profiles can be scaled to distributions that differ by constant factors from those used here [18]. For new height of updraft column $\mathcal{H}$, new generating function $\mathcal{G}$, new vertical air speed $\mathcal{W}_{max}$, and new constant fall speed $\mathcal{V} = \mathcal{W}_{max}/w_{max}$, the new solutions denoted by $\mathcal{M}_N$ are given by

$$\mathcal{M}_N = \frac{M\mathcal{G}\mathcal{H}}{GH} , \qquad (20)$$

and apply at points $z \frac{\mathcal{H}}{H}$, where z is the height where M applies.

Consider the one-dimensional, steady-state incompressible form of Eq. (11), with constant fall speed V:

$$0 = -(V + w)\frac{\partial M^*}{\partial z} + wG \; . \qquad (21)$$

This equation with $V < 0$ can be used to describe the development of precipitation M in the absence of a cloud phase; with $V = 0$ it describes the development of m. The solution of (21) for M^* is

$$M^*(z_2) - M^*(z_1) = \int_{z_1}^{z_2} \frac{wG}{w+V} dz \; . \qquad (22)$$

Equation (22) has been used to determine the profiles presented and discussed below.

Case 1. <u>The cloud conversion term is identically zero.</u> In this case there is no precipitation anywhere in the updraft column. Equation (18) becomes

$$m(z_2) - m(z_1) = \int_{z_1}^{z_2} G dz \; . \qquad (23)$$

Figure 3 shows this distribution of cloud for the case where $z_1 = 0$; $0 \le z_2 \le 10^3$m; $G = (2 \times 10^{-3} - 2 \times 10^{-6} z)$ gm m^{-4};[3] and $m(z_1)$, the cloud content at the base of the updraft, is zero. Note that the updraft distribution does not appear in Eq. (23) and, therefore, does not affect the shape of the steady-state cloud distribution in the absence of cloud-precipitation interactions. It is interesting to note that the shape of the profile in figure 3 with $M \equiv 0$, implies that the terms on the right of Eq. (15) tend to balance one another. Of course, they exactly compensate in this case since R_o is zero. Condensate is carried aloft as cloud by updrafts, and in this steady case diverges aloft at a rate equal to the sum of contributions due to low level convergence and condensation from the vapor phase. The model parameters for this case are tabulated in Table 1.

[3]The average value of this generating function is obviously 1 gm/m^{3}km. In Report No. 2 of the Contract, [21], cloud and precipitation profiles for a constant generating function are also illustrated.

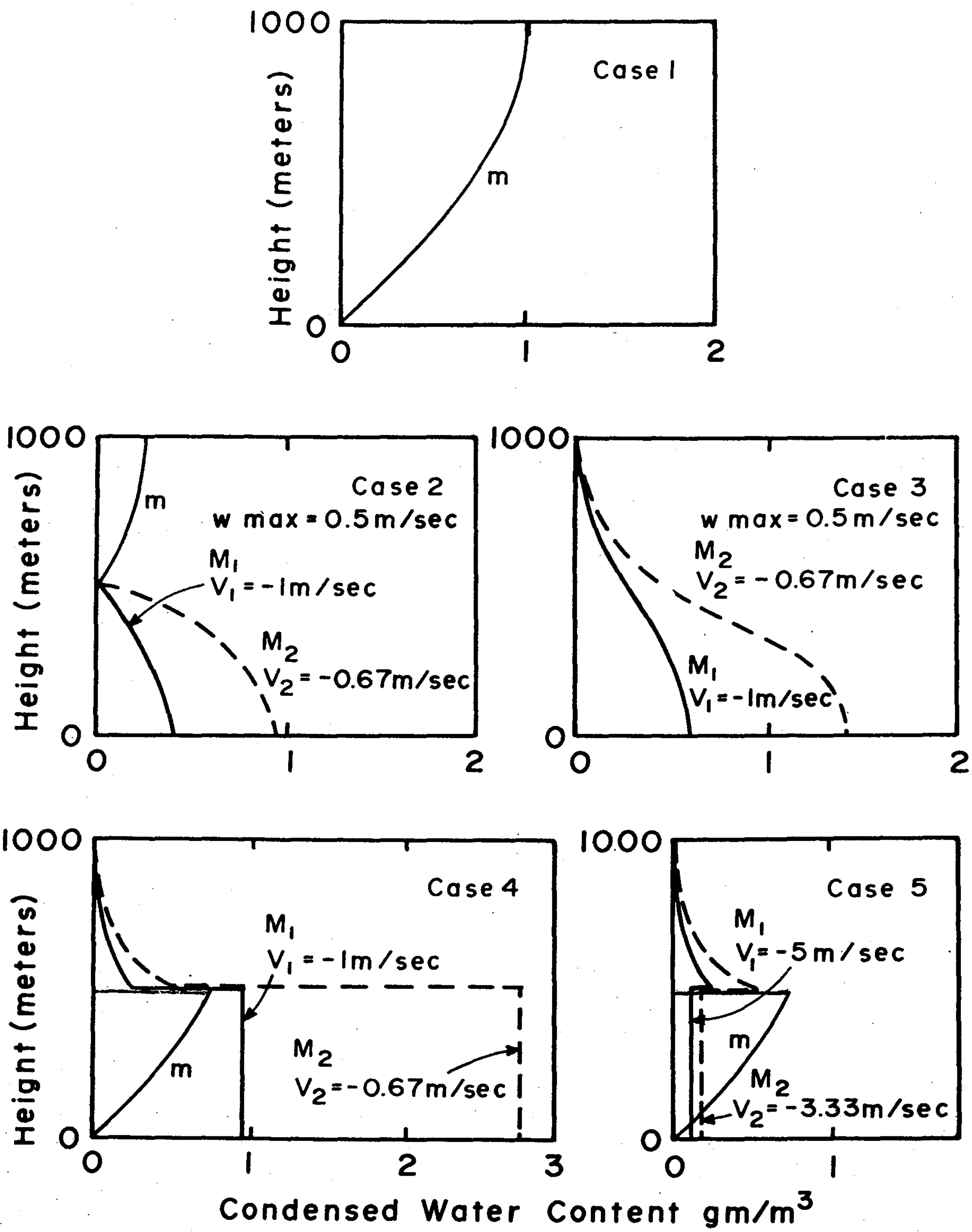

Figure 3. - Steady-state profiles of cloud and precipitation for example extrema of microphysical processes.

Table 1
Cloud and precipitation distributions in idealized one-dimensional cases*

Case 1

z	m	w	M	R	$\int_0^z wGdz$
1	1.0	0	0	0	0
0.5	0.75	0.5	-	-	.11
0	0	0	0	0	.33

z		V_1	V_2	$w+V_1$	$w+V_2$	M_1	M_2	R_1	R_2
Case 2									
1	0.5	-	-	0	0	0	0	0	0
0.5	0	-	-	.5	0	0	0	0	0
0.5	0	-1	-.67	-.5	-.17	0	0	0	0
0	0	-1	-.67	-1	-.67	.38	.95	.38	.65
Case 3									
1	0	-1	-.67	-1	-.67	0	0	0	0
0.5	0	-1	-.67	-.5	-.17	.19	.49	.10	.08
0.5	0	-1	-.67	-.5	-.17	.19	.49	.10	.08
0	0	-1	-.67	-1	-.67	.57	1.42	.57	.95
Case 4									
1	0	-1	-.67	-1	-.67	0	0	0	0
0.5	0	-1	-.67	-.5	-.67	.19	.49	.10	.08
0.5	.75	-1	-.67	-.5	-.17	.94	2.73	.47	.46
0	0	-1	-.67	-1	-.67	.94	2.73	.94	1.82
Case 5									
1	0	-1	-.67	-1	-.67	0	0	0	0
0.5	0	-1	-.67	-.5	-.17	.19	.49	.10	.08
0.5	.75	-5	-3.33	-4.5	-2.83	.10	.16	.47	.46
0	0	-5	-3.35	-5	-3.35	.10	.16	.52	.54

*This table lists the values of m and M at z = 0, z = 500 m and z = 1000 m with updrafts $w = .002(z = .001z^2)$ for corresponding numbered cases discussed in the text. The values of w and $\int wGdz$ listed under Case 1 are the same for all the others. M_1 (gm. m.$^{-3}$) and R_1 (gm. m.$^{-2}$ sec.$^{-1}$) are the precipitation water content and rate in the case V_1 = -1m. sec.$^{-1}$ M_2 and R_2 apply to the case V_2 = -.67 m. sec.$^{-1}$

Case 2. Cloud conversion is zero above the level of nondivergence; below, there is precipitation without cloud. The conditions of this case imply that precipitation is absent at high levels and that the cloud condensed there is lost by divergence. At low heights, cloud is immediately converted to precipitation.

In this and following cases, the parabolic updraft distribution

$$w = \frac{4w_{max}}{H}\left(z - \frac{z^2}{H}\right) \qquad \begin{array}{l} 0 \le z \le H \\ H = 10^3 \text{ meters} \end{array} \tag{24}$$

is assumed. The level of nondivergence in this model distribution is at $z = H/2$. Then Eq. (23) with $z_1 = H/2 = 500$ m, and $m(z_1) = 0$ describes the distribution of m above the level of nondivergence. For the distribution of M below that level, we have immediately from (22)

$$M(z_1) = M(z_2) - \int_{z_1}^{z_2} \frac{wG}{w+V}\, dz \quad , \tag{25}$$

where $M(z_2) = 0$, $z_2 = H/2 = 500$ m, and $0 \le z_1 \le H/2$. This integral has been evaluated for $V = -1$ m/sec. and $V = -0.67$ m/sec. and the profiles of m and M are shown in figure 3 (left-center). The cloud and precipitation parameters are also given in Table 1. (The analytical solution of Eq. (25) is given in [18].)

Case 3. The cloud conversion and collection terms are large everywhere and all condensate appears immediately as precipitation. This is the cloudless case discussed elsewhere in detail [18, 19, 20]. For constant V, as noted above, the steady surface precipitation rate at updraft cores always exceeds the vertically integrated condensation rate. The profiles for this case shown in figure 3 (right midheight), and tabulated in Table 1, are derived from Eq. (24) and (25) with $z_2 = H = 10^3$m., $0 \le z_1 \le H$; $M(z_2) = 0$, and two values for V, $V = -1$ m. sec.$^{-1}$ and $V = -0.67$ m. sec.$^{-1}$

Case 4. Above the level of nondivergence cloud is nonexistent; the cloud at each height below equals the total condensation in saturated air risen from the surface. This case implies a distribution of microphysical effects which is opposite from Case 2. As discussed in Section 3, the present case is the condition of maximum precipitation rate at the updraft base for specified fall speed and maximum updraft. In this case the profiles of M from $z = H$ to $z = H/2$ are developed independently of precipitation below $z = H/2$, and the profile of m at low heights is the same as that calculated in Case 1 above.

The calculation of the M profile through the level of nondivergence (where the collection efficiency is assumed to be discontinuous) is based on conservation of water substance. At this level, precipitation M falling at speed V + w collects all cloud m rising at speed w. Because conditions are steady, net transport of cloud and precipitation immediately above and below this level must be equal, i.e.,

$$(mw)_{below} + M(V + w)_{below} = (mw)_{above} + M(V + w)_{above} \,. \quad (26)$$

In this case, it is assumed that $m_{above} = 0$ and $V_{above} = V_{below}$; continuity demands also that $w_{above} = w_{below}$. With these conditions and the numerical values assumed or calculated from Eqs. (23), (24), and (25), Eq. (26) gives the numerical value of M_{below} which is constant between the level of nondivergence and the ground because the condensation process in the lower layer is assumed to contribute only to cloud. Note that although M is constant between the level of nondivergence and the ground, the precipitation rate R must increase following the descent of M because of horizontal convergence. From another point of view, note that the precipitation rate at any level is defined by

$$R = -M(V + w) \,. \quad (27)$$

Since V and w have opposite signs, the magnitude of R increases as w decreases to zero at the ground, following the descent of constant M. Profiles of M and m in this Case 4 are illustrated in figure 3 (left bottom) and tabulated in Table 1.

Case 5. This is the same as Case 4 except that a five fold increase of precipitation falling speed occurs at the level of nondivergence. A discontinuous change of V approximates the fall speed changes that commonly occur at the melting level. The precipitation content M below the level of nondivergence as determined from Eq. (26), is much smaller than in Case 4 (see figure 3, right bottom). The increased fall speed in the lower layer tends to minimize the effects of horizontal convergence, and the surface precipitation rates are also greatly reduced from those of Case 4, as can be seen in figure 3 and by comparison of tabulated values in Table 1. The mechanism associated with reduction of precipitation rate at an updraft center due to increasing falling speed following the descent of M is schematically illustrated by figure 5 in [18].

In summary, for the five cases treated above, note that the tabulated values show steady-state surface precipitation rates from zero to five times the vertically integrated condensation rates. Although the ratios of precipitation fall speed to updrafts in these examples are small compared to those that commonly occur in widespread precipitation, and the precipitation rate is, therefore, exaggerated, the role of the microphysical processes is obviously significant. In any case, of course, excesses or deficiencies of the surface precipitation rate at updraft centers compared to the condensation there are compensated by precipitation rates elsewhere, and by divergence of condensed water at various heights in the atmosphere.

6. MODELS OF MICROPHYSICAL PARAMETERS

A. Condensation and Evaporation of Cloud

As discussed in Section 2B above, Eq. (9) provides model condensation of cloud in rising saturated air, and evaporation of cloud in descending saturated air at the rates $wG = w\rho(\partial Q_s^{\prime}/\partial z)$, where w is the vertical air velocity, ρ is air density, and $Q_s^{\prime}$ is the saturation mixing ratio of water in air. In this study, a parabolic vertical profile of w (Eq. 24), and a linear decrease of G with height are assumed. Figure 4 shows how the total condensation rate in a model tropical atmosphere varies with the height H of the updraft column, when the base is at sea level, and the maximum vertical velocity is 1 m./sec.

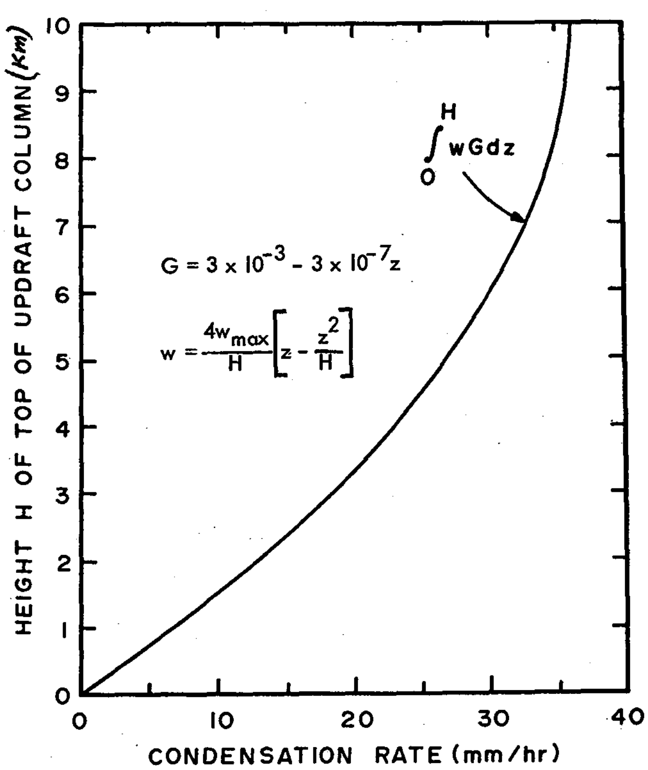

Figure 4. - Condensation rate in model saturated updrafts, parabolically distributed with height from z = 0 to H. The maximum updraft speed is 1 m./sec., and the condensation function $G = 3 \times 10^{-3} - 3 \times 10^{-7}z$ (gm.m.$^{-4}$), is representative of a tropical atmosphere.

B. The Conversion of Cloud

Implicit in Eq. (9) is the assumption that cloud shares the motion of the air, i.e., that the fall speed of cloud particles relative to the air is zero. Actually, cloud particles are distributed among small sizes and fall speeds; the cloud water content and particle distribution are of fundamental importance to the growth by coalescence of larger particles to precipitation size. In cold clouds, the presence of a few deposition nuclei among a large population of undercooled water drops favors the growth of snow crystals by a diffusion process at the expense of the liquid phase ([15], for example). The present interest, however, is to model the conversion of cloud to precipitation for the purpose of estimating the role of the rate of conversion for the development of precipitation and cloud profiles.

Everyday experience shows that there are occasions when water clouds persist for a long time without evidence of precipitation. On the other hand, various measurements show that cloud amounts greater than about 1 gm. m.$^{-3}$ are usually associated with production of precipitation [1, 29, 41, 45]. It seems reasonable to model nature in a system where the rate of cloud conversion increases with the cloud content, but is zero for amounts below some threshold. Such a process is defined by

$$\frac{dM}{dt} = -\frac{dm}{dt} = k_1(m - a), \qquad \begin{array}{l} k_1 > 0 \text{ when } m > a \\ k_1 = 0 \text{ when } m < a \end{array} \tag{28}$$

where a is the threshold value below which cloud conversion does not occur. Various effects of nature and cloud seeding can be represented by choices of k_1 and a.

C. The Drop Size Distribution in Precipitation

Observations of rain at the earth's surface by Marshall and Palmer [28] have shown that the drops are size-distributed in approximate accord with an inverse exponential law. The present study assumes that the distribution of precipitation particles has this same form throughout the depth of the updraft column, viz.,

$$N = N_0 e^{-\lambda D} \delta D \tag{29}$$

where N is the number of rain drops per unit volume of air in the diameter range δD. Thus, the effects of gravity and microphysical processes, insofar as they change the form of the distribution, are neglected.

The total number N_t of particles per unit volume in this distribution is given by integrating (29) over all diameters:

$$N_t = \int_0^{\infty} N_0 e^{-\lambda D} dD = \frac{N_0}{\lambda} \quad . \tag{30}$$

The total mass of precipitation per unit volume in the distribution represented by (29) is given by multiplying by the mass of one particle of diameter D and integrating over all diameters,

$$M = \int_0^{\infty} \frac{\pi \rho_\ell}{6} D^3 N_0 e^{-\lambda D} dD = \frac{\pi}{6} \rho_\ell N_0 \frac{\Gamma(4)}{\lambda^4} \quad , \tag{31}$$

where ρ_ℓ is the density of liquid water (or of snow or ice if the particles are so constituted), and $\Gamma(4) = 6$. In the gm. - meter - second system adopted for this study $\rho_\ell = 10^6$ gm. m.$^{-3}$ and

$$\lambda = 42.1 N_0^{0.25} M^{-0.25} \quad . \tag{32}$$

The parameter λ is also conveniently related to the median volume diameter D_0, the diameter which divides the distribution into parts of equal water content. Expand $e^{-\lambda D}$ in power series:[4]

$$e^{-\lambda D} = 1 - \lambda D + \frac{\lambda^2 D^2}{2!} - \frac{\lambda^3 D^3}{3!} + \cdots \quad . \tag{33}$$

The integral (31) over a range $0 \le D \le D_0$ is by definition M/2. We have

$$\boxed{\frac{D_0^4}{4} - \frac{\lambda D_0^5}{5} + \frac{\lambda^2 D_0^6}{6 \cdot 2!} - \frac{\lambda^3 D_0^7}{7 \cdot 3!} + \ldots = \frac{1}{2} \frac{\Gamma(4)}{\lambda^4}} \quad . \tag{34}$$

The solution of (34) is readily obtained numerically and has been presented by Atlas [3] and others: $\lambda = 3.67/D_0$. Eq. (29) can be rewritten:

[4] Integration of equations like (31) is straightforward without power series, when the exponent to D is an integer, as in this case.

$$N = N_0 \left(\exp - \frac{3.67D}{D_0} \right) \delta D \qquad (35)$$

where, from consideration of (32),

$$D_o = .087 N_o^{-.25} M^{.25} \text{ meters} \quad . \qquad (36)$$

For a particular M the parameter N_o determines the relative number of small drops in the distribution. The order of magnitude of N_o in natural rains is about $10^7 m^{-4}$, and is only slowly variable over a wide range of M [28]. Thus the number of large drops increases substantially with the precipitation content.

D. The Fall Speed of Precipitation

The vertical motion relative to the air of size-distributed rain drops is given by the parameter V in Eq. (8). Insofar as the vertical advection of precipitation is concerned, a basic assumption of this study is that the precipitation moves as though all the particles fall at the same speed V_o, the terminal velocity of the median diameter particle. The expression

$$V = -130\, D^{1/2} \text{ m./sec.} \qquad (37)$$

after Spilhaus [43], is accurate to within about 10% for drop diameters greater than about .9 mm. Use (37) to substitute for D_o in (36). Then

$$V_o = -38.3\, N_o^{-.125} M^{.125} \text{ m./sec.} \qquad (38)$$

V_o varies only very slowly with the shape parameter N_o and with the total precipitation content M.

E. The Rainfall Rate

The rain falling out of a circulating air mass is the most essential feature of the water budget. Where the updraft w is zero, as is the case at the ground, the rainfall rate R is

$$R = MV \text{ gm. m.}^{-2} \text{ sec.}^{-1} \tag{39a}$$

$$R = 3.6MV \text{ mm. hr.}^{-1} \tag{39b}$$

Substitute Eq. (38) into Eq. (39b) to obtain

$$R = 138\ N_o^{-.125}\ M^{1.125} \text{ mm./hr.} \tag{40}$$

When $N_o = 10^7\ m^{-4}$,

$$R = 18.35\ M^{1.125} \text{ mm./hr.} \quad (w = 0) \quad . \tag{41}$$

F. The Radar Reflectivity Factor of Precipitation

The radar reflectivity factor is the summation of drop diameter sixth powers, i.e.,

$$Z = \int_0^{\infty} N_0 e^{-\lambda D} D^6\, dD = N_0 \frac{\Gamma(7)}{\lambda^7} = 720 \frac{N_0}{\lambda^7} \tag{42}$$

Substitution from Eq. (32) yields

$$Z = 3.2 \times 10^{-9}\ N_o^{-.75} M^{1.75} (\text{meters}^3) \tag{43a}$$

$$Z = 3.2 \times 10^{+9}\ N_o^{-.75} M^{1.75} (\text{mm.}^6\ \text{m.}^{-3}) \quad . \tag{43b}$$

The units shown in (43b) are those usually used by radar-meteorologists. When $N_0 = 10^7$ m.$^{-4}$

$$Z = 1.8 \times 10^4\ M^{1.75} \text{ mm.}^6/\text{m.}^3 \quad . \tag{44}$$

Equations (40) and (44) can be combined and M eliminated to give

$$Z = 197R^{14/9} \quad , \tag{45a}$$

where Z is in mm.^{6}/m.^{3} and R is in mm./hr. The coefficient is close to 200 accepted as a standard by many authors.

Instead of (39b) and (38), we can, as in [23], use the following more precise equation to define rainfall rate,

$$R = \int_0^\infty NMV\,dD = \int_0^\infty (N_0 e^{-\lambda D})\left(\frac{\pi\rho}{6} D^3\right)(130\, D^{\frac{1}{2}})\,dD \quad . \tag{39c}$$

This implies that

$$Z = 210\ R^{14/9} \quad . \tag{45b}$$

The difference between (45a) and (45b) is due to the nonlinear relationship between drop mass and fall speed.

G. Collection of Cloud by Rain

The rate at which volume is swept out by one precipitation particle of diameter D_i falling at speed V_i is $-\pi D_i^2 V_i/4$ (where $V_i < 0$) and the rate of accumulation of cloud by a single precipitation particle is

$$\frac{\delta M_i}{\delta t} = -\frac{\pi D_i^2}{4} E_i V_i m \quad , \tag{46}$$

where E_i is the average efficiency with which the cloud particles of total mass m per unit volume, are caught.

The rate of growth of the liquid water content M for the entire distribution of precipitation particles is given by substitution of (37) into (46) and integration over all the particles, i.e.,

$$\frac{dM}{dt} = \int_0^\infty \frac{\delta M}{\delta t} N\,dD = \int_0^\infty \frac{130\pi E N_0 m}{4} D^{2.5} e^{-\lambda D}\,dD \quad . \tag{47}$$

If E is independent of D

$$\frac{dM}{dt} = 6.96 \times 10^{-4} \, E N_o^{.125} \, m M^{.875} \quad . \tag{48}$$

The appearance of N_o to the one-eighth power in Eqs. (38) and (48) indicates that variations of the shape of precipitation particle distributions must be quite large to affect the course of precipitation development significantly. This situation changes slightly if the collection efficiency is a function of D. The integral in Eq. (46) has been studied for the functions

$$E = E_\infty (1 - e^{-\gamma D}) \tag{49a}$$

and

$$E = E_o e^{-\gamma D} \tag{49b}$$

which have interest in connection with both natural precipitation and attempts to modify the collection efficiency artificially. Eq. (49a) is associated with even less dependence of the rate of cloud collection on N_o than constant E. For Eq. (49b), however, the shape parameter N_o is important when γ is large.

Hardy [14] has summarized the data of several investigators. The collection efficiency of raindrops larger than .5 mm. in diameter, for cloud drops larger than 15μ in diameter, is between .8 and 1 and varies only slowly with the rain and cloud drop diameters. The collection efficiency of small raindrops for smaller cloud drops is less and is size dependent. Although these data suggest that Eq. (48) with constant E, is a fair first approximation to the accretion process, there is evidently need for more comprehensive treatment of the development and motion of raindrop size distributions accompanying accretion (Berry [6], for example).

H. Evaporation of Rain

A simple form for the evaporation term in Eqs. (8) and (9) is obtained by modeling Kinzer and Gunn's expression, tabulated in the Smithsonian Tables ([42], Table 117); this describes the rate of change of mass of a freely falling water drop:

$$\frac{\delta M_i}{\delta t} = \left[4\pi a \left(1 + \frac{Fa}{s} \right) \right] \left[D(\rho_a - \rho_b) \right] \text{g/sec} \quad . \tag{50}$$

In Eq. (50), a is the drop radius, s is the equivalent thickness of the transition shell outside the drop, F is a dimensionless factor, D is the coefficient of diffusion, ρ_a is the saturation vapor density at the surface of the drop, and ρ_b is the vapor density of the environment.[5] Kinzer and Gunn's tabulations of the first bracketed term are nearly independent of ambient temperature and are fitted to an accuracy of about ±20% by

$$4\pi a\left(1 + \frac{Fa}{s}\right) = 2.24 \times 10^3 \, D^{1.6} \text{ meters} . \tag{51}$$

where D is now the drop diameter in meters.

The second bracketed term in Eq. (50) is a nearly linear function of the relative humidity, and is also temperature dependent. However, Table 108 in Smithsonian Meteorological Tables shows that this term can be related linearly to the saturation deficit $m < 0$ in Eq. (7) to an accuracy of about ±25%:

$$D(\rho_a - \rho_b) = 10^{-5} m \text{ (grams m.}^{-1}\text{sec.}^{-1}\text{)} . \tag{52}$$

Combination of Eqs. (51) and (52) yields a relatively simple expression for the rate of evaporation of a single drop, accurate within about ±40% for most diameters, ambient temperatures, and humidities:

$$\frac{\delta M_i}{\delta t} = 2.24 \times 10^{-2} m D^{1.6} \text{ gm/sec} . \tag{53}$$

The greatest errors in Eq. (53) occur, of course, when the error of the two terms combined in it are in the same direction. When (53) is integrated over all diameters in an assumed size-distribution, the net error is reduced by combination of errors of opposite sign associated with various particle sizes. The rate of change due to evaporation of the water content in the entire distribution of precipitation particles is approximately:

$$\frac{dM}{dt} = 2.24 \times 10^{-2} N_0 m \int_0^{\infty} e^{-\lambda D} D^{1.6} dD \tag{54}$$

---

[5] This equation and Eqs. (51) and (52) use notation of Kinzer and Gunn. Elsewhere in this report, a is the cloud conversion threshold (see Section 6A above) and D is the drop diameter.

or, with Eq. (32),

$$\frac{dM}{dt} = 1.93 \times 10^{-6} N_o^{.35} mM^{.65} \quad . \tag{55}$$

N_o constant in Eq. (55) does some additional violence to the physics, since the evaporation process actually decreases the relative number of small drops.

I. Summary

The mathematical representations of microphysical parameters and processes considered in this section are tabulated in Table 2 and illustrated in figure 5.

Table 2. - Mathematical models of microphysical parameters

Microphysical process	Mathematical representation	Factors most used in this study
Condensation and evap. of cloud	$\frac{4w_{max}}{H}(z - \frac{z^2}{H})(A+Bz)$gm.m.$^{-3}$sec.$^{-1}$	$A = 3\times10^{-3}$gm.m.$^{-4}$ $B = -3\times10^{-7}$gm.m.$^{-5}$ $H = 6\times10^{3}$ meters
Autocnvrsn of cloud	$k_1(m - a)$gm.m.$^{-3}$sec.$^{-1}$	$k_1 = 10^{-3}$sec.$^{-1}$ $a = 0.5$ gm.m.$^{-3}$
Median Volume diameter raindrop	$.087\ N_o^{-.25}\ M^{.25}$ meters	$N_o = 10^7$ m^{-4} $N_o^{.125} = 7.50$
Fall speed of rain	$38.6\ N_o^{-.25}\ M^{.125}$ m./sec.	$N_o^{-.35} = 282$
Rainfall rate at the ground	$38.3\ N_o^{-.125}M^{1.125}$gm.m.$^{-2}$sec.$^{-1}$ $138\ N_o^{-.125}M^{1.125}$mm.hr.$^{-1}$	$N_o^{-.125} = .133$ $N_o^{-.25} = .0178$
Radar reflectivity of precipitation	$3.2 \times 10^9 N_o^{-.75}M^{1.75}$mm.^{6}/m.^{3}	$N_o^{-.555} = 1.29\times10^{-4}$ $N_o^{-.75} = 5.63\times10^{-6}$
Accretion of cloud by rain	$6.96\times 10^{-4}EN_o^{.125}mM^{.875}$gm.m.$^{-3}$sec.$^{-1}$	$E = 1$
Evaporation of rain	$1.93\times10^{-6}N_o^{.35}mM^{.65}$gm.m.$^{-3}$sec.$^{-1}$	

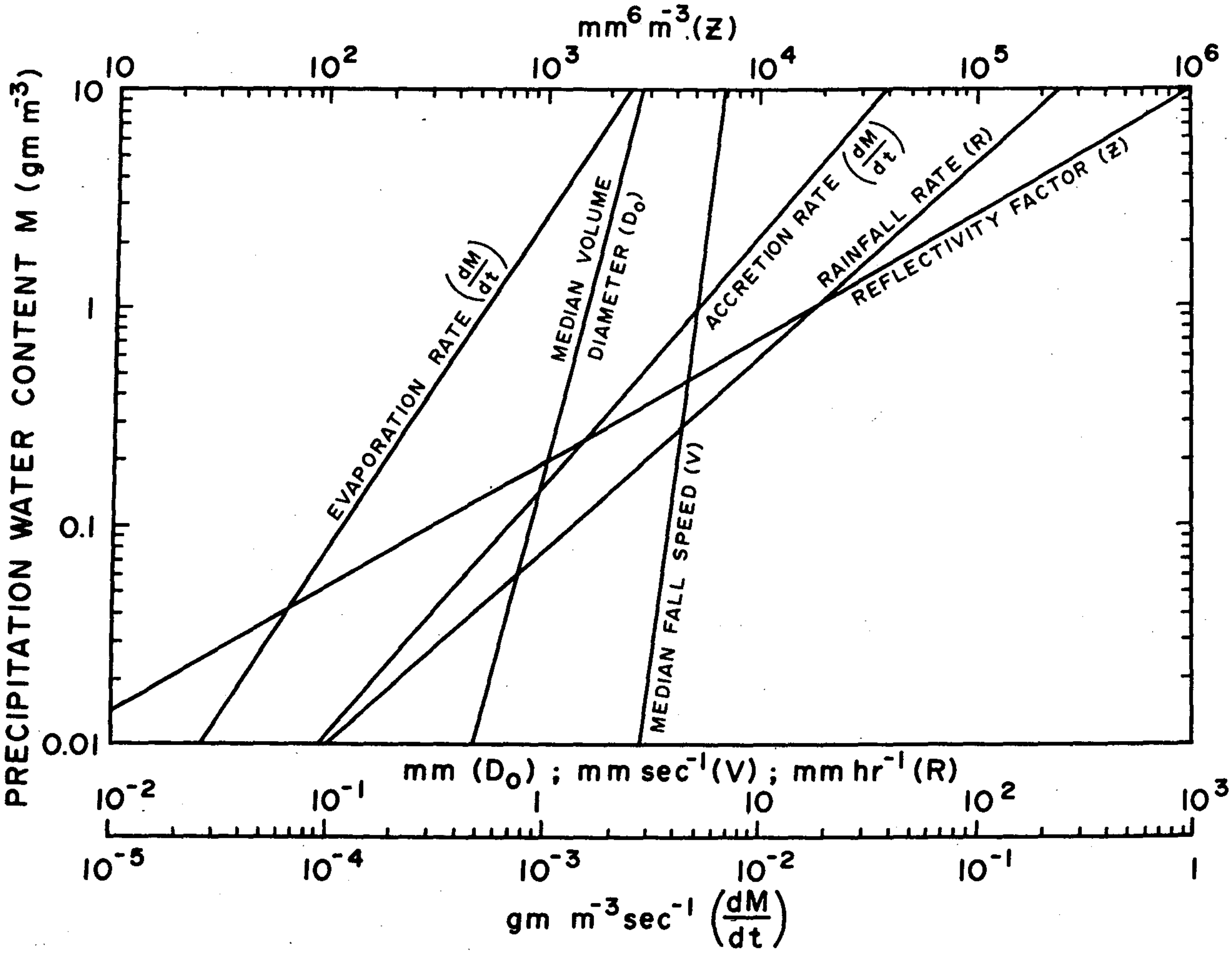

Figure 5. - Graphical representation of microphysical parameters in the model. Accretion and evaporation rates apply with 1 gm. m.$^{-3}$ cloud content and saturation deficit, respectively, and all curves are based on $N_o = 10^7$ m.$^{-4}$. See Table 2.

Substitution of the expressions in Table 2 into Eqs. (8) and (9) leads to Eqs. (8a) and (9a) which describe in density units the response of the water content of air to the air motions and microphysical processes.

The following principal assumptions are implicit in this system.

(1) Cloud is condensed water that fully shares the air motion.

(2) Cloud forms in rising saturated rising air, and evaporates in saturated descending air at the rate $w(A + Bz) = -w\rho(dQ_s/dz)$, where Q_s' is the saturation mixing ratio of water in air. Air containing cloud is always saturated, and unsaturated air never contains cloud.

(3) Cloud changes to raindrops distributed in size according to an inverse exponential distribution at the rate $k_1(m - a)$, where the magnitude of k_1 and a may be selected to simulate various processes and rates.

(4) Precipitation particles once formed are assumed to be distributed in size according to an inverse exponential law and to collect cloud particles or evaporate in subsaturated air according to approximations to the natural accretion and evaporation processes.

(5) Precipitation shares the horizontal motion of the air but the vertical mass transport of precipitation is based on the fall speed of the median diameter precipitation particle. The change of shape of a distribution by virtue of differing fall speeds within it, and by evaporation, condensation, and accretion processes is omitted.

$$\frac{\partial M}{\partial t} = -u\frac{\partial M}{\partial x} - v\frac{\partial M}{\partial y} - w\frac{\partial M}{\partial z} + 38.6\, N_0^{-0.125}\frac{\partial}{\partial z} M^{1.125} + Mw\frac{\partial \ln \rho}{\partial z}$$
$$+ k_1(m-a) + k_2 E N_0^{0.125} m M^{0.875} + k_3 N_0^{0.35} m M^{0.65} \tag{8a}$$

$$\frac{\partial m}{\partial t} = -u\frac{\partial m}{\partial x} - v\frac{\partial m}{\partial y} - w\frac{\partial m}{\partial z} + w(A+Bz) + mw\frac{\partial \ln \rho}{\partial z}$$
$$- k_1(m-a) - k_2 E N_0^{0.125} m M^{0.875} + k_3 N_0^{0.35} m M^{0.65} \tag{9a}$$

k_1 = constant (usually 10^{-3} in this paper) when $m > a$, otherwise $k_1 = 0$.

$k_2 = 6.96 \times 10^{-4}$ when $m > 0$; otherwise $k_2 = 0$.

$k_3 = 1.93 \times 10^{-6}$ when $m < 0$; otherwise $k_3 = 0$.

7. A MODEL OF THE ONSET OF PRECIPITATION

Consider the cloud conversion and accretion terms as they appear in Table 2 and in Eqs. (8a) and (9a), operating in a deep model cloud of uniform water content m without vertical air motion. The cloud is assumed to change to precipitation everywhere at the same rate and the advection terms due to the vertical gradient of precipitation therefore vanish. In these circumstances the equations describing the amounts of cloud and precipitation are

$$\frac{dM}{dt} = - \frac{dm}{dt} = k_1(m - a) + k_2 m M^{.875} \tag{56}$$

$$k_1 > 0 \text{ when } m > a$$

$$k_2 > 0 \quad (k_2 = 6.96 \times 10^{-4} EN_o^{\ .125}) \ .$$

Since there is no vertical motion and the condensation process is inactive, the following condition must be satisfied:

$$M + m = m_o, \quad 0 \le t \le \infty \quad , \tag{57}$$

where m_o is the amount of cloud when t = 0. If the exponent of M in (56) is changed from +0.875 to +1.0, exact integration is facilitated while the essential nature of the formulation is not altered. Then substitution of (57) into (56) with altered exponent yields

$$\frac{dM}{dt} = - \frac{dm}{dt} = k_1(m - a) + k_2 m(m_o - m) \ . \tag{58}$$

The interval t_a required for the cloud amount to decrease from the amount m_o to one half that amount is a convenient measure of the time of onset of precipitation.

$$t_a = \int_{m_o}^{m_o/2} \frac{dm}{k_2 m^2 - (k_1 + k_2 m_o) m + k_1 a} \ . \tag{59}$$

The integral of the right hand side depends on the sign of the discriminant $\mathcal{D}$ of the denominator; this can be shown to be positive.[6]

[6] The discriminant is $\mathcal{D} = k_1^2 + 2k_1k_2m_o + k_2^2m_o^2 - 4k_1k_2a$. That $\mathcal{D} > 0$ can be shown in the following way. Note first that k_1, k_2, m_o, and a are all positive. Therefore, the first three terms on the right-hand side are positive. Set $m_o = a$. If $\mathcal{D} > 0$ when $m_o = a$, it is obvious that $\mathcal{D} > 0$ when $m_o > a$. Thus, $\mathcal{D}(m_o = a) = k_1^2 + 2k_1 k_2 a + k_2 a^2 - 4k_1k_2a$ and $\mathcal{D}(m_o = a) = (k_1 - k_2a)^2$. Obviously the minimum value of the expression on the right-hand side is zero and $\mathcal{D}$ is, therefore, positive.

Then (60)

$$t_a = \frac{1}{\left[(k_1 + k_2 m_o)^2 - 4k_1 k_2 a\right]^{\frac{1}{2}}} \ln \frac{2k_2 m - (k_1 + k_2 m_o) - \left[(k_1 + k_2 m_o)^2 - 4k_1 k_2 a\right]^{\frac{1}{2}}}{2k_2 m - (k_1 + k_2 m_o) + \left[(k_1 + k_2 m_o)^2 - 4k_1 k_2 a\right]^{\frac{1}{2}}} \Bigg|_{m_o}^{m_o/2} .$$

Figure 6 shows the onset parameter t_a in relation to the conversion rate k_1, the initial cloud content m_o, and the accretion coefficient k_2, for the case where the conversion threshold $a = m_o/2$. Note that when $k_1 \gg k_2$, the time t_a is a very slowly varying function of k_2. And when $k_1 \ll k_2$, t_a is a very slowly varing function of k_1. In other words, if the coalescence (autoconversion) process among the many tiny cloud drops is relatively rapid, the collection of cloud by raindrops is of little consequence to the rate of depletion of cloud; and if the collection of cloud by rain is relatively rapid, then the magnitude of the rate of cloud conversion is not critical (so long as cloud conversion is more than zero). The design and analysis of experiments aimed at securing knowledge and control of processes which govern natural precipitation events needs to be considered in the light of this result.

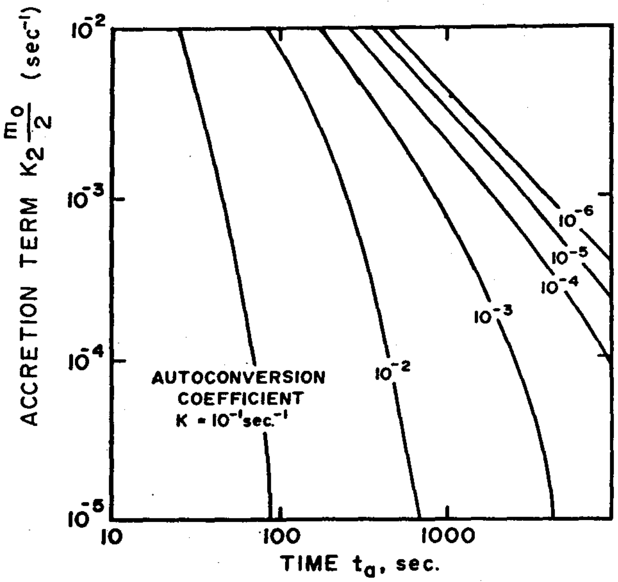

Figure 6. - Precipitation onset parameter t_a in relation to the accretion parameter $k_2 = 7 \times 10^{-4} E N_o^{.125}$ and autoconversion rate k_1. It is assumed that m_o=2a.

After cloud amounts are reduced by accretion to magnitudes below a, where autoconversion is zero, the further depletion of cloud is defined by the accretion process alone. When at t_a, M, m = $m_o/2$, we have at later times,

$$m = \frac{m_o}{1 + \exp[k_2 m_o (t - t_a)]} (\text{conversion threshold } a = \frac{m_o}{2}) \quad . \qquad (61)$$

Equations (60) and (61) define the curves in figure 7, which detail the time-dependent transfer of condensate from cloud to precipitation phases for three values of $(k_2/k_1)(m_o/2)$. Curves of the

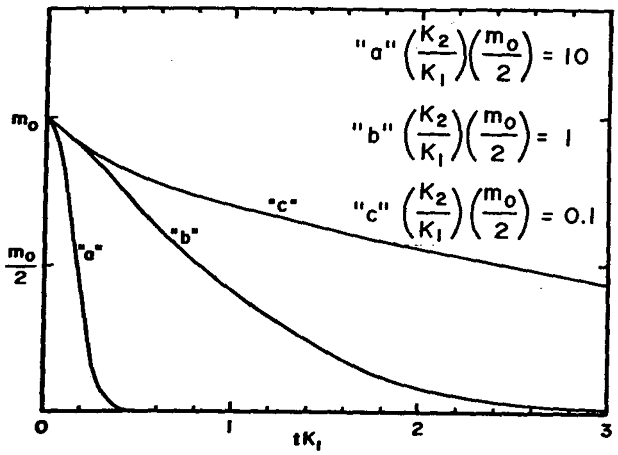

Figure 7. - The time-dependent decrease of cloud water accompanying precipitation development in a uniform model cloud of infinite vertical extent. The starting cloud content is m_o. k_1 is the rate of autoconversion to precipitation by cloud in excess of $m_o/2$, and k_2 is the accretion parameter.

precipitation content mirror those of m in figure 7; they start at M = 0 and asymptotically approach m_o as time increases.

The present model is a crude one and does not provide new basic knowledge concerning the microphysical processes affecting precipitation production. Rather, we here seek to model what is already known about precipitation formation and to learn more about how the macrophysical aspects of precipitation distributions are related to the strength of microphysical processes.

In figure 6, the region $10^{-3} < k_2 m_o/2 < 10^{-2}$ holds special interest because it is here that some empirical data are reasonably represented. For example, where $k_2 m_o/2 = 5 \times 10^{-3}$ we can have $a = 1.0$ gm. m.$^{-3}$, $m_o = 2$ gm. m.$^{-3}$, E = 1, and $n_o = 10^7$ m^{-4}. The k_1's illustrated in the figure imply onset times ranging from about one minute to one hour. In most of the following sections the value $k_1 = 10^{-3}$ sec.$^{-1}$ is used, indicating an onset time of about 8 minutes for other representative parameters.

8. NUMERICAL DETERMINATION OF VERTICAL PROFILES OF CLOUD AND PRECIPITATION

A. Relationships between Microphysical Parameters and the Onset of Precipitation

The one-dimensional forms of Eqs. (8a) and (9a) for an incompressible atmosphere have been solved by a digital computer, programmed to use the finite difference scheme discussed in Appendix B. In the examples here, the initial condition is everywhere saturation without cloud or precipitation. The updraft distribution is defined by Eq. (24) with H = 6 km.; the collection efficiency E = 1, and $N_o = 10^7$ m^{-4}, except where otherwise indicated. The generating function $G = 3 \times 10^{-3} - 3 \times 10^{-7} z$ gm. m^{-4}, is representative of the tropical troposphere. This section discusses the role of the model microphysical parameters in shaping the onset of precipitation.

(1) The conversion threshold a

The model provides that conversion of cloud to precipitation does not start until the cloud content produced in saturated updrafts has exceeded the magnitude a. Thereafter, cloud responds to its accretion by relatively large precipitation particles, in addition to processes of vertical advection and condensation. Often in the model, the amount of cloud which can coexist in equilibrium with accretion by precipitation is less than the amount required to initiate precipitation. When this is the case, the time dependent solutions for cloud and precipitation are characterized by an initial pulse whose magnitude increases with the difference between the equilibrium precipitation content and the magnitude of the conversion threshold a, as illustrated in figure 8. The precipitation pulse or gush represents the rapid deposition of condensation products accumulated as cloud over a relatively long time period.

The real atmosphere's analogue to the conversion threshold can be height dependent. In some circumstances, for example, precipitation may be quickly initiated by the ice crystal process above the melting level, while denser cloud persists below. Or, we can conceive that a paucity of deposition nuclei may cause the reverse to be true. The influence of height variations of the conversion threshold on precipitation onset is illustrated in figure 9. The magnitude of the initial pulse of precipitation is particularly large when the conversion threshold is large in

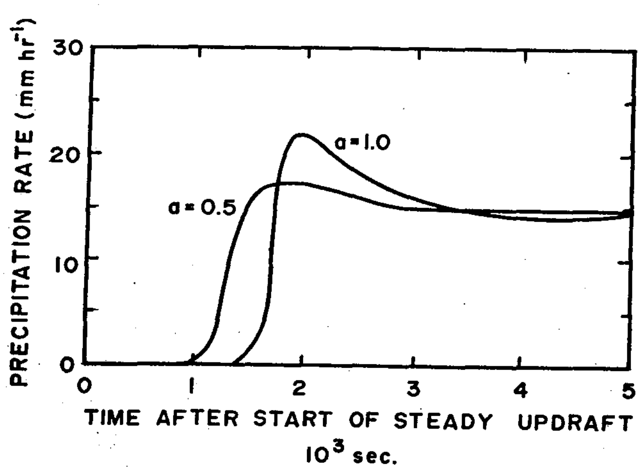

Figure 8. - Precipitation transients in relation to the cloud conversion threshold parameter a. The atmospheric model considers a saturated updraft column 6 km. deep with maximum vertical velocity .5m/sec., and other parameters given in Table 2.

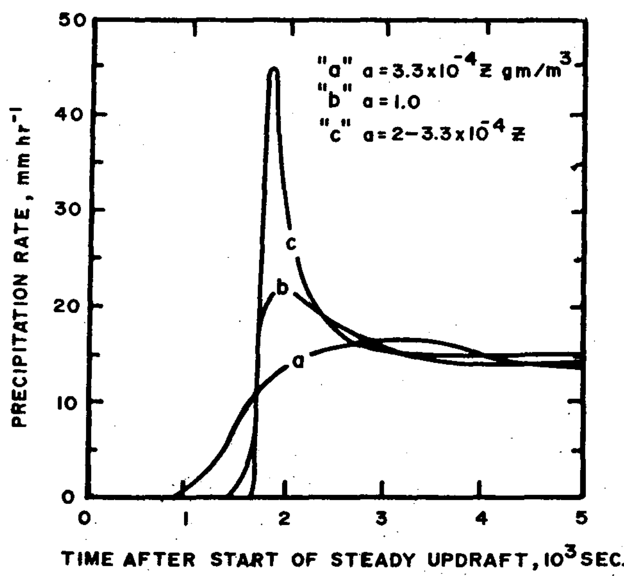

Figure 9. - Precipitation transients in relation to height variations of the parameter a. Curves c and a are associated with initial precipitation formations near cloud top and base, respectively. Curve b also appears in figure 8.

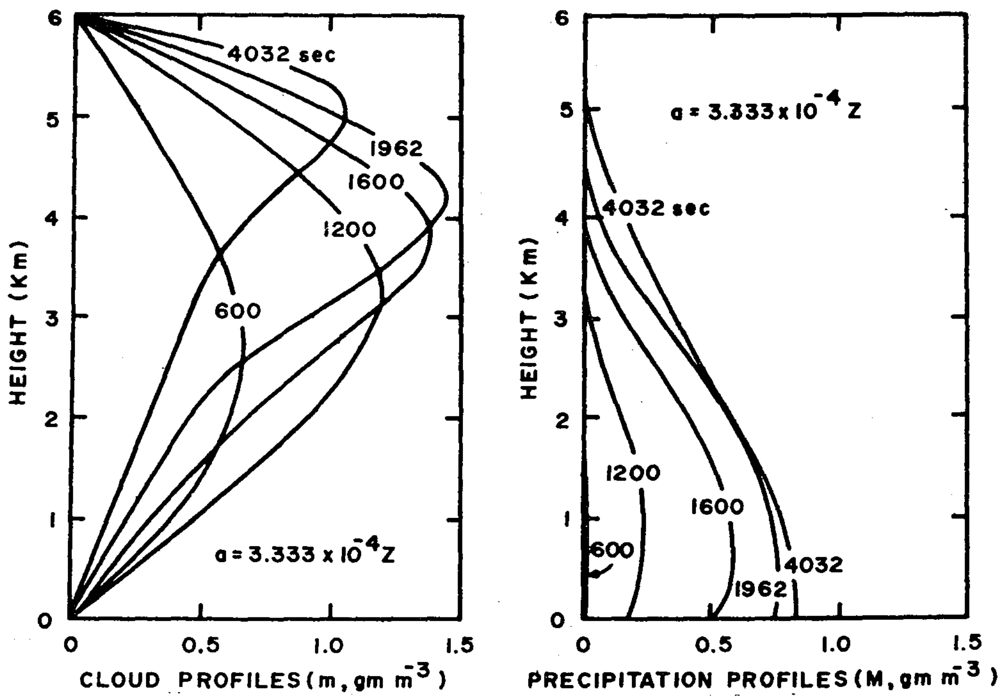

Figure 10. - Cloud and precipitation profiles at different times after the start of steady updrafts in a saturated air column, where precipitation forms first in the cloud base. See Curve "a" in figure 9.

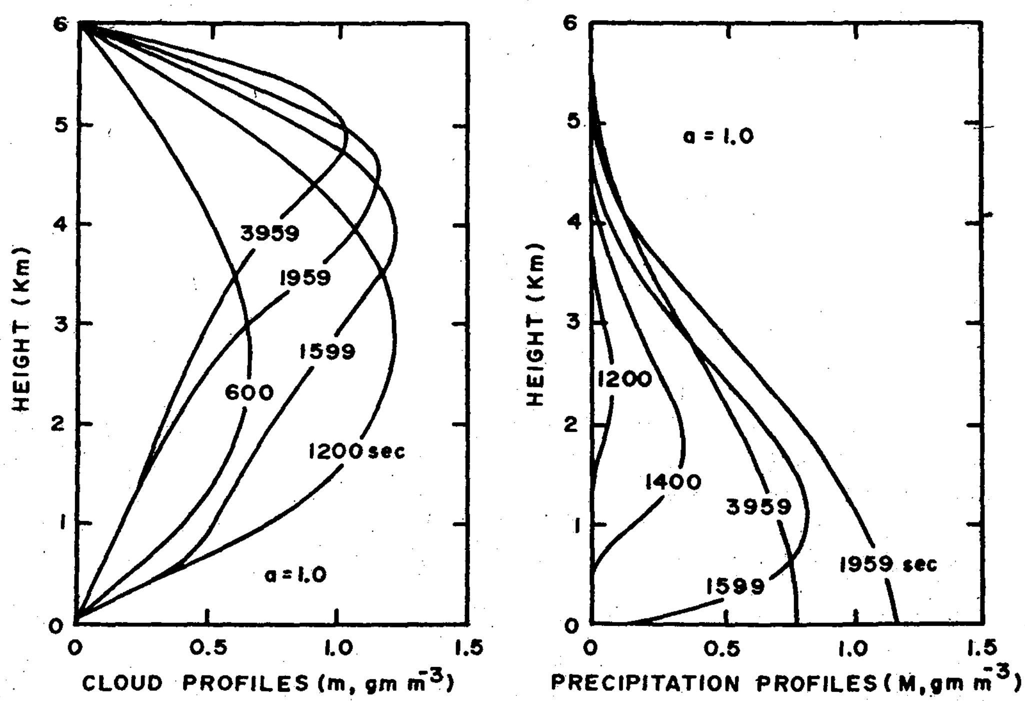

Figure 11. - Profiles of cloud and precipitation associated with curve "b" in figure 9.

low levels and decreases with height. In such cases, the autoconversion process is absent at low altitudes, and cloud there becomes dense and contributes through the accretion process to the development of the initial precipitation which originates at higher levels. The various interactions between cloud and precipitation development implied by different distributions of the conversion threshold are illustrated by the vertical profiles of precipitation and cloud in figures 10, 11, and 12. Vertical profiles are discussed in detail in Section 8B, below.

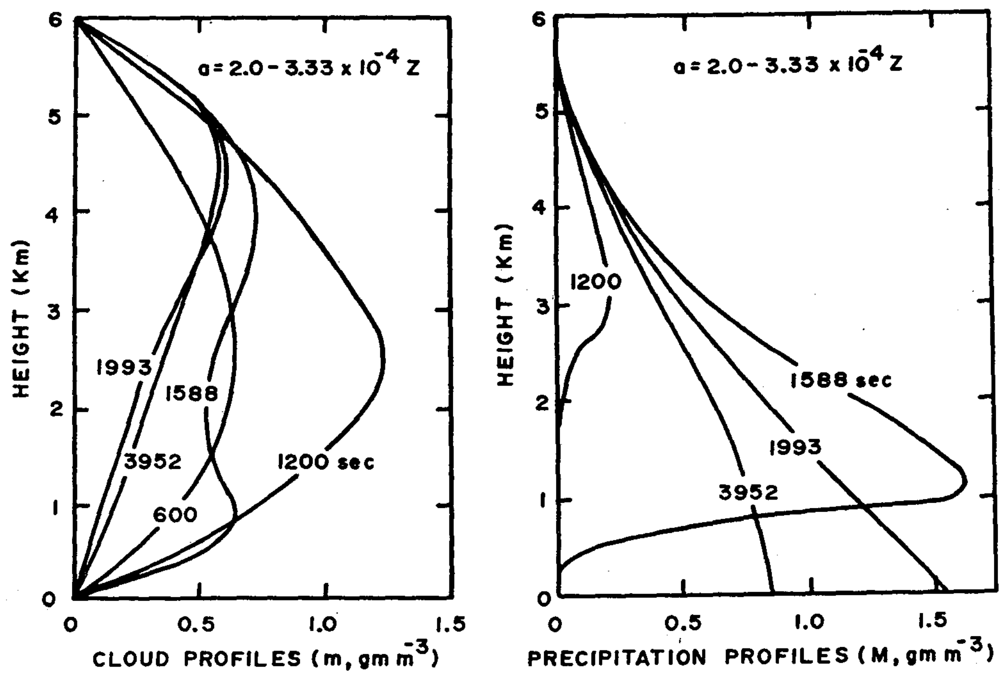

Figure 12. - Profiles of cloud and precipitation associated with curve "c" in figure 9.

Fluctuations of precipitation rate during showers have been associated with updraft variations and electrical effects [30]. The present analysis shows that rain gushes, marking the onset of showery precipitation, might occur in a model system embracing only continuity and simplified formulations of the microphysical processes. It should be recognized, however, that dynamical implications of the varied water distributions are not considered here, and that electrical effects are implicit in the model microphysical processes. (See also [22], [38].)

(2) The cloud conversion rate k_1

In the model, the parameter k_1 is the rate of autoconversion to precipitation of cloud content in excess of the conversion threshold a. When k_1 is large, the approach to a steady-state condition is expedited after m exceeds a; when k_1 is small, the cloud content continues longer to increase in the updrafts after precipitation starts (especially if the accretion process is also weak). Thus the height of a pulse-shaped transient near the start of precipitation is enhanced as the value of k_1 decreases. This is illustrated for three values of k_1 in figure 13. Nearly the same steady state is ultimately approached in all these cases because the cloud content in equilibrium with precipitation for the indicated choice of parameters is less than the conversion threshold at most levels, and the magnitude of k_1 (as that of a) is, therefore, rather unimportant after the steady-state condition in these cases has been established.

Decreasing the conversion parameter k_1 affects precipitation development in much the same way as increasing conversion threshold a.

(3) The collection efficiency E

The model permits study of the role in the precipitation process of the efficiency with which precipitation collects cloud. Figure 14 shows the development of precipitation at the ground in a case where the collection efficiency E is unity and in a case where E = 0. The steady-state precipitation rate is lower in the latter case, because more condensate remains as cloud aloft and is spread horizontally by high level divergence of the wind. This is shown clearly by the vertical profiles in Section 8B, below. When E is greater than zero, two processes can contribute to precipitation formation in the model; when E is relatively very small or zero, the autoconversion process is the only important one.

(4) The precipitation drop size parameter N_o

For at least two reasons, the parameter N_o affects the cloud and precipitation distributions. First, the rate of cloud collection for fixed M, m, and E increases slowly as N_o increases. Second, the relative number of slow-falling small drops increases with N_o, when M is constant, and the average fall speed of the whole distribution decreases. However, both the collection and fall speed equations involve the eighth root of N_o, and order-of-magnitude change of this distribution shape parameter is necessary to alter cloud and precipitation distributions significantly.

Figure 15 shows the time variation of precipitation at the ground accompanying three values of N_o. The middle curve is associated with an N_o typical of natural rain. When N_o is very small, particles fall rapidly and precipitation starts earlier at the ground. When N_o is as large as 10^{10} m^{-4}, however, the average particles are only the size of drizzle; their very slow falling speed is associated with both the delayed arrival of

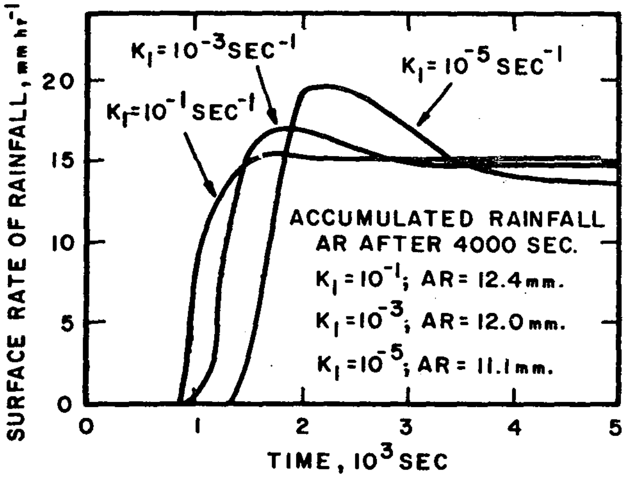

Figure 13. - Precipitation onset in relation to the conversion rate k_1. Other model parameters are listed in Table 2.

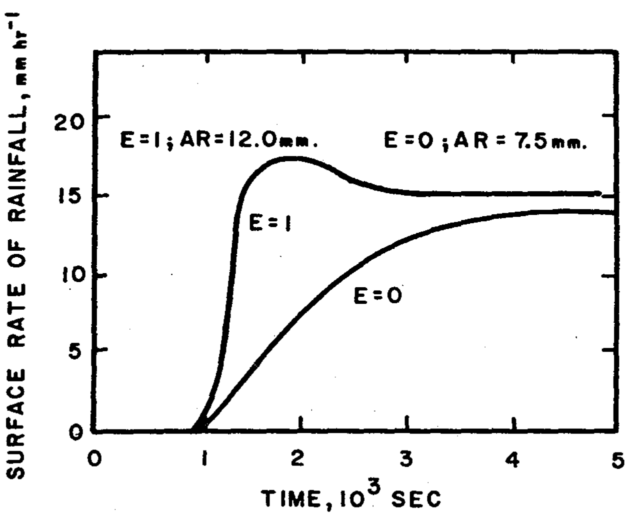

Figure 14. - Precipitation onset in relation to the collection efficiency E.

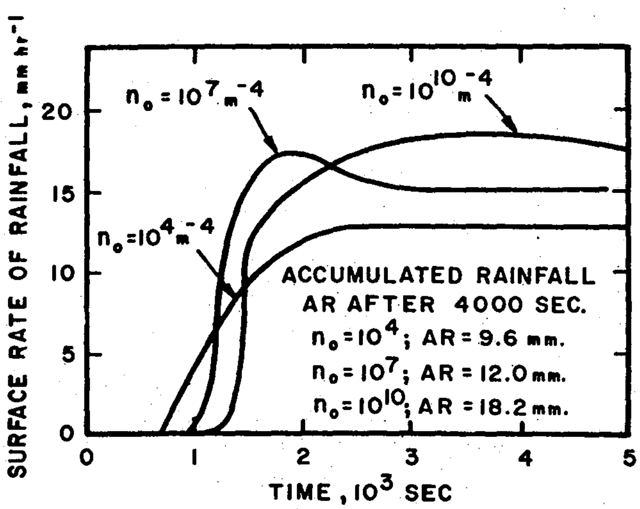

Figure 15. - Precipitation onset in relation to the drop size distribution parameter N_o. The curve for $N_o = 10^7$ also appears in figures 8, 9, 13, and 14.

steady conditions, and the larger rate of steady precipitation of this case.

B. Relationships between Microphysical Parameters and Steady-State Profiles of Cloud and Precipitation

This section discusses the role of the microphysical parameters in shaping the steady-state distributions of precipitation and cloud in model updraft columns. The initial conditions and the parameters w_{max}, H, and G are the same as noted in Section 8A above. In Section 8A the discussion of transients is illustrated mainly by graphs of the development with time of the precipitation rate at the ground. The figures in the present section indicate steady-state vertical profiles of cloud and precipitation. However, these profiles' indications are not strictly correct especially near the top of the updraft, since very long problem time is required to attain the steady-state there. This corresponds to weak cloud advection associated with weak updrafts there. If autoconversion is not a factor, vertical currents should bring finite cloud amounts indefinitely close to the upper boundary after a sufficiently long time. Steady-state analytic solutions have been derived from simpler models, and are illustrated in figure 2 (top and middle) in this paper and in figure 1 in [20].

(1) The conversion threshold a

When the conversion threshold a is quite large, the steady-state cloud amount is determined solely by a balance among condensation, vertical advection, and accretion processes. When a is small, however, the autoconversion and accretion processes both contribute to depletion of cloud, and the steady-state cloud content is therefore reduced.

The effect of varying a between particular values is shown in figure 16. When a is large, the cloud content in the upper atmosphere tends to be large because it is here that precipitation is light and relatively ineffective in removing cloud. Some of the large amounts of cloud aloft are lost to precipitation at the updraft center by virtue of horizontal divergence of the wind, and the precipitation at the ground is, therefore, slightly reduced in this case.

Note that in both cases, the cloud amount below 3.5 km. is less than a, and is locally regulated by accretion, condensation, and advection, without autoconversion.

The effect of height variations of the conversion threshold are illustrated in figures 10, 11, and 12 in the preceding Section.

(2) The cloud conversion rate k_1

Comparison of the steady-state profiles in figures 16 and 17

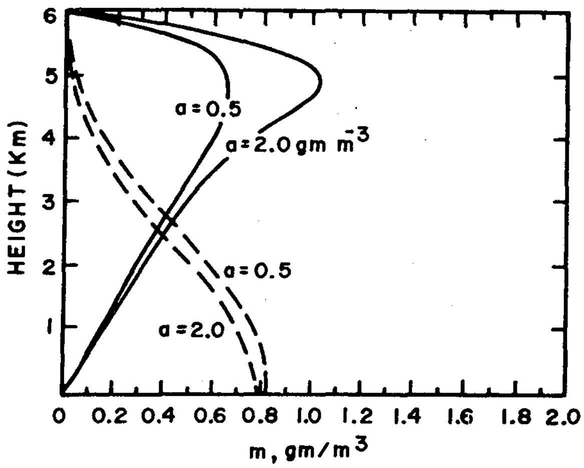

Figure 16. - Steady-state profiles of cloud and precipitation in relation to the cloud conversion threshold a.

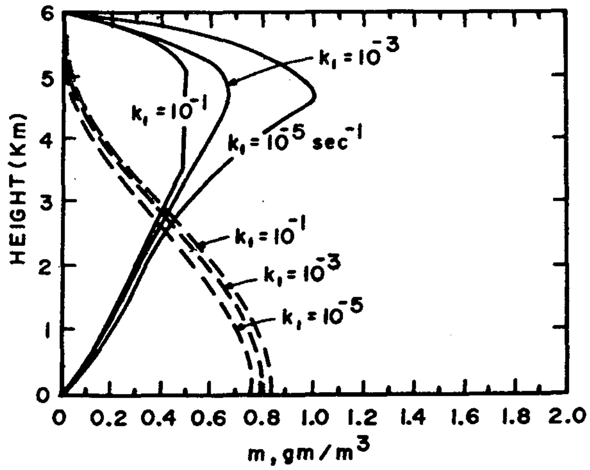

Figure 17. - Steady-state profiles in relation to the cloud conversion rate parameter k_1.

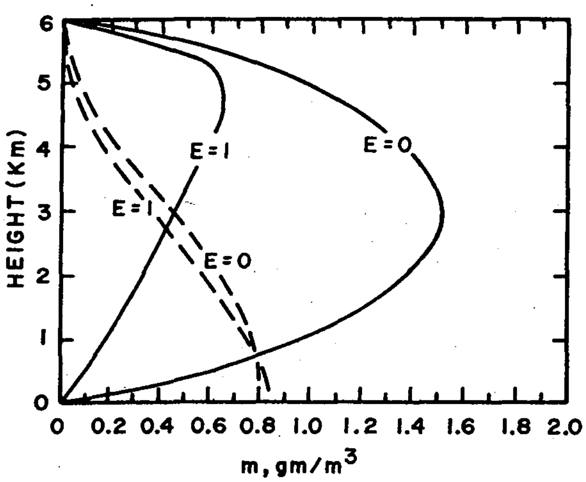

Figure 18. - Steady-state profiles in relation to the collection efficiency E.

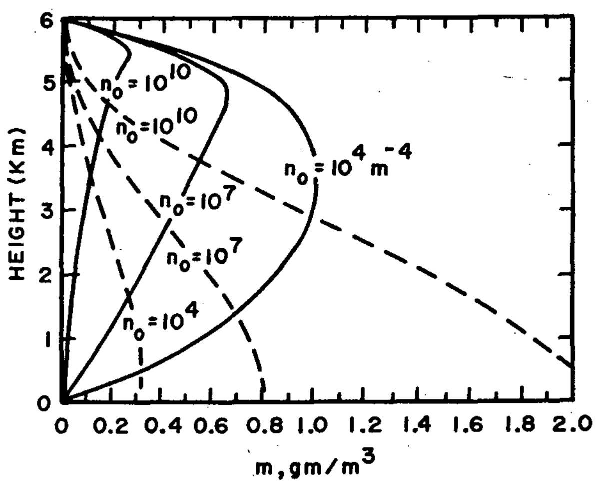

Figure 19. - Steady-state profiles in relation to the drop size distribution parameter N_o.

shows that the roles of k_1 and a are similar. Indeed, the cloud and precipitation profile corresponding to $k_1 = 10^{-5}$, a = 0.5 in figure 17 is virtually identical to that for $k_1 = 10^{-3}$, a = 2.0 in figure 16. The similarity is not surprising, since autoconversion is made small either by increasing a or by decreasing k_1.

(3) The collection efficiency E

Note figure 18 which illustrates the role of the collection efficiency E. When the collection efficiency is zero, the accretion process no longer contributes to depletion of cloud, and the cloud content rises. The curve shown for E = 0 applies to a balance among condensation, advection, and cloud autoconversion processes.

The increased cloud amount with E = 0, and the associated increased strength of autoconversion, compensates almost completely for the absence of the model accretion process, insofar as precipitation production is concerned. This is true as long as k_1 alone permits most of the cloud to convert to precipitation before being spread by horizontal divergence at high levels. In the present case, the conversion time constant 1/k is much smaller than the time that it takes an air parcel to ascend from low to high levels in the column (1/k = 1000 secs., but H/w_{max} = 12,000 secs.).

In the present case, we can consider a highly simplified form of Eq. (9a), viz.,

$$0 = -w\frac{\partial m}{\partial z} + wG - k_1(m - a). \qquad (62)$$

Eq. (62) applies to the steady state in an incompressible atmosphere without horizontal advection and without accretion or evaporation processes. This is the problem whose solution by finite differences is shown in figure 18.

Eq. (62) has a maximum which satisfies the equation

$$m_{max} = \frac{wG}{k_1} + a \qquad (63)$$

Generally, the magnitude of m_{max} increases as k_1 decreases. Equation (63) alone does not give the location of m_{max} and, therefore, does not give its magnitude. We know, however, that the maximum numerical value of m at any particular point is never larger than the steady-state cloud content at that point in a non-precipitating atmosphere.

When $1/k_1 \ll H/w_{max}$, the cloud profile is accurately defined by Eq. (23),[7] cloud is spread horizontally by divergence at high altitudes and cloud contributes little to rain production at places beneath the updraft column.

(4) The precipitation drop size parameter N_0

Much of the explanation of the curves shown in figure 19 is given in Section 8A (4). When N_0 is large, raindrops are relatively small and fall slowly; however, their total number and cross section is so greatly increased that accretion of cloud is also enhanced. Therefore, cloud amounts in this case are small. The precipitation content M is increased when N_0 is large and fall speeds small because there is then more time for the precipitation to develop from condensation in the updrafts. And the enhancement of the precipitation rate MV at updraft centers when fall speeds are small, is explained by the divergence term in Eq. (15) and by figure 1. The volume contributing to the precipitation which falls on a given section of ground, increases as fall speeds decline in relation to updrafts.

C. The Amount of Cloud which Coexists with Precipitation in the Steady State.

It is shown here that the amount of cloud which coexists with precipitation in the steady state, is probably only weakly related to the updraft speed, or condensation rate. One can perceive in advance of formal analysis, that as the condensation rate increases, the tendency for increased cloud is compensated by its more rapid accretion by increased amounts of precipitation.

Examination of the steady-state cloud profiles in figures 16-19 shows that the distributions are principally determined by condensation and accretion except where $E = 0$. A steady-state model incorporating these processes alone can be examined analytically with interesting results. Consider the case where updraft speeds are small compared to precipitation fall speeds and condensate changes efficient to precipitation. Then the precipitation content at each height is fairly approximated by the equation

$$R \doteqdot - MV_0 \doteqdot \int_z^H wGdz \quad . \tag{64}$$

[7] In the compressible case with zero accretion, the steady-state m-profiles as k_1 approaches 0, approach the curves discussed in Section 4 of this report (Eq. 16).

When the only process depleting cloud is its collection by precipitation, and when vertical advection of cloud is absent or comparatively weak, the equilibrium cloud content is defined by

$$wG = k_2 mM^{.875} \quad , \tag{65}$$

where the left term is the condensation rate and the right represents accretion. When V is defined by Eq. (38), (64), and (65) can be combined. Then

$$m = \frac{wG}{7\times10^{-4}\, EN_0^{0.125}\left[\dfrac{\int_z^H wG\,dz}{38.6\, N_0^{-0.125}}\right]^{0.778}} \quad . \tag{66}$$

The significance of (66) is more apparent when it is written in the form

$$m = \frac{wG}{\left(38.6^{-0.778}\right) 7\times10^{-4} EN_0^{0.222}\left[\overline{wG}\ \ (H-z)\right]^{0.778}} \quad , \tag{67}$$

where $\overline{wG}$ is the average value of wG in the interval H - z and wG applies at height z. Eq. (67) shows that the steady-state value of m is quite insensitive to the magnitudes of w, G, and the shape parameter N_0; m increases with the 2/9 power of the first two quantities and decreases as $N_0^{2/9}$ increases. However, m is markedly dependent on the collection efficiency E. Also, increased depth H of the updraft column without changes of shape of the updraft distribution and condensation functions, is associated with a markedly diminished cloud content m, since m is proportional to $H^{-.778}$. This can be understood in terms of the increased precipitation content in deeper updrafts, and associated increased rate of cloud accretion.

A plot of Eq. (66) based on calculations with w_{max} = 1 m./sec. and other parameters listed in Table 2, is given in figure 20. For comparison, steady-state cloud profiles determined from the finite difference forms of Eqs. (8a) and (9a) with maximum updrafts of 0.5 and 2.0 m./sec. are also shown. Agreement between the curves is good below 4 km., where the roles of cloud advection and autoconversion in the complete system (8a) and (9a) are relatively small. In the upper atmosphere where M is very small, the neglect of vertical advection

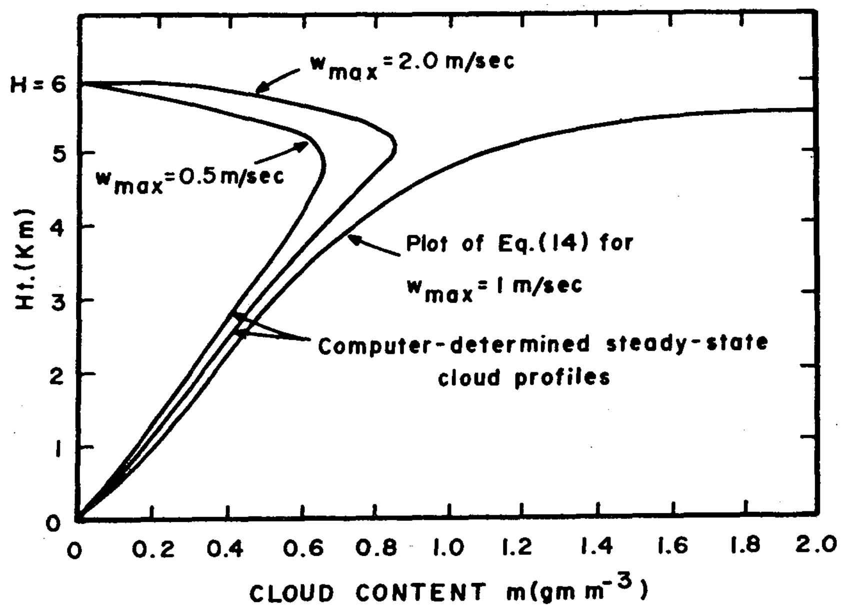

Figure 20. - Solution of Eq. (65), a model cloud profile where advection and auto-conversion are zero. Agreement with numerical results is good where advection and autoconversion are small compared with other processes affecting cloud development. Parameters not given here are listed in Table 2.

in Eq. (66) leads to the prediction of indefinitely large cloud contents; however, the cloud content in any situation can never exceed that accumulated in a saturated air parcel rising from the surface without precipitation.

It should be noted that Eq. (66) can not be applied when collection efficiencies are very low, updrafts are comparable to or larger than fall speeds, or with extrema of the other parameters. The computer results verify the indication of Eq. (66) that steady-state cloud contents in stratiform rain are very weakly related to the updraft speed. This is also discussed in [47].

D. Roles of Updraft Strength and Duration in Model Cloud and Precipitation Development

(1) Specified vertical displacement of the air at a very rapid rate

A given amount of lifting may be produced by a slow updraft operating over a long period of time or by a stronger updraft operating for a proportionately shorter period. A limiting case of special interest is associated with a particular vertical displacement of the air, occurring at a rate so rapid that condensation of cloud is the only effective process. The cloud profile resulting from such a rapid limited vertical displacement is calculated as follows:

Consider the model condensation function,

$$G = \frac{dm}{dz} = A + Bz \text{ [cf. compressible form Eq. (16)].} \quad (68)$$

Then

$$m_2 = A(z_2 - z_1) + \frac{B(z_2^{\,2} - z_1^{\,2})}{2} + m_1 \quad , \tag{69}$$

where m_2 is the cloud amount at z_2 associated with a parcel lifted from height z_1 where its cloud content was m_1.

Consider the updraft distribution Eq. (24). This is the basis for defining the displacement to z_2 of particles starting from any height z_1.

$$z_1 = \frac{z_2 H}{(H - z_2)\exp 4\mathbb{D} + z_2} \quad , \tag{70}$$

where the displacement parameter $\mathbb{D} = \frac{w_{max} t}{H}$. Substitution of (70) into (69) yields

$$m_2 = m_1 + Az_2(1 - \alpha) + \frac{Bz_2^{\,2}}{2}(1 - \alpha^2) \quad , \tag{71}$$

where $\alpha = \frac{z_1}{z_2}$ is defined by (70). When m_1 is a function of z_1, Eq. (70) is also used to substitute for other terms in z_1 in (71).

Figure 21 shows for saturated initial conditions and various values of the displacement parameter in Eq. (70), the associated cloud profiles. These profiles occur when the displacement time is so short that precipitation processes are not operative. For all $\mathbb{D} > 2.5$ (about) the cloud profiles are almost the same, and are almost exactly the steady-state cloud profile except at height H (6 km. in these cases).

Consider the development of precipitation in the updraft column following establishment of the cloud profiles shown in figure 21. This problem has been treated numerically for the indicated parameter values listed in Table 2. The results are shown in figure 22.

With small values of $\mathbb{D}$, the cloud conversion and cloud collection processes proceed very slowly in the tenuous clouds generated. As $\mathbb{D}$ increases, the rate of precipitation generation is increased and the onset time of precipitation at the ground decreases. For $\mathbb{D} > 1/2$, the occurrence of the maximum precipitation

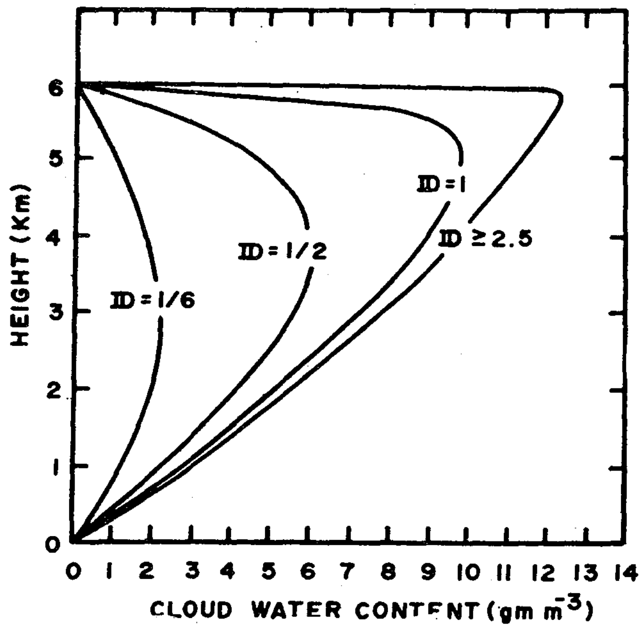

Figure 21. - Cloud profiles resulting from vertical displacement of saturated air without cloud autoconversion or accretion. The displacement parameter $D = W_{max}t/H$ and other parameters are listed in Table 2.

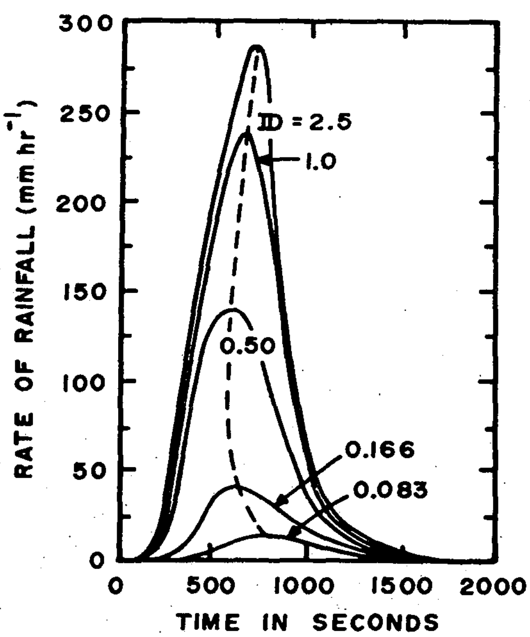

Figure 22. - Precipitation rate at the surface vs time associated with cloud profiles initially as shown in figure 22, and other parameters listed in Table 2.

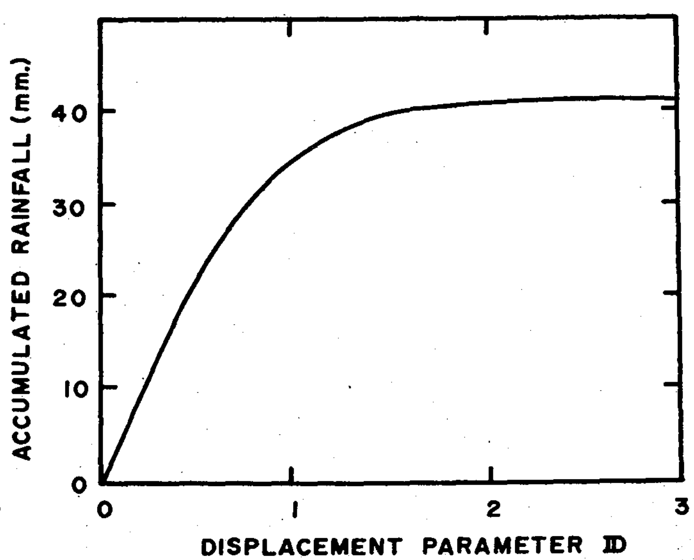

Figure 23. - The total rainfall accumulated at the ground, as derived from the curves in figure 22.

rate at the ground is delayed because precipitation formation is centered at successively higher levels (cf. figure 21) and the terminal speed of the particles comprising precipitation increases only as the eighth root of the precipitation content M, i.e., only slowly with M.

Figure 23 shows the total rainfall accumulated beneath an updraft core as a function of $\mathbb{D}$ for these cases where vertical air displacement is complete before precipitation processes have time to operate, and for the parameters listed in Table 2. The total precipitation per unit area beneath an updraft column in these cases is proportional to $\mathbb{D}$ only when $\mathbb{D}$ is small, and is almost insensitive to $\mathbb{D}$ when $\mathbb{D} > 1$. Continuity requires, however, that larger values of $\mathbb{D}$ be associated with a larger extent of cloudiness in the high atmosphere, and larger amounts of precipitation plus evaporation at places removed from the updraft centers.

(2) Various updraft speeds and durations

Figure 24 shows the time dependence of the precipitation rate at the surface for various combinations of w_{max} and T, each combination associated with the same displacement parameter $\mathbb{D} = 1/6$. Since the total air displacement is quite small, very little cloud is exported to the environment even when updrafts are strong, and the total precipitation received at the ground is about the same in all cases. Notice, however, that the precipitation curves have nearly the same shape and amplitude for updrafts of 2, 5, and ∞ meters/second. In each of these cases, cloud formation is substantially completed before precipitation development is far advanced. The earlier onset time for stronger updrafts in these cases is closely related to the earlier completion of the cloud formation process. The similar curves suggest

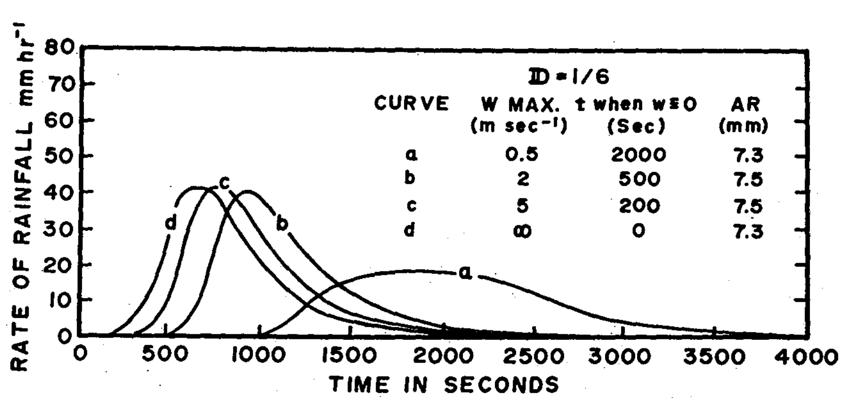

Figure 24. - Surface rainfall rate vs. time for several combinations of updraft magnitudes and durations, each associated with the same displacement parameter $\mathbb{D} = 1/6$.

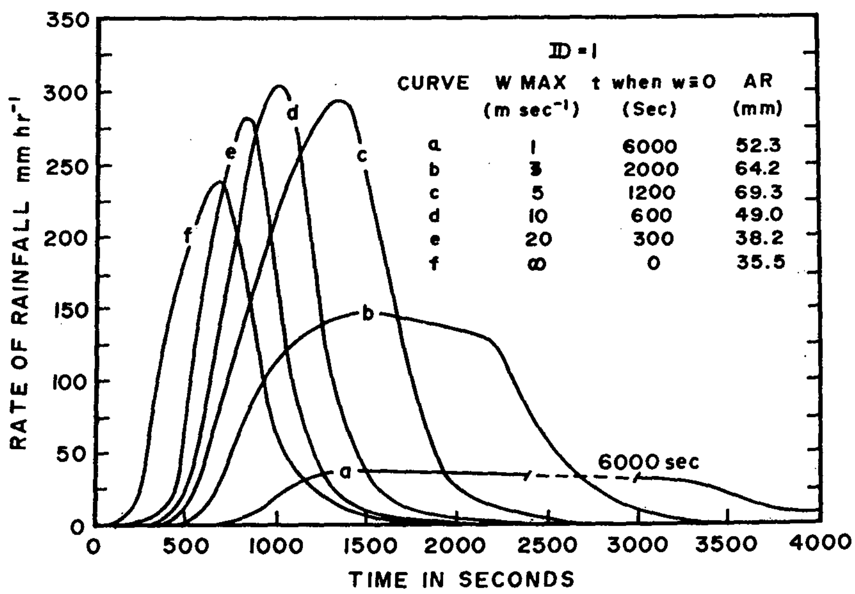

Figure 25. - Similar to figure 24 but with ID = 1. Parameters not listed are given in Table 2.

limitations in our ability to infer the intensity of convective currents from the shape of curves depicting precipitation rate vs time. The displacement of air is accurately measured by the total precipitation, however, in this case where the total displacement is small.

Figure 25 shows the time dependence of the precipitation rate beneath the updraft column for some w_{max}, T combinations associated with ID = 1. The typical displacement of air parcels is now a large fraction of the total depth of the updraft column. The stronger updraft cases are associated with appreciable high-level export of cloud from the updraft column, and with an associated reduction of the total precipitation received beneath the updraft. Cloud in these strong-updraft cases is removed from the updraft column by high level divergence before it has time to change to precipitation.

Notice that peak precipitation rate and total accumulation are maximized when maximum updrafts are about the same as typical precipitation fall speeds. While the updraft persists in such cases, much precipitation is suspended in the middle of the updraft column and grows there to large values by collecting cloud which would otherwise be carried to high levels and lost by effects of horizontal divergence. An additional boost to the precipitation rate in the intermediate updraft cases, however, is due to strong horizontal convergence in the lower atmosphere, explained in figure 1 and related text.

Figures 24 and 25 indicate that the precipitation rate in nature should not be expected to increase indefinitely with updraft speed. For defined total displacement of air consistent with the development of atmospheric water contents in the observed meteorological range, the peak precipitation rate at the ground is a maximum when maximum vertical air velocities are of the same order as the fall speed of precipitation particles, and decreases for faster updrafts. With increasing magnitude of large and rapid displacement a greater portion of the condensation products are spread by horizontal divergence aloft. Some condensation products may descend to the ground outside the updraft and a greater portion is exposed to possible loss by evaporation when updrafts are very strong.

E. Development of Cloud and Precipitation in an Initially Unsaturated Updraft Column

Figure 26 shows the development of cloud and precipitation profiles in an initially unsaturated model updraft column where the maximum updraft speed is 0.5 m./sec. Microphysical parameters and others are given in Table 2. Notice that the cloud profile undergoes substantial changes during most of the 8000-second duration of the updraft illustrated, whereas the precipitation profile undergoes most of its development in only one-third of this time. The lowering of the cloud base after 3500 seconds is due to ascent from beneath the cloud base, of air which becomes progressively moister by evaporation

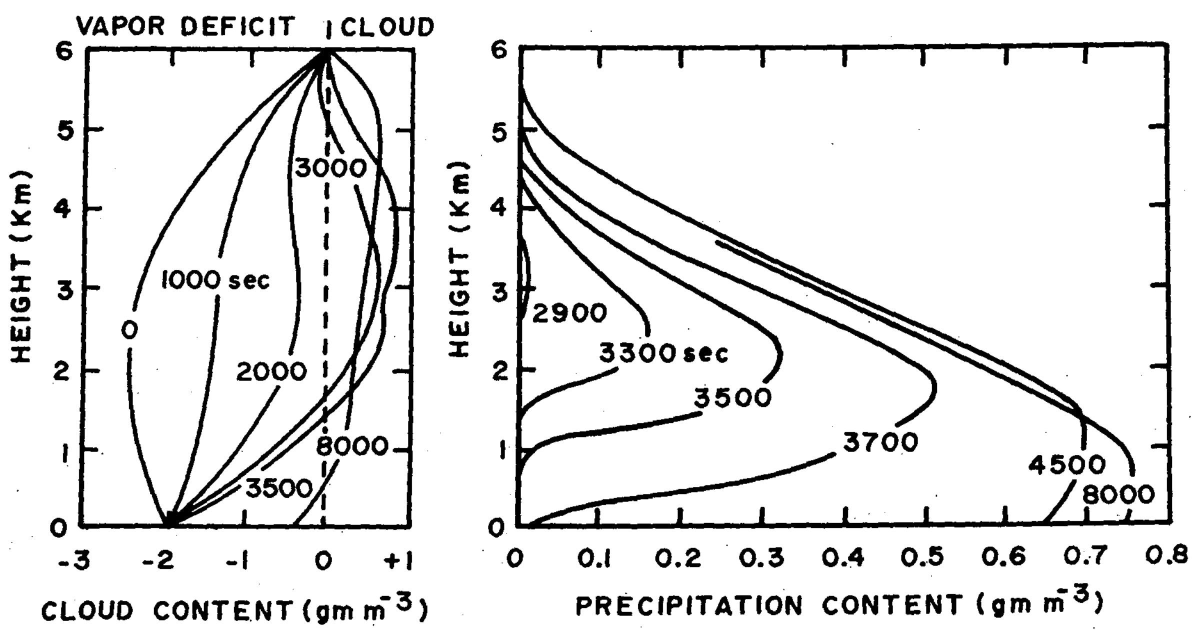

Figures 26a and 26b. - Vertical profiles of vapor, cloud, and precipitation in a circulation initially unsaturated.

of precipitation. After 8000 seconds, in this example, the cloud and precipitation profiles change only little as long as the updraft is unchanged. At zero height, where there is no airflow, evaporation of precipitation causes the saturation deficit m to approach zero asymptotically with time.

9. A TWO-DIMENSIONAL RECTILINEAR CIRCULATION CELL MODEL

A. The Model Circulation

In the following pages we consider vapor, cloud, and precipitation distributions in the two-dimensional rectilinear air circulation:

$$u = \frac{2Lw_{max}}{\pi H}\left(\frac{2z}{H} - 1\right)\sin\frac{2\pi x}{L} \qquad 0 \le x \le \frac{L}{2} \qquad 0 \le z \le H \quad , \tag{72}$$

$$w = \frac{4w_{max}}{\pi H}\left(z - \frac{z^2}{H}\right)\cos\frac{2\pi x}{L} \qquad 0 \le x \le \frac{L}{2} \qquad 0 \le z \le H \quad , \tag{73}$$

$$\Psi = \frac{2Lw_{max}}{\pi H}\left(z - \frac{z^2}{H}\right)\sin\frac{2\pi x}{L} \qquad 0 \le x \le \frac{L}{2} \qquad 0 \le z \le H \quad . \tag{74}$$

These equations satisfy the continuity equation

$$\frac{\partial u}{\partial x} + \frac{\partial w}{\partial z} = 0 \tag{75}$$

and, therefore, refer to an incompressible atmosphere. Essential features of wind-water relationships are not obscured by treating an incompressible atmosphere in the present context. Streamlines of this model wind field are shown by figure 27.

A computer program devised for calculating the development of cloud, precipitation, and vapor distributions in this circulation is described in [21], Reports 4 and 5 (also, see appendix B of this paper). The same program has been used to define the purely advective properties of (72), (73), and (74), with the result shown in figure 28. The advective properties are important because they provide a rational criterion for regulating the circulation, and some criterion must be found since dynamical equations are absent from the model. Figure 28 shows that overturning of air is substantially completed in this circulation when $t = 1.35H/w_{max}$, and this interval defines the duration of circulations studied below.

It should be noted that at x = 0 the circulation defined by Eqs. (72), (73), and (74) is identical to the updraft columns treated in previous sections of this paper.

B. Water Budget Parameters Independent of Circulation Intensity and Microphysical Processes

The efficiency of precipitation production must be judged in terms of the available mass of water substance, measured by the budget parameters discussed below.

(1) Total water

The total mass of water substance in the region of interest is composed of vapor, cloud, and precipitation. The total vapor divided by horizontal area and density, corresponds to the usual definition of precipitable water. The term "precipitable water" appears to be a misnomer, however, because the fraction of the

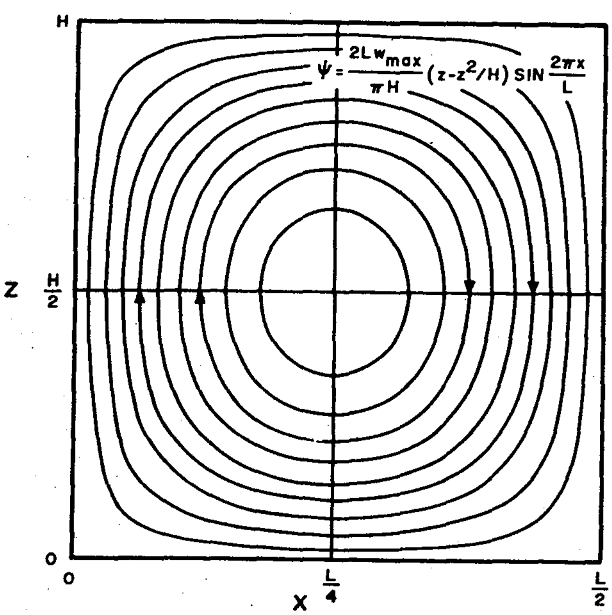

Figure 27. - Streamlines of the model wind field given by Eqs. (72), (73), and (74).

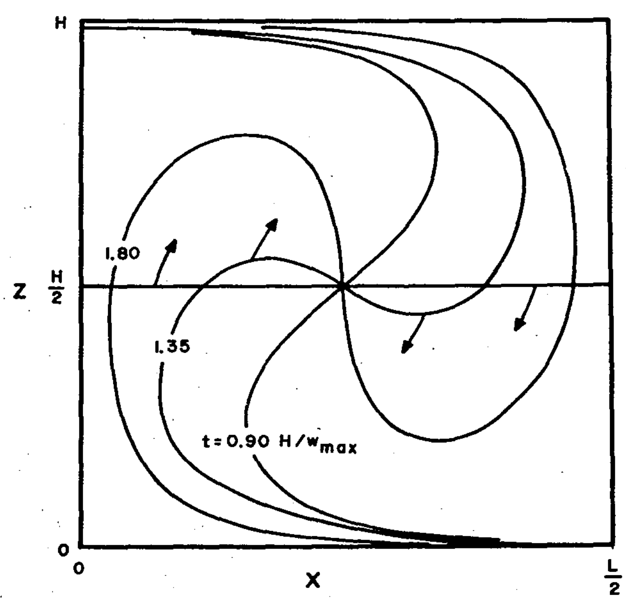

Figure 28. - Loci of a line initially horizontal and advected in the flow shown in figure 27.

total vapor which precipitates depends on its initial distribution, the wind field, and microphysical processes, as is shown below. The author supports Myers suggestion [31] that the term "precipitable water" be replaced by "liquid equivalent."

Consider first a saturated atmosphere without clouds or precipitation - in this the total water is the total vapor. In the model incompressible atmosphere the vertical lapse of saturation vapor density Q_s is the condensation function

$$G = -\frac{\partial Q_s}{\partial z} \quad , \tag{76}$$

from which it follows immediately that

$$Q_s(z) = \int_z^{H'} G\,dz + Q_s(H') \quad , \tag{77}$$

where $Q_s(H')$ is the saturation vapor density at the reference level H'.[6] The function $G = (3 \times 10^{-3} - 3 \times 10^{-7} z)$ gm. m.$^{-4}$ between $z = 0$ and $z = 10^4$m (where $Q_s = 0$ in the model), is used here as an approximation to an atmosphere with moisture content like the tropics.

The total amount of vapor in a saturated section of the x - z plane of height H, length L/2, and unit depth (into the page) is

$$\int_0^H \int_0^{L/2} Q_s\,dx\,dz = \frac{HL}{2}\left[H\left(1.5 \times 10^{-3} - 10^{-7} H\right) + Q_s(H)\right] \quad , \tag{78}$$

where $Q_s(H)$ is determined from (77) by setting $H' = 10^4$m, $Q_s(H') = 0$, $z = H$, and $Q_s(z) = Q_s(H)$:

$$Q_s(H) = 15 - 3 \times 10^{-3} H + 1.5 \times 10^{-7} H^2 \quad . \tag{79}$$

[6]Eq. (76) assumes that local and individual changes of vapor density are the same, e.g., that the analogous saturated real atmosphere has a moist - adiabatic lapse rate. See also discussion related to Eqs. (7) and (9) in this paper.

The terms excluding $Q_s(H)$ in (78) measure the maximum condensable water in a region of depth H, as discussed in the following paragraph. In the saturated area of square cross section where $H = L/2 = 6 \times 10^3$ meters, the total water is exactly 2.808×10^8 gm. m.$^{-1}$

(2) Maximum condensable water

This is the amount of water condensed when all the air in a given region is lifted to the highest elevation H in the region. The maximum condensable water is defined in the model saturated atmosphere by the equation

$$\text{Max. condensable water} = \frac{H^2 L}{2} (1.5 \times 10^{-3} - 10^{-7} H) . \qquad (80)$$

In the volume with square cross section discussed above, the maximum condensable water is exactly 1.944×10^8gm. m.$^{-1}$

(3) Circulation-condensable water

The circulation-condensable water is the mass of vapor that would be condensed if an hypothesized field of motion prevailed long enough to carry all the air parcels to the highest elevations of their streamlines. At $x = L/4$ is the maximum height to which the wind field pictured in figure 28 lifts an air parcel. This height is found from Eq. (74):

$$z_{max} = \frac{1}{2} \left\{ H + \left[H^2 - 4z(H-z) \sin \frac{2\pi x}{L} \right]^{\frac{1}{2}} \right\} , \qquad (81)$$

where x and z are initial coordinates.

A saturated parcel lifted from z to z_{max} condenses an amount of water $Q_s(z) - Q_s(z_{max})$. This difference of saturation vapor densities must be summed over the whole region, i.e.,

$$\text{Circ. Condensable water} = \int_0^H \int_0^{L/2} \left[\int_z^{z_{max}} G dz \right] dx dz \cdot \qquad (82)$$

Equation (82) has been calculated by computing the bracketed term at an array of 121 grid points with the aid of (81), then horizontally and vertically summing the numbers in the array by

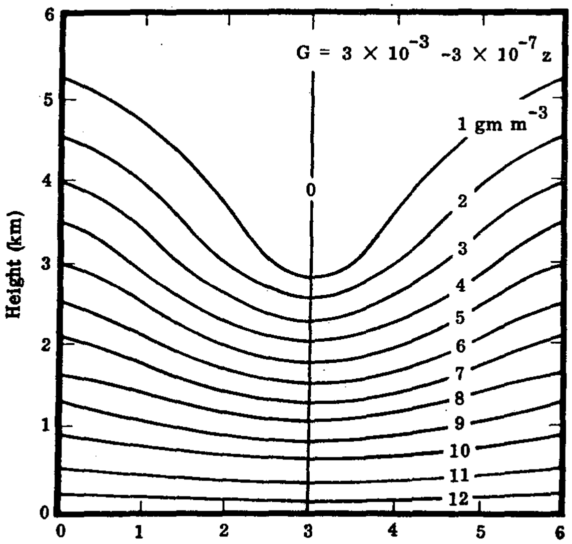

Figure 29. - Distribution of circulation-condensable water in an initially saturated atmosphere which circulates as shown in figure 27. The generating function $G = 3 \times 10^{-3} - 3 \times 10^{-7}z$.

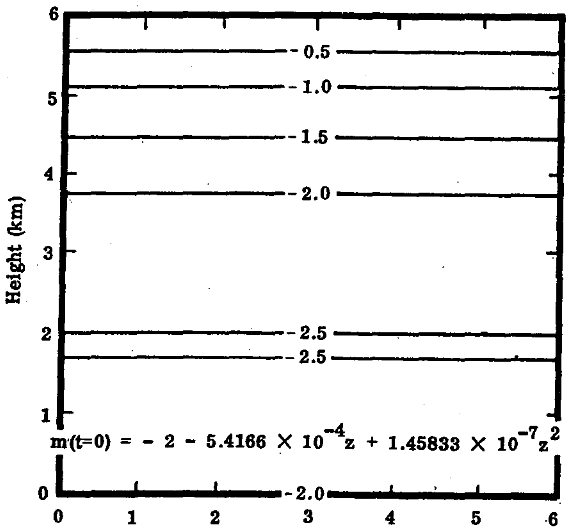

Figure 30a. - Initial distribution of saturation deficit in a model unsaturated atmosphere.

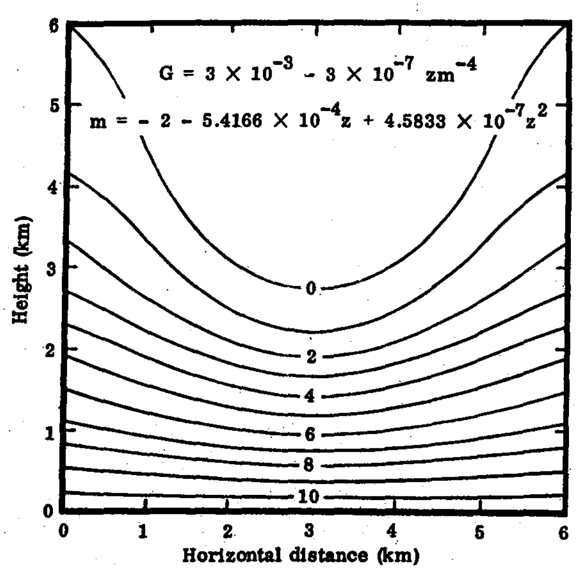

Figure 30b. - Distribution of circulation-condensable water in the atmosphere shown in figure 30a, which circulates as shown in figure 27.

Table 3

Budget parameters in two model atmospheres whose circulations are described by Eqs.(72) through (74) and where $H = L/2 = 6 \times 10^3$ m; $G = 3 \times 10^3 - 3 \times 10^{-7}z$ gm. m.$^{-4}$

Initial moisture condition	Duration of Circulation with $w_{max} = 2.5$ m./sec.	Water Condensed	$\frac{\text{Condensed}}{\text{circ.cdnsbl.}}$
Saturation Everywhere			
1. Total 28.08×10^7 gm.m.$^{-1}$	1080 secs.$= .45 \frac{H}{w_{max}}$	4.0×10^7	.26
2. Max. cond. 19.44×10^7	2160 secs.$= .90 \frac{H}{w_{max}}$	7.5×10^7	.48
3. Circ. Cond. 15.48×10^7			
$\frac{(2)}{(1)} = .69$; $\frac{(3)}{(1)} = .55$	3240 secs.$= 1.35 \frac{H}{w_{max}}$	10.2×10^7	.66
Unsaturated			
1. Total = 21.33×10^7 gm.	1080 secs.$= .45 \frac{H}{w_{max}}$	1.1×10^7	.12
2. Max. cond. = 12.69×10^7	2160 secs.$= .90 \frac{H}{w_{max}}$	3.5×10^7	.37
3. Circ. cond. = 9.50×10^7	3240 secs.$= 1.35 \frac{H}{w_{max}}$	5.5×10^7	.58
$\frac{(2)}{(1)} = .60$; $\frac{(3)}{(1)} = .45$	4000 secs.$= 1.67 \frac{H}{w_{max}}$	6.7×10^7	.71

successive applications of the trapesoidal rule. The distribution of circulation-condensable water in each part of an atmosphere which is initially saturated and circulates as shown in figure 27, is shown in figure 29; in this case the total circulation-condensable water is 1.548×10^8 gm. m.$^{-1}$

In the unsaturated atmosphere whose initial moisture distribution is illustrated in figure 30a, the circulation-condensable water, depicted in 30b, totals about 9.50×10^7 gm. m.$^{-1}$

(4) Condensed water

This quantity is defined as the amount of condensate produced during a given duration of an hypothesized field of motion. In this study, wind and water fields are studied over the interval associated with substantial overturning of the air strata. Such an interval is less than that associated with the transport of all air parcels to the maximum elevations of the steady streamlines; therefore, the circulation-condensable totals noted in the preceding paragraphs are not fully realized.

The condensed water is generally larger than the amount of condensate present in the model air circulation at a given time. Some condensate changes to precipitation, some of this falls out of the circulating area and some evaporates, some condensate in the form of cloud is carried to the downdraft part of the circulation and evaporates.

The computer program mentioned in Section 9A above has been used to determine the water condensed as a function of time in the circulation of figure 27. This has been accomplished by setting the conversion threshhold a = 0, having k_1 large, and setting evaporation = 0. Such choices of microphysical parameters lead to the immediate conversion of cloud to precipitation and its descent to the ground in the model. The condensed water at any problem time is the sum of precipitation in the air with that already at the ground.

Since all of the precipitation comes from vapor, the amount of precipitation should be represented by the net decrease of vapor content in the circulation since the start of calculations. In practice, truncation error leads to appreciable divergence of these measures. In the absence of a clear indication that the change of saturation deficit or the directly calculated precipitation accumulation more accurately describes precipitation at the ground, both quantities are included in calculations of the condensed water parameters depicted in Table 3 and figure 31.

C. Water Distributions in Weak and Strong Circulations Initially Saturated and Unsaturated

The development of vapor, cloud, and precipitation distributions in model circulations has been calculated with the microphysical parameters listed in Table 2. Figures 32 and 33 show sample pages of the computer product which is the basis for most of the discussion in this section. The numerical procedure is discussed in Appendix B.

Figure 34 illustrates the changing water distributions in a cell which is initially saturated, and in which the maximum updraft is 2.5 m./sec. The cloud passes through a dense transient stage, then thins in response to accretion. Substantial overturning of the air has occurred at the time represented in the fourth picture (lower left). At this time, denoted by T_1, winds are equated to zero and subsequent calculations follow the fallout of precipitation in still air. Notice that the cloud base lifts rapidly after updrafts cease - this is a response to the highly efficient accretion process when it is no longer balanced by condensation. The high cloud persisting long after updrafts cease seems analogous to many natural shower events.

Fall speeds of precipitation range about 6 m. sec.$^{-1}$ in this case, and are sufficiently larger than updrafts to produce nearly steady-state cloud and precipitation profiles at and near the left-hand boundary before the time T_1.

Some budget parameters associated with figure 34 are plotted in figure 35. Note the temporary increase of precipitation rate following cessation of updrafts. Note also the difference between the saturation deficit and the accumulated precipitation. This difference, properly zero, grows while the air circulates and remains steady after the air

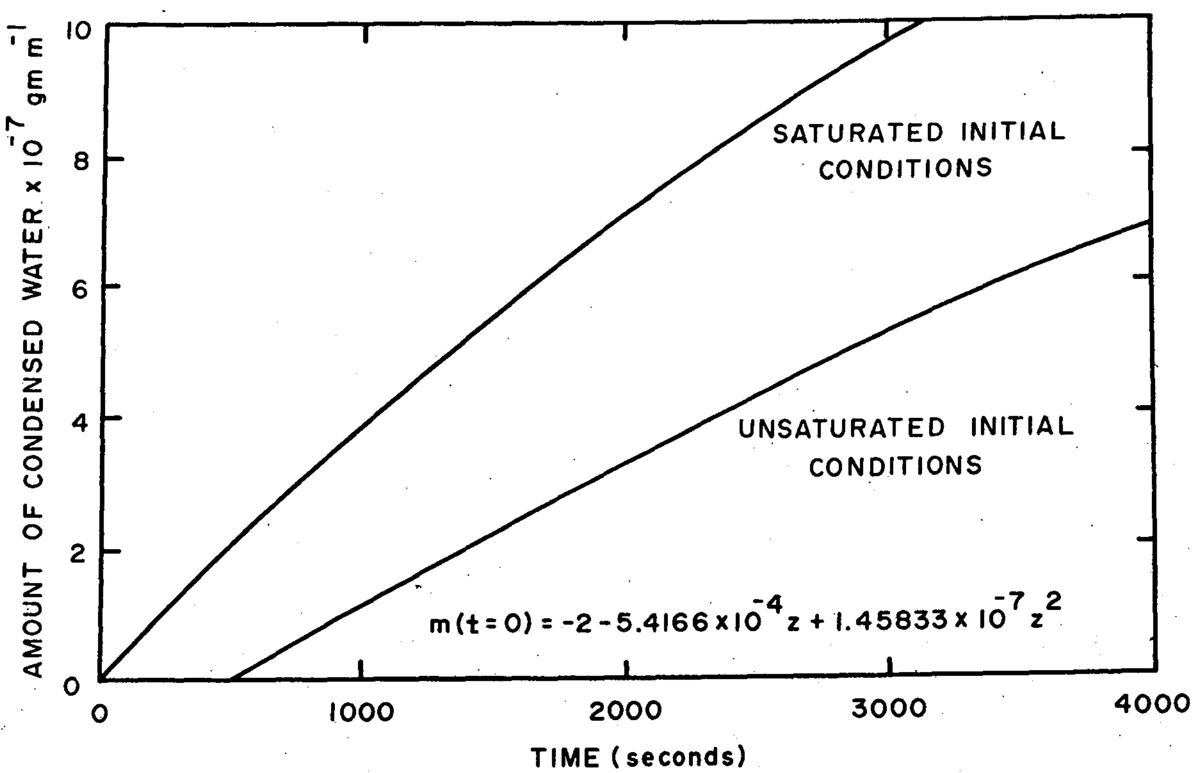

Figure 31. - Total water condensed in the circulation shown in figure 27, when the maximum updraft is 2.5 m./sec., for model saturated and unsaturated initial conditions.

circulation is equated to zero. A similar discrepancy was observed by the author [19], in calculations of precipitation and vapor based on a centered difference approximation to the differential equations, and such also appear in many other works ([33] for example). More confidence would be attached to the results if the magnitude of this discrepancy were reduced, and a better approach to representation of accumulated precipitation is obviously desirable. Future studies of similar problems should include consideration of finite difference schemes which treat the budget parameters more precisely.

The changing water distributions accompanying maximum updrafts of 10 m./sec. are illustrated in figure 36. In this case, maximum updrafts substantially exceed precipitation fall speeds, which range up to 7.5 m./sec., and appreciable precipitation at the ground is therefore delayed until time T_1, when the supporting updraft ceases. However, the maximum rainfall rate in this case is near 300 mm./hr. (1"/5 min.) corresponding to the largest rates usually observed during intense showers [10, 36].

TIME STEP NUMBER = 72 TIME = 1335. SECONDS

TAU (LAST TIME STEP TO THIS TIME STEP) = 14. TAU (THIS TIME STEP TO NEXT TIME STEP) = 14.

PRECIPITATION CONTENT, CAPITAL M, IN GR./CU. M. CLOUD AND VAPOR CONTENT, SMALL M, IN GR./CU. M.
VALUES OF PRECIP H2O ARE PREFIXED BY M VALUES OF CLOUD H2O ARE IMMEDIATELY BELOW THE PRECIP H2O VALUES FOR EACH HEIGHT LEVEL

H IN METERS	DISTANCE FROM UPDRAFT CORE IN METERS 0.	400.	800.	1200.	1600.	2000.	2400.	2800.	3200.	3600.	4000.	4400.	4800.	5200.	5600.	6000.
6000.	M 0.	M 0.	M 0.	M 0.	M 0.	M 0.	M 0.	M 0.	M 0.	M 0.	M 0.	M 0.	M 0.	M 0.	M 0.	M 0.
	0.	0.	0.	0.	0.	0.	0.	0.	0.	0.	0.	0.	0.	0.	0.	0.
5600.	M 0.10	M 0.07	M 0.07	M 0.06	M 0.06	M 0.05	M 0.04	M 0.03	M 0.02	M 0.01	M 0.00	M 0.00	M 0.00	M 0.00	M 0.00	M 0.
	0.84	0.81	0.80	0.79	0.76	0.73	0.69	0.64	0.56	0.46	0.29	0.09	-0.12	-0.32	-0.49	-0.46
5200.	M 0.27	M 0.22	M 0.20	M 0.18	M 0.16	M 0.14	M 0.12	M 0.09	M 0.05	M 0.02	M 0.01	M 0.00	M 0.00	M 0.00	M 0.00	M 0.
	0.76	0.78	0.79	0.78	0.76	0.73	0.69	0.63	0.55	0.42	0.19	-0.10	-0.42	-0.70	-0.89	-0.95
4800.	M 0.51	M 0.44	M 0.40	M 0.37	M 0.33	M 0.28	M 0.23	M 0.17	M 0.10	M 0.05	M 0.01	M 0.00	M 0.00	M 0.00	M 0.00	M 0.
	0.67	0.71	0.72	0.71	0.69	0.66	0.62	0.56	0.47	0.29	0.00	-0.38	-0.78	-1.13	-1.36	-1.48
4400.	M 0.84	M 0.75	M 0.69	M 0.62	M 0.54	M 0.46	M 0.36	M 0.26	M 0.16	M 0.07	M 0.02	M 0.01	M 0.00	M 0.00	M 0.00	M 0.
	0.61	0.64	0.64	0.63	0.61	0.57	0.53	0.45	0.32	0.09	-0.29	-0.76	-1.23	-1.62	-1.88	-2.04
4000.	M 1.25	M 1.14	M 1.04	M 0.93	M 0.80	M 0.66	M 0.52	M 0.36	M 0.21	M 0.10	M 0.03	M 0.01	M 0.00	M 0.00	M 0.	M 0.
	0.55	0.57	0.58	0.57	0.54	0.50	0.44	0.33	0.14	-0.20	-0.68	-1.23	-1.75	-2.16	-2.45	-2.64
3600.	M 1.71	M 1.58	M 1.45	M 1.29	M 1.10	M 0.90	M 0.68	M 0.46	M 0.25	M 0.11	M 0.04	M 0.01	M 0.00	M 0.00	M 0.00	M 0.
	0.50	0.52	0.52	0.51	0.48	0.44	0.36	0.20	-0.11	-0.59	-1.17	-1.78	-2.33	-2.76	-3.06	-3.26
3200.	M 2.22	M 2.07	M 1.89	M 1.67	M 1.42	M 1.14	M 0.83	M 0.52	M 0.27	M 0.12	M 0.03	M 0.01	M 0.00	M 0.00	M 0.00	M 0.
	0.45	0.46	0.46	0.45	0.43	0.38	0.27	0.01	-0.47	-1.09	-1.77	-2.41	-2.96	-3.38	-3.68	-3.89
2800.	M 2.75	M 2.57	M 2.35	M 2.07	M 1.74	M 1.36	M 0.94	M 0.55	M 0.27	M 0.11	M 0.03	M 0.00	M 0.00	M 0.00	M 0.00	M 0.
	0.40	0.41	0.41	0.40	0.38	0.32	0.14	-0.30	-0.97	-1.70	-2.43	-3.08	-3.62	-4.03	-4.32	-4.52
2400.	M 3.26	M 3.06	M 2.80	M 2.45	M 2.03	M 1.52	M 0.96	M 0.53	M 0.24	M 0.08	M 0.02	M 0.00	M 0.00	M 0.00	M 0.00	M 0.
	0.35	0.36	0.36	0.36	0.33	0.23	-0.10	-0.77	-1.57	-2.38	-3.12	-3.76	-4.27	-4.66	-4.93	-5.14
2000.	M 3.73	M 3.52	M 3.21	M 2.78	M 2.24	M 1.57	M 0.92	M 0.46	M 0.18	M 0.05	M 0.01	M 0.00	M 0.00	M 0.00	M 0.00	M 0.
	0.30	0.31	0.31	0.31	0.27	0.10	-0.47	-1.31	-2.20	-3.03	-3.77	-4.38	-4.87	-5.23	-5.50	-5.70
1600.	M 4.14	M 3.91	M 3.55	M 3.04	M 2.34	M 1.49	M 0.81	M 0.35	M 0.11	M 0.02	M 0.00	M 0.00	M 0.00	M 0.00	M 0.00	M 0.
	0.26	0.26	0.27	0.26	0.20	-0.13	-0.89	-1.81	-2.73	-3.56	-4.27	-4.85	-5.31	-5.66	-5.92	-6.15
1200.	M 4.47	M 4.21	M 3.80	M 3.17	M 2.28	M 1.32	M 0.62	M 0.22	M 0.05	M 0.01	M 0.00	M 0.00	M 0.00	M 0.00	M 0.00	M 0.
	0.21	0.21	0.21	0.21	0.10	-0.40	-1.22	-2.13	-3.00	-3.78	-4.44	-4.99	-5.43	-5.78	-6.05	-6.36
800.	M 4.69	M 4.41	M 3.92	M 3.14	M 2.05	M 1.05	M 0.41	M 0.11	M 0.01	M 0.00	M 0.00	M 0.00	M 0.00	M 0.	M 0.	M 0.
	0.15	0.15	0.15	0.14	-0.04	-0.60	-1.33	-2.10	-2.83	-3.49	-4.07	-4.55	-4.95	-5.28	-5.59	-6.08
400.	M 4.81	M 4.49	M 3.90	M 2.92	M 1.71	M 0.73	M 0.21	M 0.04	M 0.00	M 0.00	M 0.	M 0.	M 0.	M 0.	M 0.	M 0.
	0.08	0.08	0.08	0.04	-0.23	-0.67	-1.17	-1.69	-2.18	-2.63	-3.03	-3.38	-3.68	-3.93	-4.19	-4.64
0.	M 4.81	M 4.44	M 3.72	M 2.56	M 1.28	M 0.43	M 0.08	M 0.01	M 0.00	M 0.00	M 0.	M 0.	M 0.	M 0.	M 0.	M 0.
	0.	0.	0.	0.	0.	0.	0.	0.	0.	0.	0.	0.	0.	0.	0.	0.

Figure 32. - One page of the output of the computer program for calculating distribution of cloud vapor and precipitation content in model two-dimensional circulations.

Note in figure 36 the complex changes in the cloud distribution accompanying precipitation development. A cloud maximum persists at low levels midway between the cloud core (left-hand boundary of circulation) and the cloud boundary, because the accretion process is strongest at the cloud core when precipitation amounts are largest.

Budget parameters for the strong updraft case illustrated in figure 36 are shown in figure 37. Here, the precipitation rate and accumulation at the ground are negligible until the updraft ceases, and much larger amounts of precipitation are stored aloft while updrafts persist, than in the weak updraft model.

The development of water distributions in the model atmosphere initially unsaturated (figure 30), is illustrated in figures 38-41. Less water condenses in these cases and a greater proportion of condensate evaporates again before reaching the ground because the air is generally drier and a greater volume of air remains subsaturated.

TIME STEP NUMBER = 72 TIME = 1335. SECONDS

TAU (LAST TIME STEP TO THIS TIME STEP) = 14. TAU (THIS TIME STEP TO NEXT TIME STEP) = 14.

HEIGHT IN METERS	CLOUD WATER IN GR/SQ M	PRECIP. WATER IN GR/SQ M	CLOUD + PRECIP WATER IN GR/SQ M	DEFICIT (CLOUD + VAPOR) IN GR/SQ M
6000.	0.	0.	0.	0.
5600.	2.81105E 03	1.79219E 02	2.99027E 03	2.34338E 03
5200.	2.67536E 03	5.25337E 02	3.20070E 03	1.64718E 03
4800.	2.31409E 03	1.05021E 03	3.36430E 03	5.47788E 02
4400.	1.91778E 03	1.73919E 03	3.65698E 03	-7.95262E 02
4000.	1.57263E 03	2.56466E 03	4.13729E 03	-2.32534E 03
3600.	1.30762E 03	3.48154E 03	4.78916E 03	-4.05210E 03
3200.	1.08467E 03	4.42998E 03	5.51466E 03	-6.00111E 03
2800.	8.91795E 02	5.33756E 03	6.22935E 03	-8.17500E 03
2400.	7.30200E 02	6.12570E 03	6.85590E 03	-1.05173E 04
2000.	5.80974E 02	6.72116E 03	7.30214E 03	-1.28529E 04
1600.	4.50223E 02	7.07271E 03	7.52293E 03	-1.48267E 04
1200.	3.26952E 02	7.15381E 03	7.48076E 03	-1.58149E 04
800.	2.12761E 02	6.97129E 03	7.18405E 03	-1.49206E 04
400.	9.74833E 01	6.55448E 03	6.65197E 03	-1.15229E 04
0.	0.	5.96272E 03	5.96272E 03	0.
TOTALS	7.15725E 06 GR/M	2.51812E 07 GR/M	3.23384E 07 GR/M	-3.96280E 07 GR/M

WATER CONTENT OF SATURATED ATMOSPHERE = 2.80800E 08 GR/M

NET SATURATION DEFICIT IN THIS ATMOSPHERE = -1.44468E 07 GR/M

TOTAL WATER IN THIS ATMOSPHERE = 2.66353E 08 GR/M

PRECIPITATION RATE AT EACH POINT AT THE GROUND IN MM/HR.

DISTANCE FROM UPDRAFT CORE IN METERS

0.	400.	800.	1200.	1600.	2000.	2400.	2800.	3200.	3600.	4000.	4400.	4800.	5200.	5600.	6000.
109.60	100.16	82.09	53.87	24.82	7.19	1.14	0.08	0.00	0.00	0.	0.	0.	0.	0.	0.

INTEGRATED PRECIPITATION RATE AT GROUND = 3.59586E 04 GR/M SEC

ACCUMULATED PRECIPITATION AT GROUND = 1.59828E 07 GR/M

Figure 33. - Computer product showing budget parameters associated with figure 32.

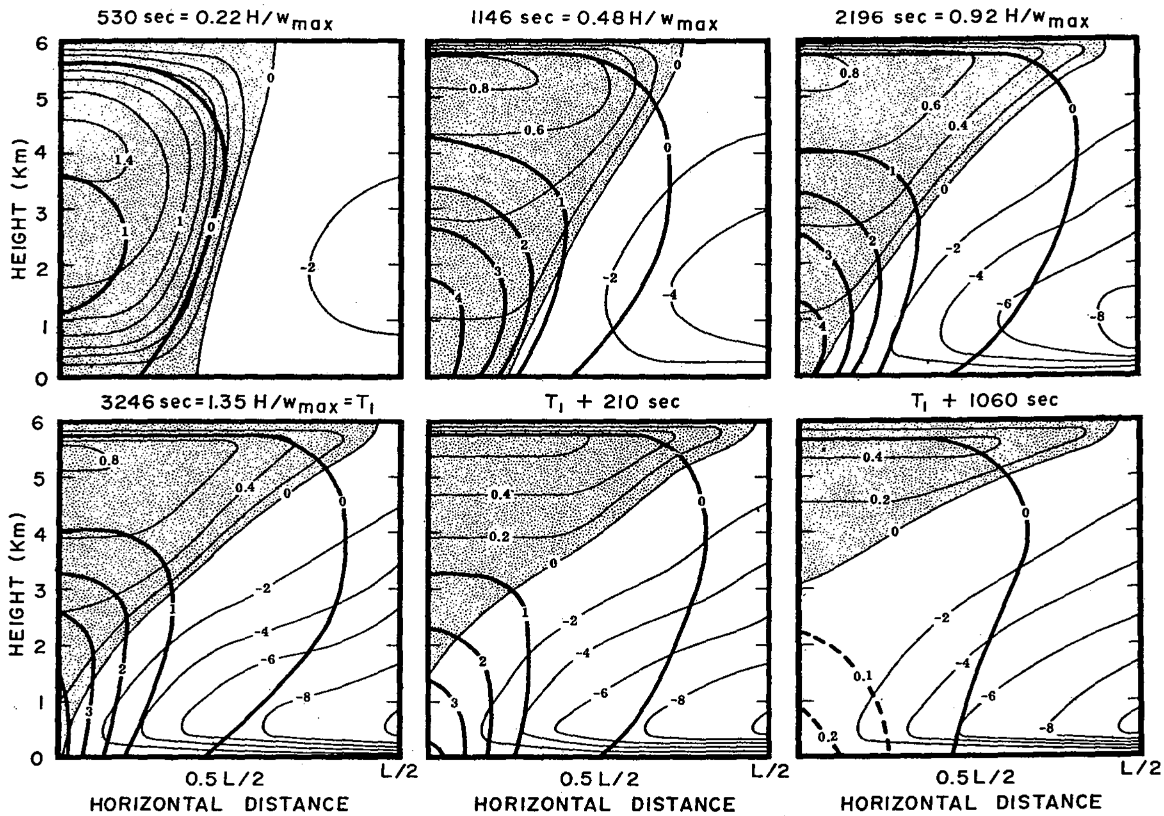

Figure 34. - Water distributions in an initially saturated atmosphere with w_{max} = 2.5 m./sec. and $N_\odot = 10^7 m^{-4}$. Heavy lines are isopleths of precipitation content, light lines in stippled area mark cloud, and light lines in clear refer to saturation deficit. Lines are labeled in gm. $m.^{-3}$

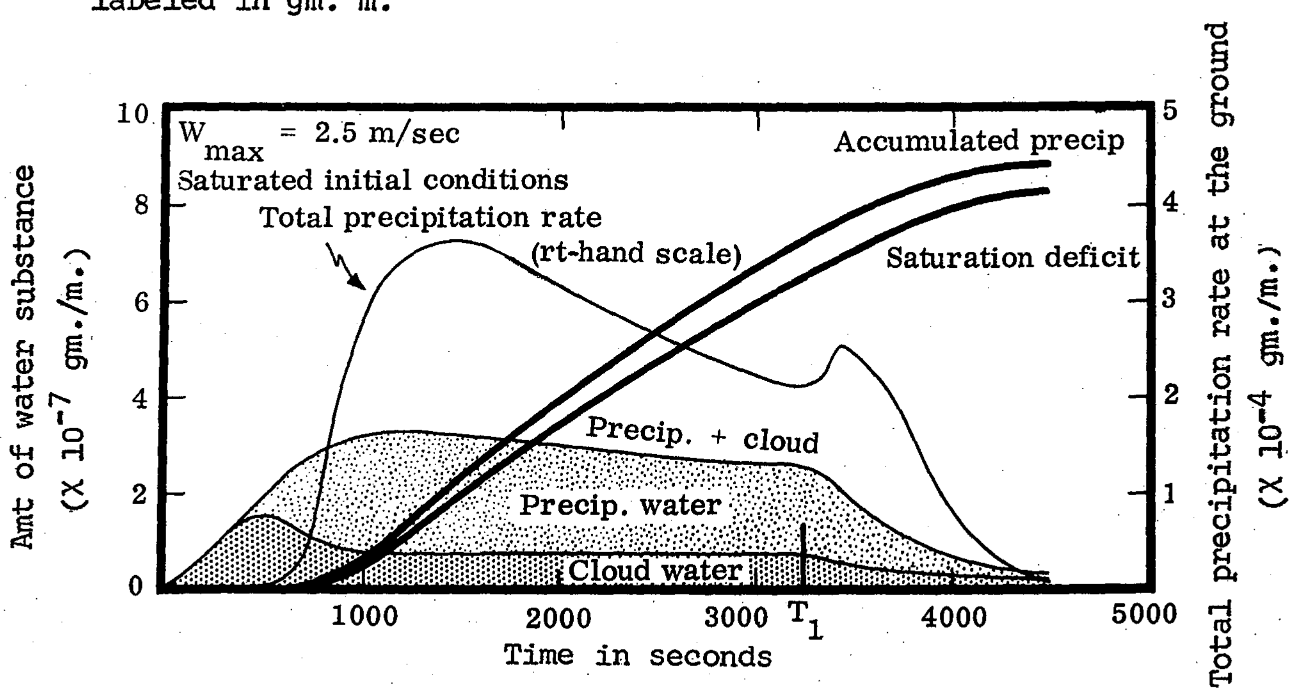

Figure 35. - Budget parameters associated with figure 34.

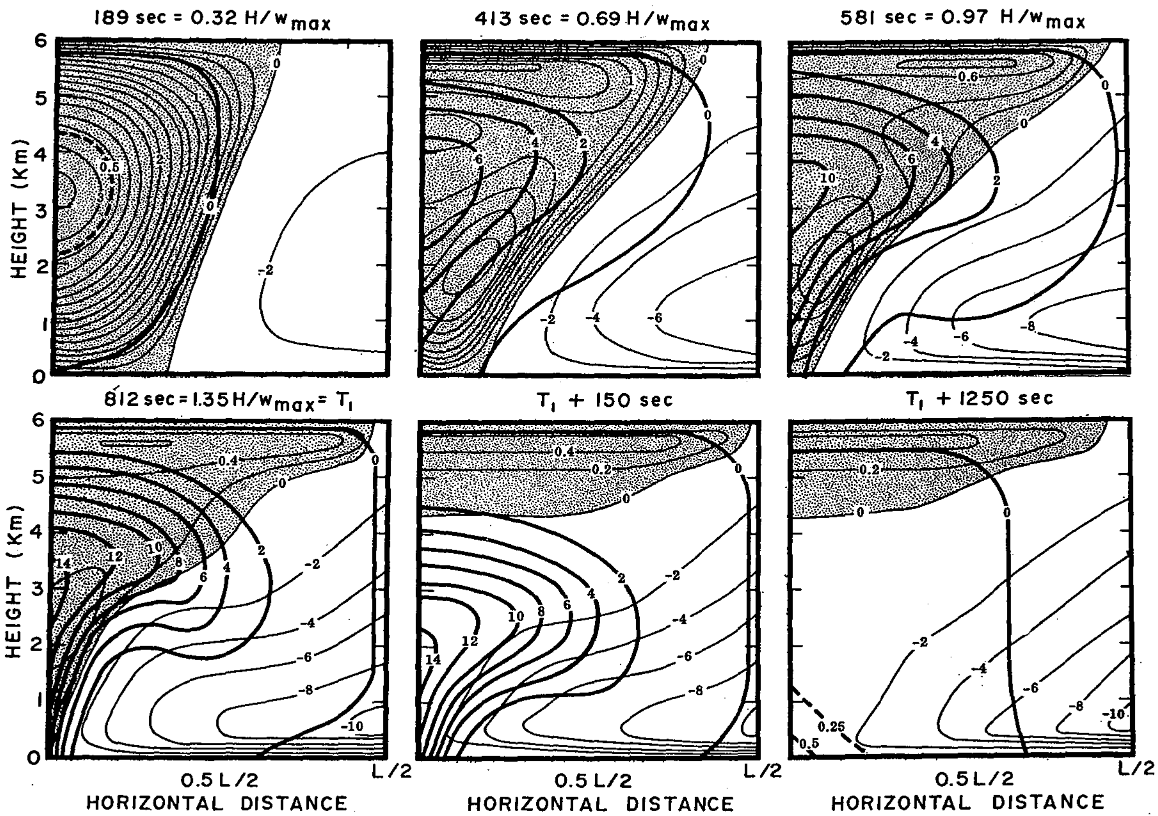

Figure 36. - Water distributions in a circulation with w_{max} = 10 m./sec.

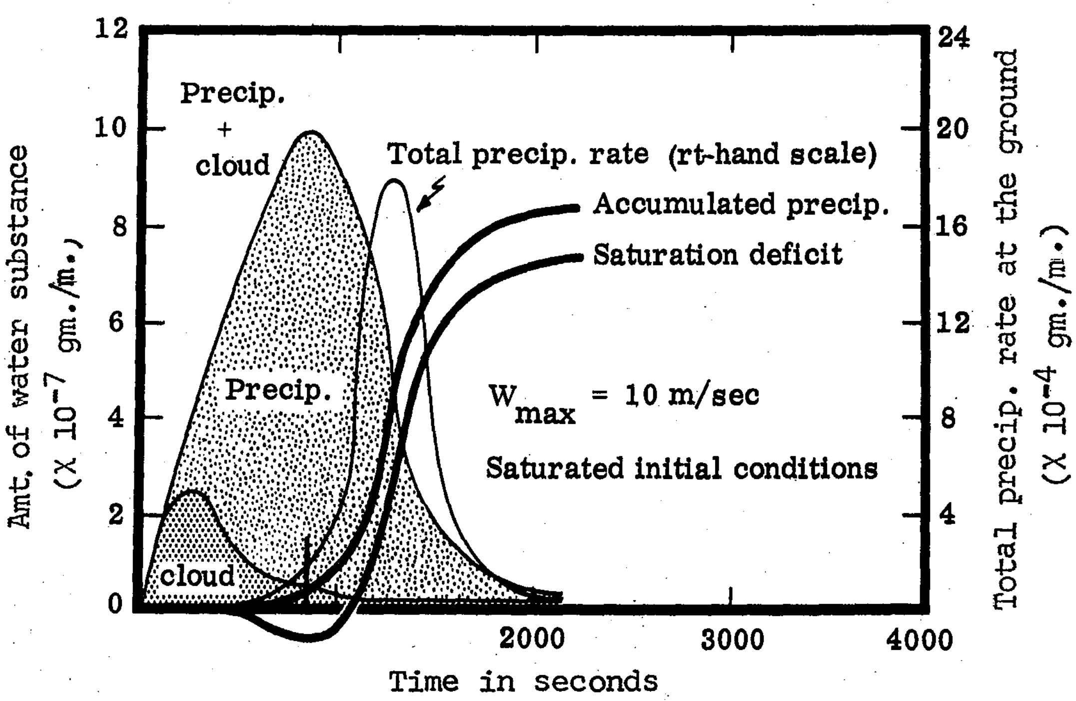

Figure 37. - Budget parameters associated with figure 36.

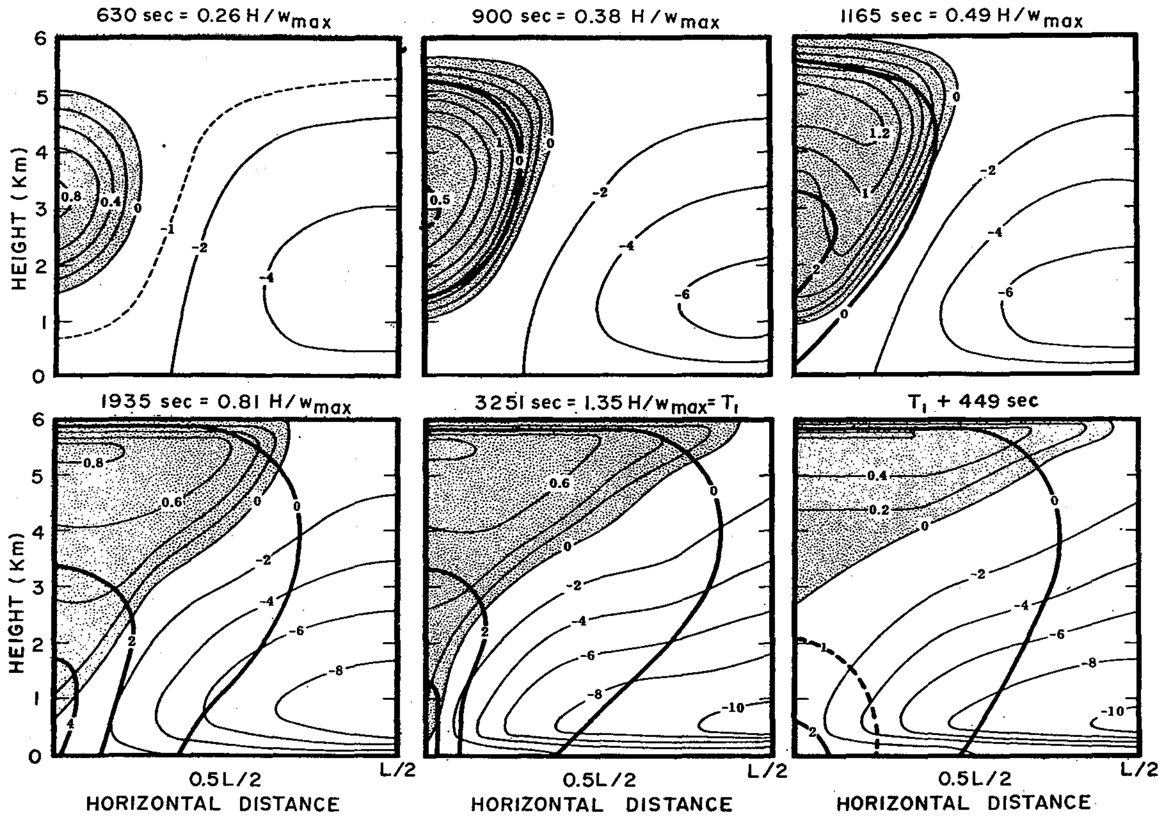

Figure 38. - Water distributions in the initially unsaturated circulation shown in figures 30a and 30b with maximum updrafts 2.5 m./sec.

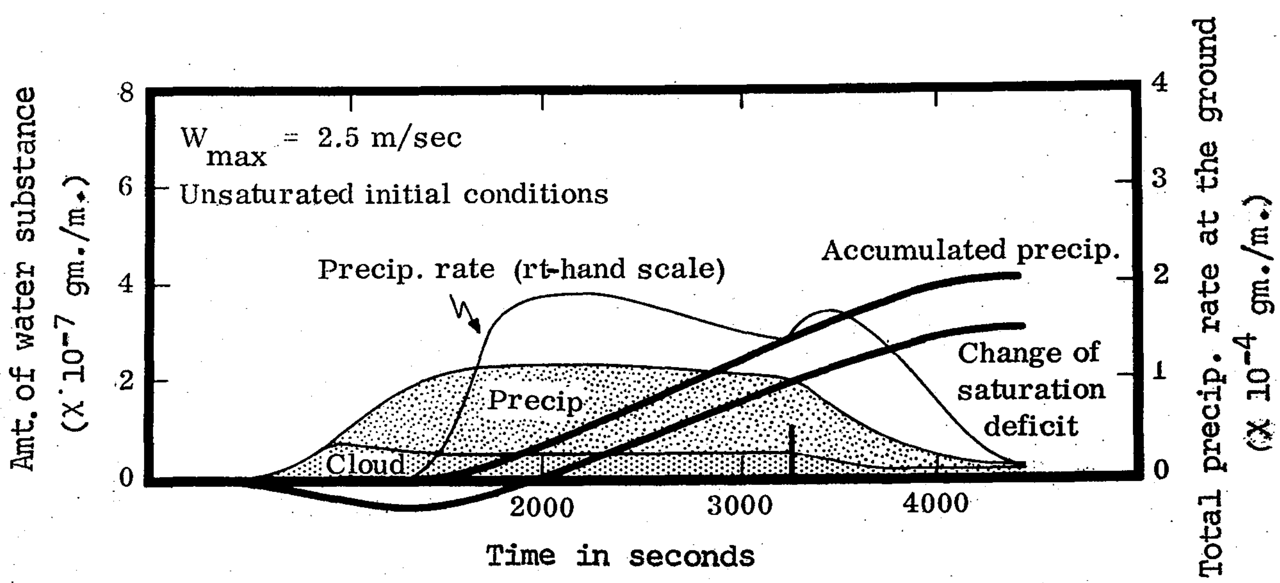

Figure 39. - Budget parameters associated with figure 38.

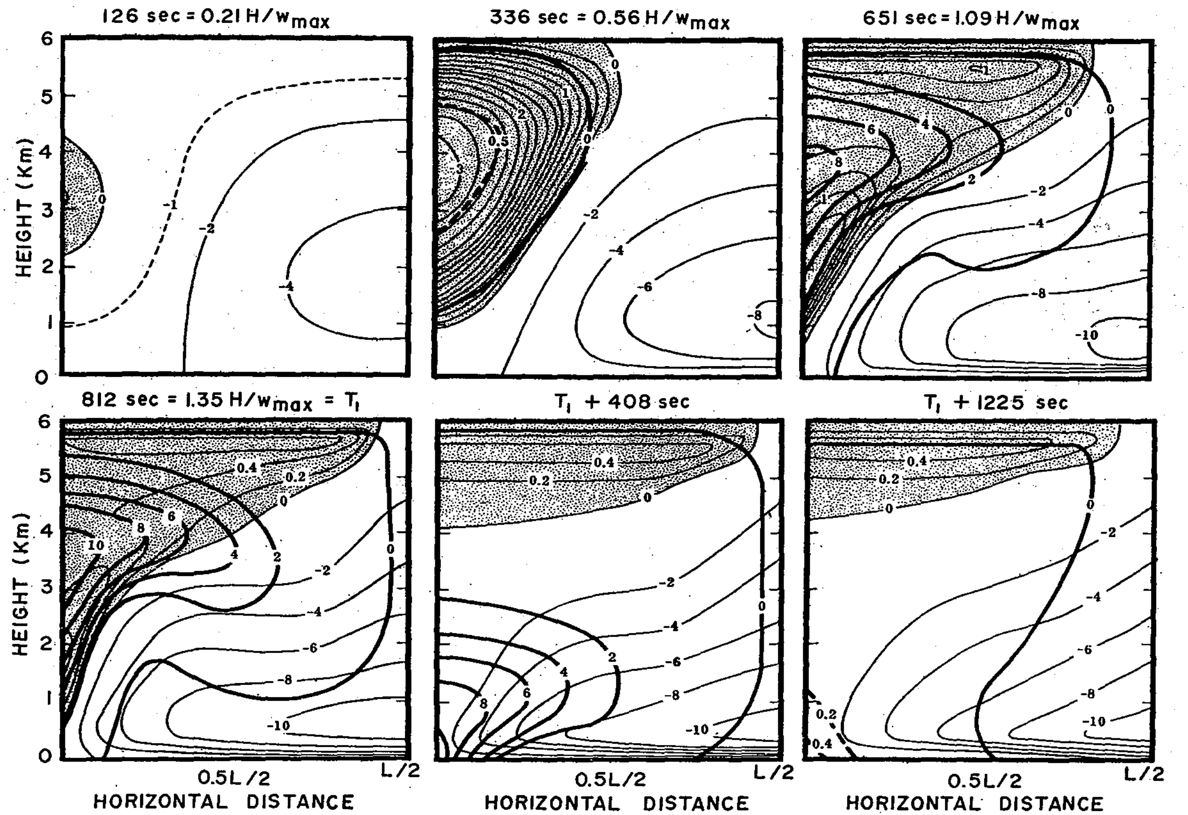

Figure 40. - Same as figure 38 except maximum updrafts are 10 m./sec.

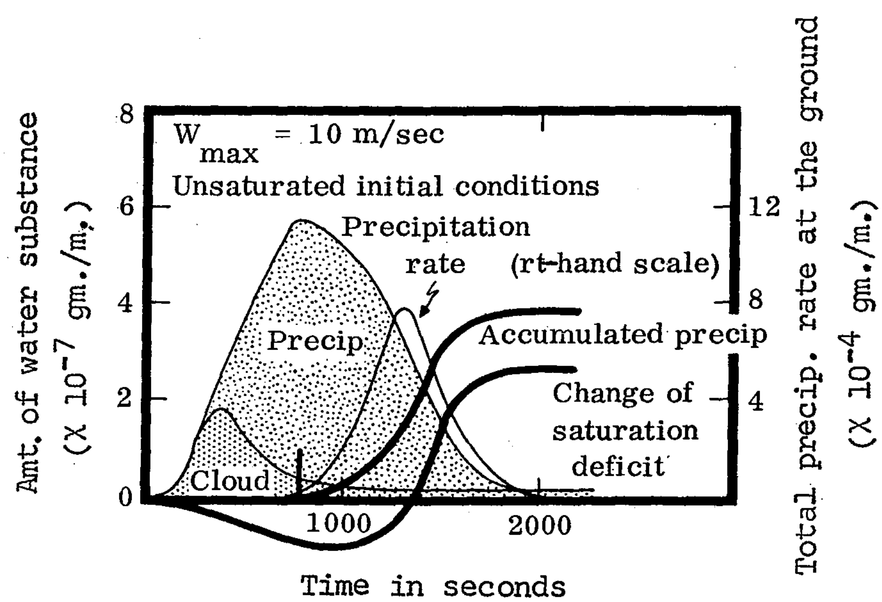

Figure 41. - Budget parameters associated with figure 40.

D. Effect of the Shape Parameter N_o on the Water Distribution in the Model Circulation Cell

Equations in Table 2 on page 29 show that the drop-size distribution parameter N_o influences the fall speed and evaporation rate of precipitation, and the rate at which precipitation collects cloud. If M and m were unchanged while N_o increased by a factor of 100, the fall speed would be reduced to .56 of the former value, the accretion rate would increase to 1.78 of the former value, and the evaporation rate would enlarge by the factor 5. However, in our model, the reduced fall speed associated with increased N_o is associated with a longer development of precipitation parcels, and hence their growth to larger values. The ultimate decrease of fall speed, therefore, is by a smaller factor than given above. The larger magnitudes of both M and N_o contribute to increased cloud collection and precipitation and evaporation rates, but these tendencies are largely offset by compensating changes of cloud and vapor m, in the model circulation.

Figure 42 shows the development of water distributions in a case where $N_o = 10^9 m^{-4}$, $w_{max} = 2.5$ m. sec.$^{-1}$, and all other parameters have exactly the same values defined in Table 2 on page 28. In other words, figure 42 shows distributions under precisely the same conditions illustrated in figure 34, except for the increase of N_o by two orders of magnitude.

Relatively slow descent and rapid evaporation of precipitation is evident in figure 42. The precipitation content at the ground should, in this case, be related to the precipitation rate by the equation $R_o = 13\ M_o^{1.125}$ mm./hr., rather than by Eq. (41) on page 24.

E. Discussion of Budget Parameters in the Model Two-Dimensional Circulation

Budget parameters based on numerical integration of the distributions displayed in figures 34-43 are presented in Table 4, and a number of interesting relationships are shown therein. Where two values are listed in columns 4, 6, 10, 15, and 16, the upper larger quantity is based on calculations of the accumulated precipitation, and the lower figure incorporates the change during problem time of the total water content within the model circulation. The difference between the two figures given suggests the uncertainty which may be attached to the calculations.

Starting with the surest and most obvious conclusion presented by Table 4, the efficiency with which condensate descends to earth in the model circulations is highest (>80%) for cases of saturated initial conditions and slow overturning of air. In such cases, more of the precipitation formed descends to the ground through the same saturated updraft which produces it. Descending air in which a small part of the precipitation is exposed to the evaporation process, is not very dry, and the evaporation process therein is correspondingly slow.

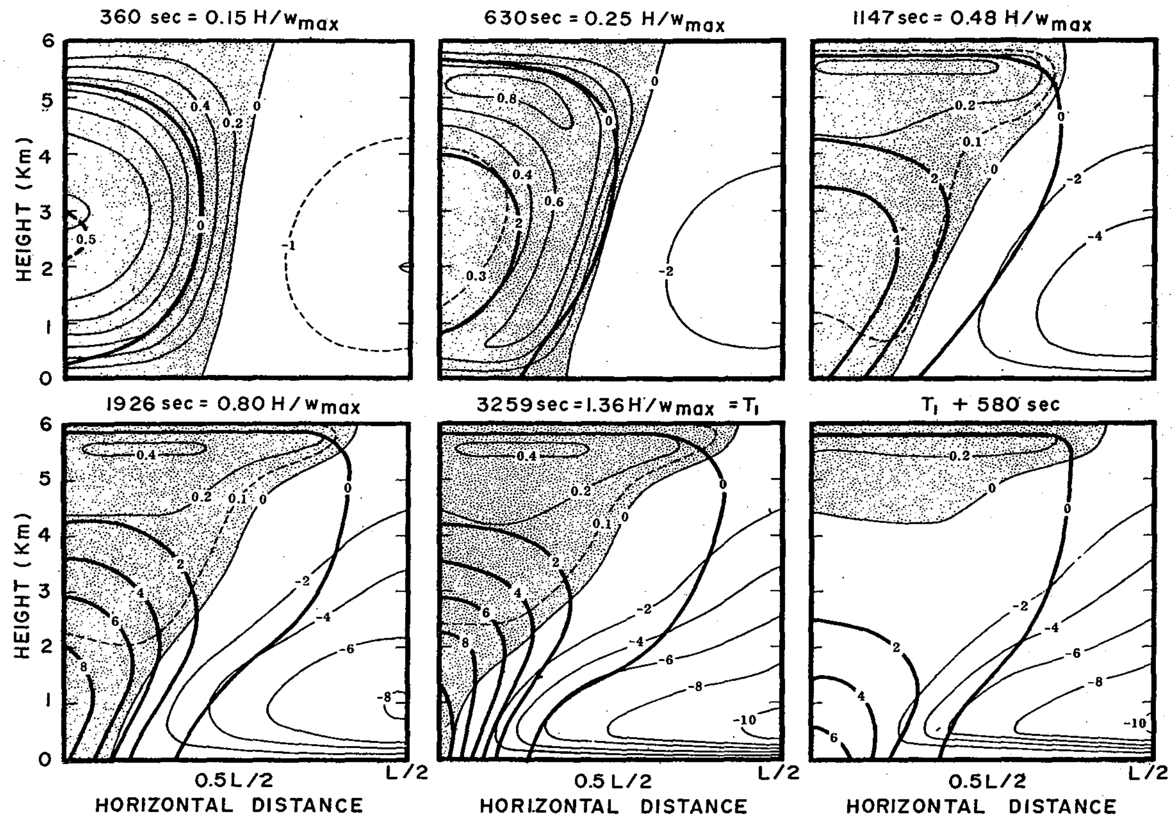

Figure 42. - Developing water distributions for saturated initial conditions with w_{max} = 2.5 m./sec. as in Figure 34, but with $N_o = 10^9 m^{-4}$.

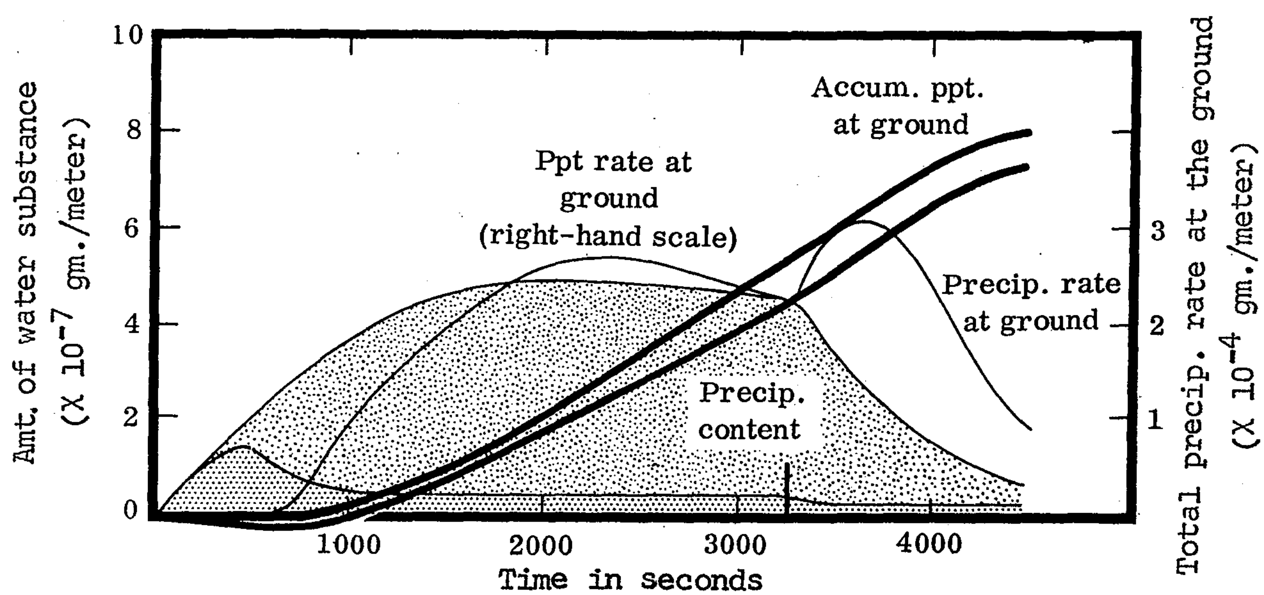

Figure 43. - Budget parameters associated with figure 42.

Table 4

Water budget parameters associated with model circulations illustrated in figures 34 - 43.

Case	2	3	4	5	6	7
Initial Water Content	w_{max}	T_1	Ppt on gnd at T_1	Ppt aloft at T_1	Total Ppt 4 + 5	Cloud at T_1
gm./m.	m./sec.	sec.	(grams per meter) $\times 10^{-7}$			
1. 28.08×10^7 (Saturated)	2.5	3253 (3240)	6.94 6.20	1.89	8.83 8.09	.66
2. 28.08×10^7	10	812 (810)	.28 -.73	9.46	9.74 8.73	.48
3. 28.08×10^7 (with $n_o = 10^9$)	2.5	3259 (3240)	5.21 4.31	4.17	9.38 8.48	.27
4. 21.33×10^7 (Unsaturated)	2.5	3251 (3240)	2.94 1.75	1.57	4.52 3.32	.59
5. 21.33×10^7	10	812 (810)	.003 -1.18	5.52	5.52 4.24	.52
6. 21.33×10^7 (with slow evaporation)	10	812 (810)	.004 -1.18	5.52	5.54 4.38	.52

$T_1 = 1.35 \frac{H}{w_{max}}$; for $t > T_1$, w, u = 0

T_2 = time when calculations stop

In columns 3 and 9, numbers in parentheses represent singular moments in problem time, and the others represent the closest time for which printout is available.

8	9	10	11	12	13	14	15	16
Total condensate at T_1 (6+7)	T_2	Precip. on grd at T_2	Precip. aloft T_2	Cloud aloft T_2	Total Cond. at T_2 10+11+12	Amt. evap. between T_1 & T_2 (av.)	Ppt x 100 / Amt. Cond.	Ppt x 100 / Total Water
	sec.	(grams	per meter) x 10^{-7}				per cent	
9.49 8.75	4912 (5000)	8.58 8.08	.040	.213	8.83 8.33	.54	84 79	31 29
10.22 9.21	2535 (2500)	7.79 6.96	.016	.178	7.98 7.15	2.15	77 68	28 25
9.65 8.75	4881 (5000)	8.16 7.37	.163	.106	8.43 7.64	1.16	81 73	30 26
5.11 3.91	4911 (5000)	4.11 3.11	.031	.196	4.34 3.34	.67	62 45	19 15
6.04 4.86	2437 (2500)	3.50 2.31	.020	.169	3.68 2.50	2.35	53 35	17 11
6.06 4.90	2437 (2500)	3.93 2.69	.022	.165	4.12 2.88	1.98	59 40	19 13

Where two values are listed in columns 4, 6, 10, 15, and 16, the upper larger quantity is based on calculations of the accumulated precipitation and the lower figure incorporates the change of the total water content since the start of calculations. The difference between the numbers indicates the magnitude of truncation errors.

The efficiency is least (~45%) in the circulation which is vigorous and initially subsaturated. In this case, considerable precipitation is spread by divergence aloft and descends through descended air whose relative humidity has been further lowered from subsaturated initial conditions.

Numerical values illustrative of the above are given in column 14 of Table 4. Compare Case 1 with 2 or 4 with 5, and note how much more of the total condensed water existing when the circulations cease, evaporates in the vigorous circulation models than in weak circulations. Now compare Cases 1 with 4 or 2 with 5, and note that even though less condensate exists when circulation ceases at time T_1 in the latter cases, a greater quantity is lost by evaporation while descending toward the ground.

Table 3 shows that only 36% of total water condenses in the model saturated circulation, and just 26% in the initially unsaturated case. Although rainfall rates at the ground exceed 6"/hr. over small areas in the model, the fraction of total water precipitated is less than a third for the most efficient case, and less than a fifth with initially unsaturated conditions. If our model circulations were deeper, air parcels would be carried higher and a greater fraction of water vapor in the model would condense and precipitate.

It is interesting to note that the sums of all condensation products at the time the circulation stops (sum of columns 6 and 7 given in column 8) are greater in the strong updraft cases (cf. Case 1 with 2, and Case 4 with 5). The principal reason for this may be as follows: When the updrafts are strong, the precipitation densities aloft increase to larger magnitudes and are more effective scavengers of cloud. Precipitation evaporates slowly in downdrafts while cloud evaporates at a rate defined by the condensation function. The smaller amounts of cloud existing in the stronger circulations reduce the role of cloud evaporation in the total budget picture. Of course, this effect is more than compensated during the precipitation - fallout phase, for reasons noted in the second and third paragraphs of this section.

One may notice that the difference between sums in the unsaturated cases (Column 8 for Cases 4 and 5) is greater than the corresponding difference in the saturated cases 1 and 2. The explanation for this is not clear to the author, but might be rooted in basic properties of the numerical procedure.

Note by comparing Cases 5 and 6 that the effect of decreasing the evaporation coefficient by 30 percent increases the total precipitation by only about 10 percent. This is due in part to the fact that much of the precipitation is not subject to evaporation in this model because it descends to earth through the saturated air column established and maintained by the updraft. A second reason is that the evaporation process is self-controlled in this model to the extent that faster evaporation rates lead to more nearly saturated air and slower rates.

It is interesting to compare the efficiencies given in column 15 of Table 4 with those estimated by other investigators. Braham [8] studied thundershowers of moderate size in early stages of their growth and suggests that in an average cell 5.3×10^8 Kg is condensed and 10^8 Kg falls as rain; the typical efficiency is then about 18 percent. Newton and Fankhauser [32], however, cite a squall line example where the efficiency is about 50 percent, and suggest that the efficiency in larger isolated storms is comparable. In the case of a large isolated thunderstorm in Oklahoma in 1964, Fankhauser estimated on the basis of aircraft, radar and raingage data that 60 percent of water intercepted by the storm was deposited as rain [12]. This is larger than comparable data in Column 16 of Table 4, but is certainly plausible in view of the great vertical depth of real thunderstorm circulations compared to the circulation models treated in this paper. It should be noted that in deeper circulations, the condensed water is greater, and we should anticipate an increased percentage in Column 16 of Table 4 as the depth of circulation increases. On the other hand, much condensed water would be carried to higher levels in taller circulation cells, especially when the vertical currents are strong. Then there is more time for precipitation to evaporate again as it descends to the ground, and we expect a decline in the percentage of condensed water precipitated (Column 15) as the depth of circulation increases.

It has already been shown clearly that precipitation efficiencies are lower in drier atmospheres, other factors being constant. In a drier atmosphere, the clouds formed by any given ascent are thinner, a smaller amount of cloud changes to precipitation, and a greater part of the precipitation formed evaporates again during descent.

Mixing between cloud and environment is a process not explicitly treated in the present model; this process would tend to deplete cloud and reduce efficiencies, especially when the ambient atmosphere is dry, and this process must be most important when clouds are small.

These considerations lead the author to believe that the various efficiency magnitudes reported in the prior literature may all be reasonably representative of the convective processes with which they are associated. The present theory confirms the idea that amounts of water between none and perhaps 80 percent of the total present in the involved air mass can be discharged as precipitation. It also confirms another of nature's checks and balances: water tends to be conserved in the drier atmospheres.

10. SOME IMPLICATIONS OF THE MODEL AND SUGGESTIONS FOR FUTURE WORK

A. Interpretation of Radar Weather Data

In the example circulations shown, the total precipitation is much better defined by the total displacement of air parcels than by the rate of displacement. However, the distribution of precipitation within the air mass is very sensitive to the circulation intensity. Since the large particles of precipitation are readily detected by radar, this sensitivity provides important clues for the interpretation of radar weather data. For example, figures 44 and 45, derived from tabulations like that shown in figure 33, illustrate the temporal development of vertical profiles of horizontally integrated precipitation water content in the model circulations in figures 34 and 36. It is interesting that in both figures, the space-averaged vertical profiles show a maximum aloft, though the maximum is much greater in the stronger circulation. This suggests that the shape of averaged vertical profiles of radar echoes should measure the characteristic intensity of convection.

Figure 46 strengthens this idea. This figure shows two vertical profiles corresponding to the time- and space-averaged precipitation content in the initially saturated, strong and weak circulations. Both profiles represent averages over 5000 second intervals, and like figures 44 and 45, over both ascending and descending branches of the circulation. From this result, it is a small step to equate time and ensemble averages and to deduce a correspondence between the height profile of total water derived from scans at different elevation angles with the radar plan-position indicator (PPI), and the intensity of convection. Indeed, this has already been considered by Hamilton with remarkable results [13]. Using a CPS-9 radar with 1° beam, Hamilton found that the vertical profile of the total precipitation content

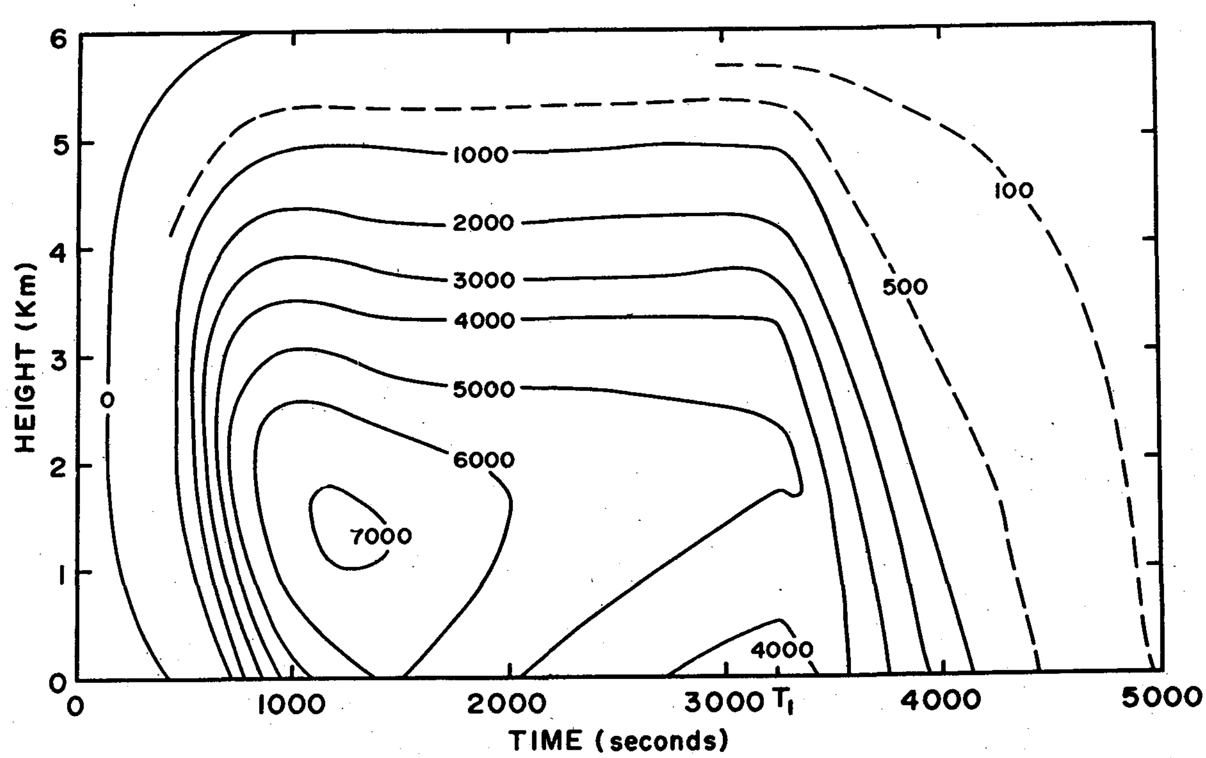

Figure 44. - Total precipitation water in grams in 1 m^2 cross sections extending horizontally at different heights through the model circulation cell 6 km. wide illustrated in figure 34, as a function of time. The circulation ceases at time T_1, and precipitation thereafter falls out.

has a maximum whose height increases with the convective energy (positive area) determined from nearby radiosonde ascents.

It should also be noted that the radar view of a particular cell is determined partly by cell size. For example, when the storm is very large, the core vertical profile should be accurately perceived. However, when the dimensions of cells are only of the order of the radar beamwidth, space-averaged data like those in figures 44 and 45 are applicable. In either event the increase of echo intensity with height should be more pronounced in the stronger circulations.

These results are also important for the estimation of rainfall by radar. Since the radar beam illuminates a volume at a height above the ground which increases with range, the reflectivities can have no correspondence as singular as the Z-R relationship, with showery precipitation at the earth's surface. The correspondence between reflectivity magnitudes and precipitation rate at the earth's surface must vary with the intensity of convection, the radar range, and the elevation of the radar beam, even when that elevation is only zero to a few degrees. The theoretical data reinforce the thought that radar data may underestimate widespread heavy rains in which updrafts are nearly uniform but less than about 2 m./sec. (substantially less than precipitation fall speeds, but corresponding to a steady

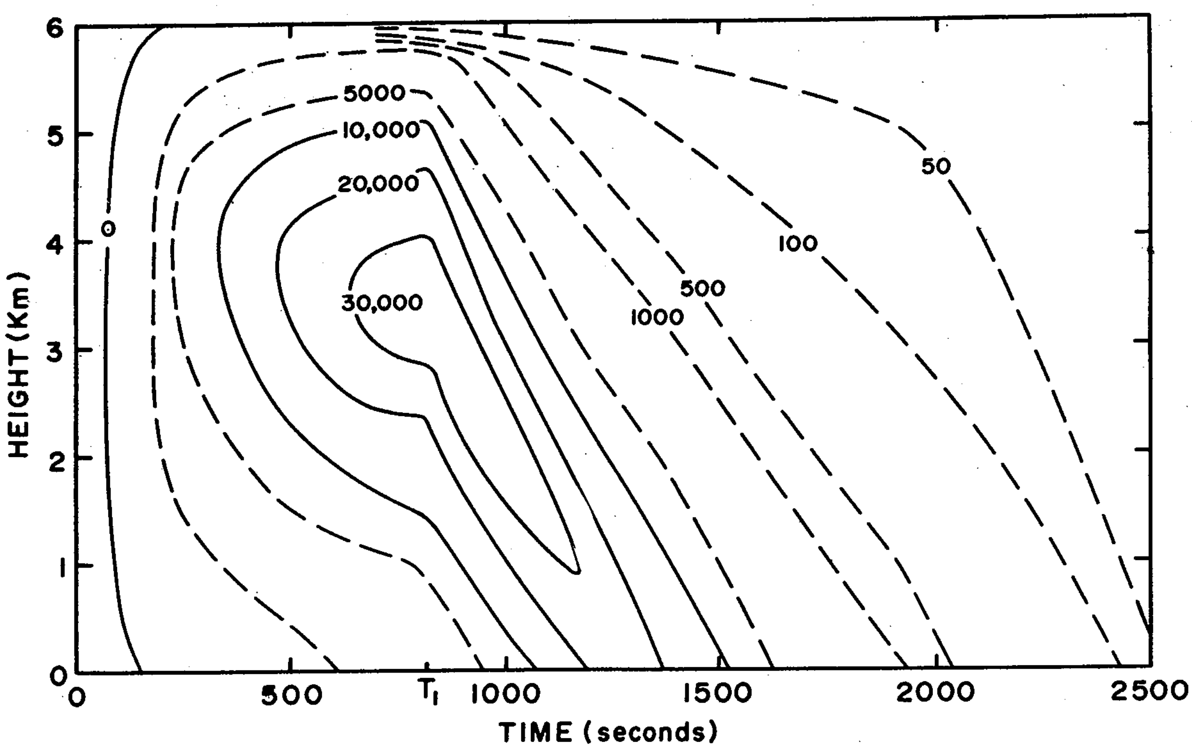

Figure 45. - Same as figure 44, except the corresponding model cell is the strong circulation illustrated in figure 36. Note that maximum accumulation of precipitation water is in the upper half of the cell during the entire time that the circulation is active.

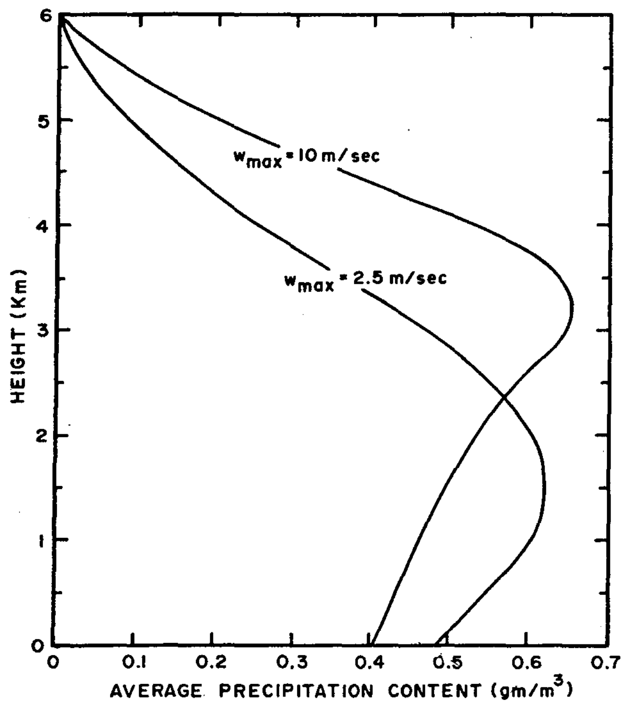

Figure 46. - Average water content in grams per cubic meter as a function of height in the model cells represented in figures 34 and 44, and 36 and 45. The average is taken over 5000 sec., during which the intense circulation is active for 810 sec., and the weak circulation for 3240 sec.

precipitation rate of about 70 mm./hr. in a tropical atmosphere). Much precipitation growth in such cases occurs in lower strata not well illuminated by the radar beam.

On the other hand, during intense convection, the radar beam at considerable range may fully illuminate the large water contents aloft which are ultimately deposited (substantially) on the ground. Errors in radar-rainfall estimates in these cases may be augmented by non-linear associations between durations of accumulation (and of observation) and durations of deposition.

Another indication of this study concerns the heights of radar echo centers. Figures 47 and 48 illustrate the temporal development of the vertical profile of precipitation content at updraft cores for maximum updrafts of 2.5 and 10 m./sec. respectively, in cases where $\mathbb{D} = 1.35$, and the circulation phase is followed by fallout of precipitation in still air. Parameter values are again those of Table 2, except the conversion threshold, $a = 1.0$ gm./m.^{3} in these cases. Note that the locus of maximum precipitation water content is lifted substantially when $w_{max} = 10$ m./sec., but descends practically from the start when $w_{max} = 2.5$ m./sec. This indicates that during early stages of convection, the maximum radar echo should be observed at higher altitudes when the updraft is strong. It is evident that with increased conversion threshold a, decreased conversion rate k_1, and increased w_{max}, the height at which appreciable precipitation and radar echoes first appear must tend to depend on the displacement parameter $\mathbb{D}$ in a way suggested by the maxima of the cloud profiles in figure 21.

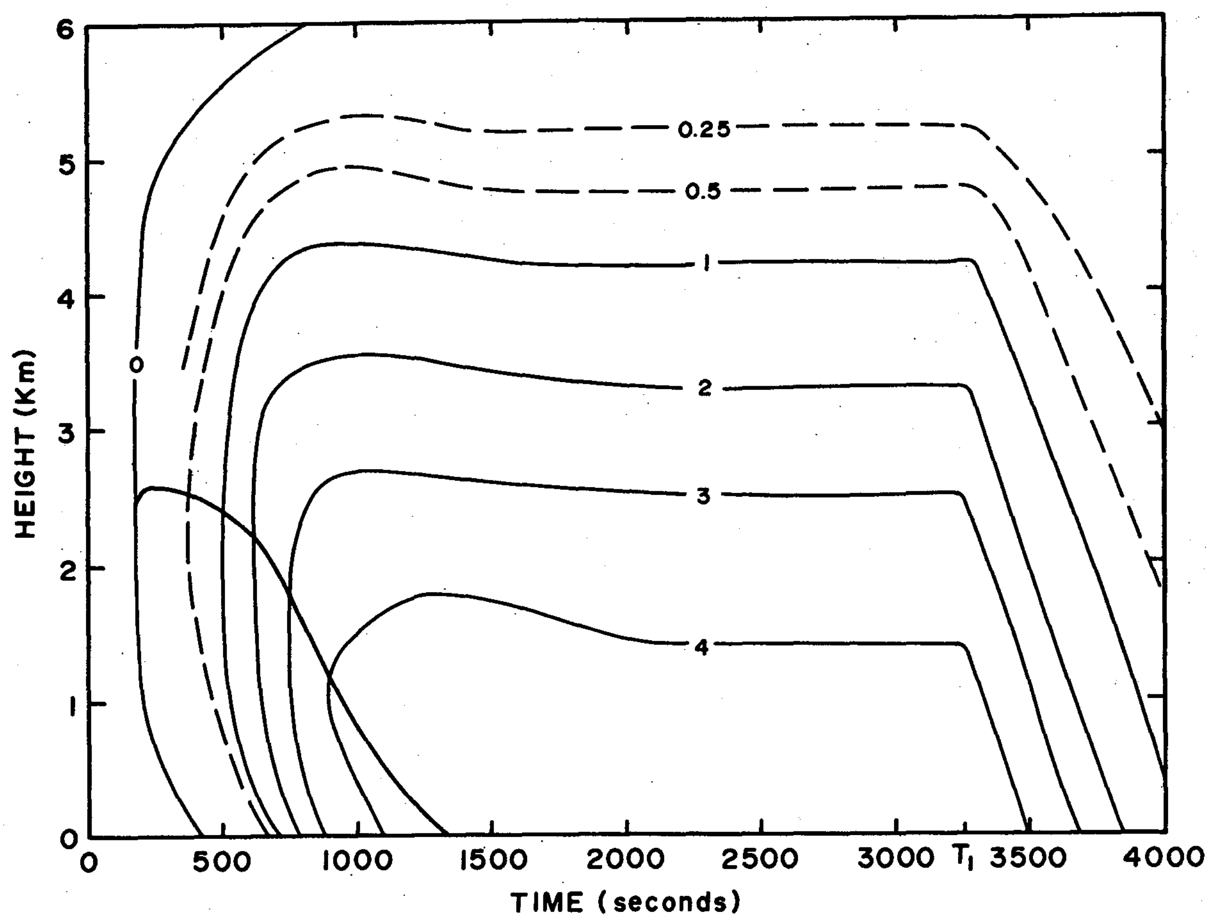

Figure 47. - Development of the vertical profile of precipitation in a saturated updraft. Isopleths are labeled in gm./m.^{3} The maximum updraft is 2.5 m./sec. and the heavy solid line marks the maximum water content in relation to problem time. After T_1 the circulation is zero and precipitation descends in still air. Parameters of Table 2 apply except the cloud conversion threshold a = 1.0 gm./m.^{3}

B. Implications of Microphysical Parameters for Weather Modification and Global Climate

(1) Weather modification

These studies indicate that the moisture content of the air, the shape and depth of the circulation, and the displacement parameter $\mathbb{D} = w_{max}\ t/H$ are important factors influencing the amount of precipitation deposited on the ground. In the kinematic framework considered here, the microphysical parameters assume secondary roles. In this connection, however, the limitations of the model should be remembered: updrafts in the real world are regulated by dynamical factors which are influenced by microphysical processes. In any event, even secondary

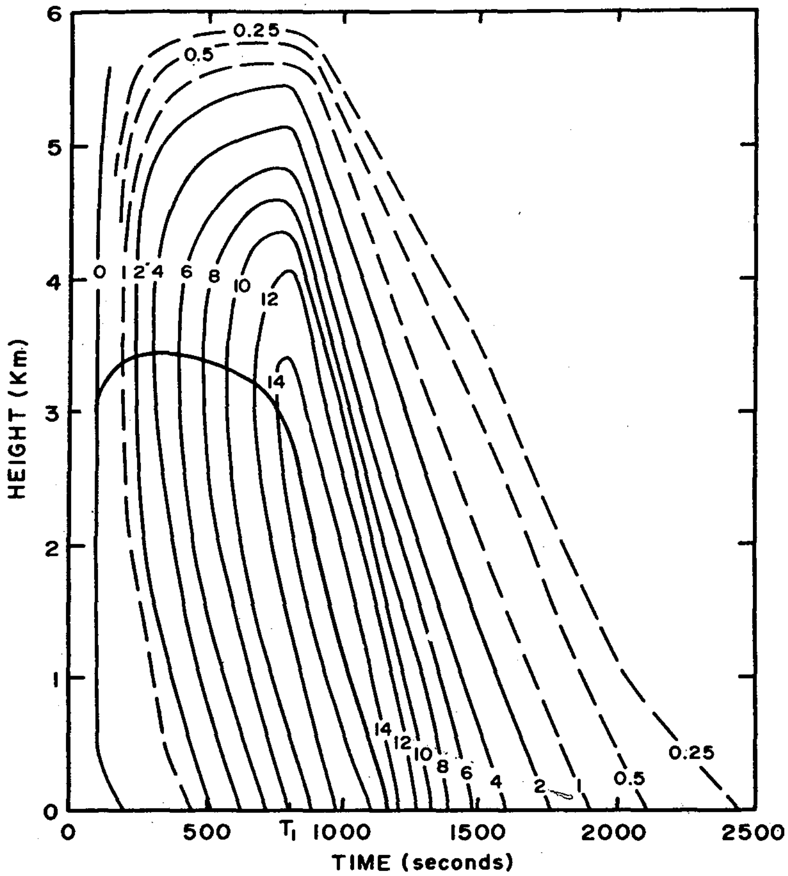

Figure 48. - Same as figure 47 except w_{max} = 10 m./sec.

effects may be important, as shown by the purely kinematic study of changes in the temporal and spatial distributions of precipitation implied by changes in the microphysical parameters.

For example, when the cloud conversion rate and collection rate are smaller, the onset of precipitation from showers is delayed; such delay might be associated with a downwind displacement of precipitation at the ground. Reduced cloud conversion and collection rates are associated with larger amounts of cloud aloft; in a situation orographically influenced, some of the increased cloud might be carried over mountains to contribute precipitation on the ordinarily dry lee side, with loss of relatively unneeded precipitation at windward. If raindrops could be made to develop smaller than natural size, they would fall more slowly, and the probability of significant precipitation downwind over a ridge would rise. Cloud amounts associated with more numerous smaller raindrops would probably decrease, however, as shown by figure 19.

When cloud conversion and accretion rates are sufficiently small, rainfall decreases, and the amount of cloud evaporated in the descending branches of the circulation increases. Moisture not precipitated is retained in the atmosphere and contributes to future precipitation. Squires and Twomey [44] in their study of differences between continental and maritime cumuli, have cited the absence of giant salt nuclei in continental air, and the presence there of many small nuclei and cloud drops, as explanations for a noticeable inefficiency of the continental clouds with respect to the release of warm rain. The effects of condensation nuclei are represented by Eq. (28) discussed in Section 6b.

If cloud conversion and accretion were made larger in a particular case, rainfall would start sooner, and its steady rate would increase, especially if the precipitation rate to begin with were considerably less than the rate of condensation.

Attempts to modify precipitation distributions might be pursued in a region where the precipitation regime is nearly steady and air trajectories known or measurable. Analyses of the weather situations, including measurements of cloud water contents and distributions of surface rainfall, should indicate approximate values of microphysical parameters and updrafts which could be incorporated into quantitative analyses to show whether appreciable benefits would accrue from their artificial modification. Cloud conversion might be assisted by introduction of relatively small numbers of giant salt nuclei and water drops. Conversion might be decreased by introducing very large numbers of very small nuclei, and Weickmann [46] has presented a preliminary quantitative analysis of such condensation nuclei seeding. Raindrops might be made smaller by introducing a surface-active agent to reduce the drops' surface tension and promote breakup. A freezing process might be aided by the well-known technique of seeding with dry ice or silver iodide [29, Chapter VII], or a freezing process might be suppressed by use of organic substances which become absorbed on the surfaces of freezing nuclei with a lowering of their activation temperature [7].

In the present model, the microphysical parameters which link the condensation and precipitation processes are much more decisive with respect to the distributions of water substance aloft, than to precipitation on the ground. This may serve to emphasize the inadequacy of the present purely kinematic treatment. The distribution of cloud and precipitation aloft are associated with thermodynamic effects which must influence the displacement parameter $\mathbb{D}$. Through this link, essentially unexplored in the present paper, the microphysical parameters may exert highly significant control of surface precipitation, at least in particular situations.

Another dynamical link between the microphysical parameters and the circulation is defined by the heat released during the freezing of undercooled cloud drops. This should be important when vertical velocity development is unstable with respect to small changes of the temperature distribution. The artificial modification of this heat source and possible implications for hurricane and cumulonimbus circulations have been discussed recently by Malkus and Simpson [27], Battan [5], Simpson et al. [39, 40], and Ruskin [37].

(2) Global climate

The cloudiness of the earth's atmosphere depends largely on the stability of clouds. When cloud conversion and accretion are smaller, less precipitation is formed and deposited at the ground, and a greater portion of condensate evaporates at high levels either in dry air diffusively entrained, or in the downdrafts which accompany updrafts. If the processes of cloud conversion and accretion were reduced on a global scale, a new state of statistical equilibrium might be attained where more atmospheric moisture and clouds would tend to offset clouds' reduced effectiveness as precipitation producers. Significantly increased atmospheric moisture and cloudiness would be associated with increased atmospheric opacity to the earth's long wave black-body radiation, and increased albedo, with accompanying temperature changes. If changes of the microphysical parameters were confined to either the warm (coalescence) or cold (ice-crystal) regimes, or if changes were substantially different for the two regimes, the shape of the mean latitudinal temperature profile might be altered, with further consequences for the shape and intensity of the general circulation. Perhaps the earth's historical and prehistorical climates have been affected by variations of the microphysical processes, responding in turn to variations of atmospheric trace constituents, or to the quality of solar radiation.

C. Other Suggestions for Further Study

Important contributions to meteorology would ensue from several kinds of further developments.

First, the framework presented here might be a basis for more realistic modeling of real weather systems. For example, the three-dimensional asymmetrical circulation suggested by Browning [9] as a model for some severe storms, could be examined in relation to the consistent distributions of associated water substance. Results compared to radar echo and other data might suggest a series of adjustments leading to more adequate representations of storm circulations and microphysical processes. Another related problem involves the development of numerical models which retain manageable computational properties while giving separate treatment to families of particles falling at different speeds. Such models would furnish improved understanding of deep and strong convection in which snow, rain, and hail are mixed at high altitudes, and rain and hail are mixed at low altitudes.

Second, the applications of continuity principles with radar data may provide important means for characterizing atmospheric transport processes. Ultimately, the heat and momentum might all be characterized in terms of echoes' statistical properties combined with other observational data. Echo properties already studied in the context of data processing include the average intensity and variance, the echo sizes, the tendency to pattern bandedness, and the echo coverage [2, 24, 48]. Development of such a science of "mesoscale turbulence" might be assisted by extension of the results presented in figures 44-46 in this paper. For example, one might answer the question "What statistical properties of the radar echo distribution are associated with vertical circulations with characterized distributions of sizes, intensities and durations?"

A third area in which more work is needed involves incorporation into a dynamical system of the continuity principles governing distributions of water substance. To provide a truer measure of the role of microphysical processes in precipitation production, such a system must allow the evolving water distributions to be felt in the fields of pressure and hence of motion. However, the formulation of a consistent and workable model so complete is very difficult.

11. APPENDICES

A. The Difference between the Horizontal Speed of Raindrops and the Horizontal Wind Speed

The precipitation-cloud models discussed in this paper are based in part on the assumption that the horizontal speed of condensate is the same as the horizontal speed of the air. The validity of this assumption must decrease with increasing size of condensation particles; a fair test of the assumption is therefore given by examination of the equation of motion for a large raindrop.

The horizontal resisting force on a spherical raindrop is given by

$$f_r = 3\pi\mu D(u-U)\,\frac{C_D R_e}{24} \quad / \,, \tag{A1}$$

where μ is the viscosity of air, u is the horizontal velocity of the air, U is the horizontal velocity of the drop, C_D is the drag coefficient, and R_e is the Reynold's number [17, p. 121]. Consider a drop falling at terminal speed through a layer wherein there is vertical shear of the horizontal wind. The drop is accelerating horizontally due to the force associated with a difference between its horizontal velocity and the horizontal air motion. This force given by Eq. (A1) is equal to the mass of the drop times its horizontal acceleration, i.e.,

$$3\pi\mu D(u-U)\,\frac{C_D R_e}{24} = \frac{\pi}{6} D^3 \rho_\ell \frac{dU}{dt} \quad , \tag{A2}$$

where ρ_ℓ is the density of liquid water. Consider a drop of radius 0.24 cm. The quantity $C_D R_e/24 \doteqdot 77$ and $\mu \doteqdot 1.8 \times 10^{-4}$ gm. cm.$^{-1}$ sec.$^{-1}$ Substitute these values in (A2) to obtain

$$\frac{dU}{dt} = 1.09(u - U). \tag{A3}$$

Nothing of importance to this development is lost by considering the case where the shear is uniform and the difference between the horizontal wind speed and drop speed is constant. Then the drop's falling speed, about 907 cm. sec.$^{-1}$ and the shear $\partial u/\partial z = S$ determines du/dt, the time rate of change of u (and U) at the drop,

$$\frac{du}{dt} = \frac{dU}{dt} = \frac{dz}{dt}\frac{\partial u}{\partial z} = 907S. \tag{A4}$$

Substitute for du/dt in (A3) from (A4) to get

$$u - U = \frac{907S}{1.09} \tag{A5}$$

When S is 0.02 sec.$^{-1}$ (20 m./sec. km., a very large value), u - U is only 16.64 cm./sec., less than 1% of representative horizontal wind speeds.

So long as u - U is small compared with the terminal fall speeds, the method employed here yields an accurate measure of u - U. The generalization to variable shear and variable u - U is obvious but of little practical interest to this work since u - U is so small.

B. Method for Numerical Solution[9]

(1) Model updraft columns

The computer program for the numerical solution of cloud and precipitation distributions in model updraft columns follows a method first suggested by P. D. Lax [25]. For computations at interior points, the equations (8) and (9) (compressibility terms omitted) are used in their divergence form

[9]The principal author of this section is Dr. E. A. Newburg, Travelers Research Center, Hartford, Connecticut.

$$\frac{\partial U}{\partial t} + \frac{\partial F}{\partial z} = B \quad , \tag{A6}$$

where U, F, and B are the vectors

$$U = \begin{bmatrix} M \\ m \end{bmatrix} ; \quad F = \begin{bmatrix} (w+V)M \\ wm \end{bmatrix} ; \quad B = \begin{bmatrix} B_1 \\ B_2 \end{bmatrix} \quad ; \tag{A7}$$

and the B's are given by

$$\begin{aligned} B_1 &= M \frac{\partial w}{\partial z} + \text{microphysical terms} \\ B_1 &= m \frac{\partial w}{\partial z} + wG + \text{microphysical terms.} \end{aligned} \tag{A8}$$

The finite difference formulation is

$$\begin{aligned} U(z,t+k) = \overline{U}(z,t) + \frac{k}{2h}\{F(z-h,t) - F(z+h,t) \\ + h[B(z+h,t) + B(z-h,t)]\} \quad , \end{aligned} \tag{A9}$$

where

$$\overline{U}(z,t) = \frac{1}{2}[U(z+h,t) + U(z-h,t)], \tag{A10}$$

and k and h are the increments of time and space, respectively.

Exceptions to (A9) occur at upper and lower boundaries and at the grid point adjacent to the upper boundary. At the upper boundary, $m = 0$ (or m may be less than 0), and M is a constant (usually zero). At the lower boundary

$$M(0,t+k) = M(0,t) + \frac{k}{h}[M(0,t)V(0,t) - M(h,t)V(h,t) + hB(0,t)]$$

$$m(0,t+k) = m(0,t) + kB(0,t), \tag{A11}$$

where the terms in $\partial w/\partial z$ are omitted from the B's.

A special equation is suggested near the upper boundary because analytic solutions of simple models show that relatively large values of cloud may exist quite near the upper boundary, at which m is zero or, in an initially dry atmosphere, negative. Such large values of m are brought there by upward air currents and persist in the absence of precipitation to collect it. Equation (A9) involves averaging which may result in fictitious cloud depletion near the upper boundary. Although this averaging tends to zero in the limit of many grid points, this boundary influence can be more effectively removed by modifying the computational method.

Accordingly, at the grid point adjacent to the upper boundary, the m - part of (A9) is modified to the form

$$m(H-h,t+k) = m(H-h,t) + \frac{k}{h}[m(H-h,t)w(H-h,t) + hB(H-h,t)] \quad . \tag{A12}$$

This equation employs no averaging in its approximation of the time derivative, and uses a one-sided approximation to the advection term.

In the cases discussed in Section 8 of this paper, $h = .01H$, and the choice of k is based on the more stringent of the classical stability criteria $k < (h/|V + w_{max}|)$ and $k < (h/|w_{max}|)$.

(2) Two-dimensional model circulations

The finite difference scheme used for numerical solution of the two-dimensional time dependent problem discussed in Section 9 above is presented in detail in Reports 4 and 5 of [21]. This scheme incorporates several ad hoc procedures, adopted under pressure of time to achieve stability. Work on cloud models subsequent to that discussed in this paper has led to replacement of these procedures with the Two-Step Lax-Wendroff Scheme, which has been described by Richtmyer [35].

The question of existence and uniqueness for the quasi-linear hyperbolic system (8) and (9) cannot be answered at present. It is a reasonable conjecture that a unique continuously differentiable solution does not exist for conditions of M,m = 0 initially. R. Courant [11] has established the existence of a continuously differentiable solution for the hyperbolic system $u_t + A(x,t,u)\, u_x + B(x,t,u) = 0$, with initial data $u(x,0) = f(x)$ on some interval of the x-axis. His method of proof requires that $A(x,t,u)$ and $B(x,t,u)$ be continuously differentiable in the domain of x, t, u under consideration. Our problem fails to satisfy this condition.

Since Courant's proof follows from the weakest hypothesis deemed reasonable for success in solving the problem, it is felt that a unique solution for the equations of clouds and rain must perforce be a generalized solution which allows discontinuities in the derivatives of the solution vector. We believe that a solution of this type might be established along the lines followed by Kuznecov and Rozdestvenski [25]. However, due to the rather abstract and purely mathematical nature of this problem we have devoted no further effort to it.

The incomplete theory of the techniques used in this investigation is not satisfying to a mathematician. However, this fact is not cause for rejection of the results of the computations. The physical reasoning underlying the mathematical formulation of this problem and the numerical results of these and similar calculations of others (e.g., P. D. Lax [26]) imply strong credibility for the results. The semi-empirical approach used here is typical in the development of new methods. As R. D. Richtmyer [34] has said, ". . . if we were to wait for convergence proofs and error estimates for the new methods, most of the computers now in use in technology and industry would come grinding to a halt."

ACKNOWLEDGMENT

The study presented above was made possible by the substantial assistance and advice of colleagues at Travelers Research Center, especially Dr. Edward A. Newburg, mathematician, Mr. Gerald Wickham, programmer, and Mr. Pieter Feteris, meteorologist, of whom the last named is now with the Illinois State Water Survey. The U. S. Army Electronics Research and Development Laboratories furnished financial support during 1961-1964 and helpful advice and encouragement from Dr. Helmut Weickmann, now with ESSA, and Mr. Marvin Lowenthal. Mrs. Horace Hudson, Dr. Gilbert Kinzer and Dr. Joanne Simpson read the manuscript before final typing and offered many useful suggestions. A difficult typing job was done by Mrs. John Horwitz and most of the illustrations were prepared by Mr. Carlos Droescher. This note of appreciation is given also to the many other persons who helped this work in various ways from time to time.

REFERENCES

1. Ackerman, B., "The Variability of Liquid Water Content of Tropical Cumuli," Journal of Meteorology, vol. 16, No. 2, 1959, pp. 191-198.

2. Armijo, L., "Statistical Properties of Radar Echo Patterns and the Radar Echo Process," NSSL Report No. 27, ESSA (In press, Journal of the Atmospheric Sciences, vol. 23, No. 5, Sept. 1966, pp. 560-568.

3. Atlas, D., "Optical Extinction by Rainfall," Journal of Meteorology, vol. 10, No. 6, 1953, pp. 486-489.

4. Bannon, J. H., "The Estimation of Vertical Currents from the Rate of Rainfall," Quarterly Journal of the Royal Meteorological Society, vol. 74, No. 1, 1948, pp. 57-66.

5. Battan, L. J., "Comments on 'Note on the Potentialities of Cumulonimbus and Hurricane Seeding Experiments,'" Journal of Applied Meteorology, vol. 4, No. 3, 1965, pp. 426-427.

6. Berry, E. X., "Cloud Droplet Growth by Collection - A Theoretical Formulation and Numerical Calculation," PhD. Thesis at University of Nevada, Reno, 1965; Available from University Microfilms, Ann Arbor, Michigan.

7. Birstein, S. J., "Absorption Studies of Heterogeneous Phase Transitions," Geophysics Research Papers No. 31, Air Force Cambridge Research Center, Bedford, Mass., 1954.

8. Braham, R. R., Jr., "The Water and Energy Budgets of the Thunderstorm and Their Relation to Thunderstorm Development," Journal of Meteorology, vol. 9, No. 4, 1952, pp. 227-242.

9. Browning, K. A., "Some Inferences about the Updraft within A Severe Local Storm," Journal of Atmospheric Sciences, vol. 22, No. 6, 1956, pp. 669-677.

10. Cole, A. E., "Surface Rates of Precipitation," Handbook of Geophysics, Air Force Cambridge Research Laboratories, Bedford, Mass., 1957, pp. 6-1 to 6-5 (see figure 6-4, p. 6-3).

11. Courant, R., "Cauchy's Problem for Hyperbolic Quasi-Linear Systems of First-Order Partial Differential Equations in Two Independent Variables," Communs. Pure and Applied Math., vol. 14, No. 3, 1961, pp. 257-263.

12. Fankhauser, J. C., "Some Physical and Dynamical Aspects of a Singular Cumulonimbus Observed by Instrumented Aircraft and Radar," Proceedings 12th Conf. Radar Meteorology, American Meteorological Society, Boston, Mass., 1966, pp. 405-413.

13. Hamilton, P. M., "Vertical Profiles of Total Precipitation in Shower Situations," Quarterly Journal of the Royal Meteorological Society, vol. 92, No. 393, 1966, pp. 346-362.

14. Hardy, K. R., "A Study of Raindrop-Size Distributions and Their Variation with Height," PhD dissertation, University of Michigan, 1963, p. 53.

15. Haurwitz, B., Dynamic Meteorology, New York, McGraw Hill, pp. 129-130.

16. Houghton, H. G., "A Preliminary Quantitative Analysis of Precipitation Mechanisms," Journal of Meteorology, vol. 7, No. 6, 1950, pp. 363-369.

17. Johnson, J. C., Physical Meteorology, John Wiley & Sons, New York, 1954

18. Kessler, E., "Kinematic Relations between Wind and Precipitation Distributions," Journal of Meteorology, vol. 16, No. 6, 1959, pp. 630-637.

19. Kessler, E., "Kinematic Relations between Wind and Precipitation Distributions, II," Journal of Meteorology, vol. 18, No. 4, 1961, pp. 510-525.

20. Kessler, E., "Elementary Theory of Associations between Atmospheric Motions and Distributions of Water Content," Monthly Weather Review, vol. 91, No. 1, 1963, pp. 13-27.

21. Kessler, E., Newburg, E., Feteris, P. and Wickham, G., "Relationships between Tropical Precipitation and Kinematic Cloud Models," Reports 1-5, Contract DA 36-039 SC 89099 between Travelers Research Center and the U. S. Army Electronics Research and Development Laboratory, 1961-1964.

22. Kessler, E., "Lightning Discharge and Precipitation," Quarterly Journal of the Royal Meteorological Society, vol. 92, No. 392, April 1966, pp. 308-310.

23. Kessler, E., "Radar Measurements for the Assessment of Areal Rainfall: Review and Outlook," Water Resources Research, vol. 2, No. 3, 1966, pp. 413-425.

24. Kessler, E., "Computer Program for Calculating Average Lengths of Weather-Radar Echoes and Pattern Bandedness," Journal of Atmospheric Sciences, vol. 23, No. 5, Sept. 1966, pp. 569-574.

25. Kuznecov, N. N. and Rozdestvensku, B. Z, "Existence and Uniqueness of the Generalized Solution of the Cauchy Problem for a Non-Homogeneous Law of Conservation," Doklady Akad. Nauk, S.S.S.R. 126 (1959) (in Russian).

26. Lax, P. D., "Weak Solutions of Nonlinear Hyperbolic Equations and Their Numerical Computation," Communs. Pure and Applied Math., vol. 7, No. 2, 1954, pp. 159-193.

27. Malkus, J. S. and Simpson, R., "Note on the Potentialities of Cumulonimbus and Hurricane Seeding Experiments," Journal of Applied Meteorology, vol. 3, No. 4, 1964, pp. 470-475.

28. Marshall, J. S. and Palmer, W. McK., "The Distribution of Raindrops with Size," Journal of Meteorology, vol. 5, No. 4, 1948, pp. 165-166.

29. Mason, B. J., The Physics of Clouds, Oxford, Clarendon Press. 1957.

30. Moore, C. B., Vonnegut, B., Vrablik, E. A., and McCaig, D. A., "Gushes of Rain and Hail after Lightning," Journal of Atmospheric Sciences, vol. 21, No. 6, 1966, pp. 646-665.

31. Myers, Vance A., "Precipitable Water," Bulletin of American Meteorological Society, vol. 43, No. 6, 1962, p. 267.

32. Newton, C. W. and Fankhauser, J. C., "On the Movements of Convective Storms, with Emphasis on Size Discrimination in Relation to Water-Budget Requirements," Journal of Applied Meteorology, vol. 3, No. 6, 1957, pp. 651-668.

33. Ogura, V., "Convection of Isolated Masses of Buoyant Fluid: A Numerical Calculation," Journal of Atmospheric Sciences, vol. 19, No. 6, 1962, pp. 492-502.

34. Richtmyer, R. D., Difference Methods for Initial Value Problems, Interscience Publishers, Inc., New York 1957 (see Chap. IV).

35. Richtmyer, R. D., "A Survey of Difference Methods for Non-Steady Fluid Dynamics," NCAR Tech. Notes, National Center for Atmospheric Research, Boulder, Colo., 1962, pp. 63-72.

36. Roys, George P., and Kessler, E., "Measurements by Aircraft of Condensed Water in Great Plains Thunderstorms," ESSA Tech. Note 49, NSSL Report No. 19, Washington, D.C., July 1966, 17 pp. (see Table 3, p. 7).

37. Ruskin, R. E., "Measurements of Water-Ice Budget Changes at -5C in AgI Seeded Tropical Cumulus," Project Stormfury Report 3-65, Dept. of Commerce and Dept. of Navy, Washington, D. C. (Also, in press, Journal of Applied Meteorology.)

38. Saunders, P. M., "Some Characteristics of Tropical Marine Showers," Journal of Atmospheric Sciences, vol. 22, No. 2, 1966, pp. 167-175.

39. Simpson, J., Simpson, R. H., Stinson, J. R. and Kidd, J. W., "Stormfury Cumulus Experiments: Preliminary Results 1965," Journal of Applied Meteorology, vol. 5, No. 4, August 1966, pp. 521-525.

40. Simpson, J., "Photographic and Radar Study on the Stormfury 5 August 1965 Seeded Cloud," Stormfury Report 4-65, Dept. of Commerce and Dept. of the Navy, Washington, D. C. (Also, in press, Journal of Applied Meteorology.)

41. Singleton, F. and Smith, D. J., "Some Observations of Drop-Size Distributions in Low Layer Clouds," Quarterly Journal of the Royal Meteorological Society, vol. 86, No. 370, 1960, pp. 454-467.

42. Smithsonian Meteorological Tables, Published by the Smithsonian Institution, Washington, D. C. (Sixth revised Edition, 1958).

43. Spilhaus, A. F., "Raindrop Size, Shape, and Falling Speed," Journal of Meteorology, vol. 5, No. 3, June 1948, pp. 108-110.

44. Squires, P. and Twomey, S., "The Relation between Cloud Drop Spectra and the Spectrum of Cloud Nuclei," Geophysical Monograph No. 5, American Geophysical Union, Washington, D. C., 1960.

45. Weickmann, H. K. and aufm Kampe, H. J., "Physical Properties of Cumulus Clouds," Journal of Meteorology, vol. 10, No. 3, 1953, pp. 204-211.

46. Weickmann, H. K., "A Realistic Appraisal of Weather Control," Journal of Applied Mathematics and Physics (ZAMP), vol. 14, Fasc. 5, 1963, pp. 528-543.

47. Wexler, R. and D. Atlas, "Moisture Supply and Growth of Stratiform Precipitation," Journal of Meteorology, vol. 15, No. 6, 1957, pp. 531-538.

48. Wilson, J., "Movement and Predictability of Radar Echoes," NSSL Report No. 28, ESSA, Washington, D. C., 1966.

SORTING OF RAINDROPS BY GRAVITY

ABSTRACT

Gravitational sorting of raindrops is examined with model distributions of raindrop sizes and terminal fall speeds. Analysis of an example situation shows how size distributions and precipitation rates at the ground depend on the initial height and thickness of the precipitation packet, and on the initial shape and breadth of the size distribution.

1. INTRODUCTION

It is commonly observed that the onset of a shower is marked by a few large raindrops. This is probably due to the large drops' relatively fast terminal fall speed, which carries them more quickly to the ground than the majority of drops comprising distributions formed aloft. Atlas [1], for example, has considered the variation of terminal fall speed with drop size in his analysis of radar and rainfall observations. Many processes including aggregation of particles, breakup, evaporation, and separation by gravity, participate in the evolution of precipitation particle size distributions. The present note is intended to clarify the role of the last named in affecting the size distribution of precipitation particles arriving at the ground.

2. EXAMPLE CASE

Consider a precipitation packet in a depth of atmosphere S and at a height H above the ground, as shown in figure 1, with the water content and particle sizes evenly distributed through S. The size distribution is given initially by

$$N = f_1(D)\,\delta D, \qquad (1)$$

where N is the number of raindrops in unit volume of air per range of diameter δD, and the fall speed of a drop can be defined by

$$V = f_2(D), \qquad (2)$$

where $f_1(D)$ and $f_2(D)$ are any suitable functions of diameter.

The rainfall rate δR due to drops within a range of diameter D is then given by

$$\delta R = \frac{\pi\rho}{6} D^3 V \delta N = \left(\frac{\pi\rho}{6} D^3\right) f_1(D) f_2(D) \delta D, \qquad (3)$$

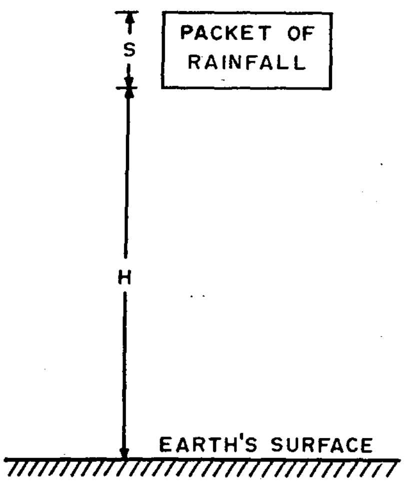

Figure 1. - Initial conditions of the problem.

where the first term in parentheses is just the mass of a single precipitation particle.

The arrival time of precipitation of size D_i at the ground from the packet at height H is

$$t_1 = \frac{H}{V_i} = \frac{H}{f_2(D_i)} \qquad (4)$$

and the duration of precipitation of this size is

$$t_2 - t_1 = \frac{S}{f_2(D_i)} \qquad (5)$$

The duration $\mathfrak{D}$ of precipitation of any size is obviously

$$\mathfrak{D} = \frac{S + H}{f_2(D_{min})} - \frac{H}{f_2(D_{max})} \qquad (6)$$

Figure 2 shows, for S and H both equal to 1 km., the times of onset and termination of drops at the ground, as a function of their size when $f_2 = 130\ D^{1/2}$ m./sec., a form suggested by Spilhaus [3]. The distance parallel to the abscissa between the two curves on figure 2 defines the duration at the ground of a given particle size originating within S. The distance parallel to the ordinate between the two curves on figure 2, defines the range of drop diameters from within S which are arriving at the ground at the same time. Figure 2 with Eq. (3) provides the basis for a complete analysis of the effect of gravitational sorting on the rainfall at the ground.

To illustrate, I have taken $f_1(D) = N_0 e^{-\lambda D}$, suggested by Marshall and Palmer [2]. A plot of R vs. D for this distribution is shown in figure 3, with $\lambda = 2.2$ mm.$^{-1}$, corresponding to a rainfall rate for the whole distribution of 25 mm./hour. The shaded portion of figure 3 shows the contribution to rainfall at the ground at 400 seconds, as determined from figure 2.

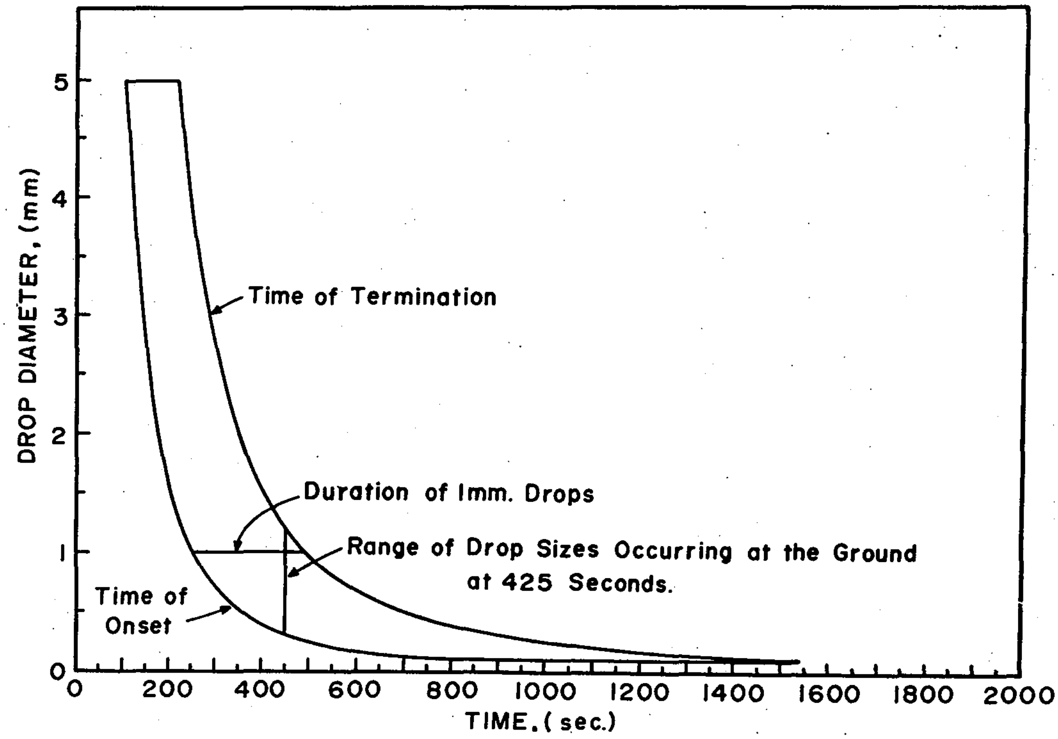

Figure 2. - Times of onset and termination of various drop sizes at the ground, for S and H in figure 1 both equal to 1 km.

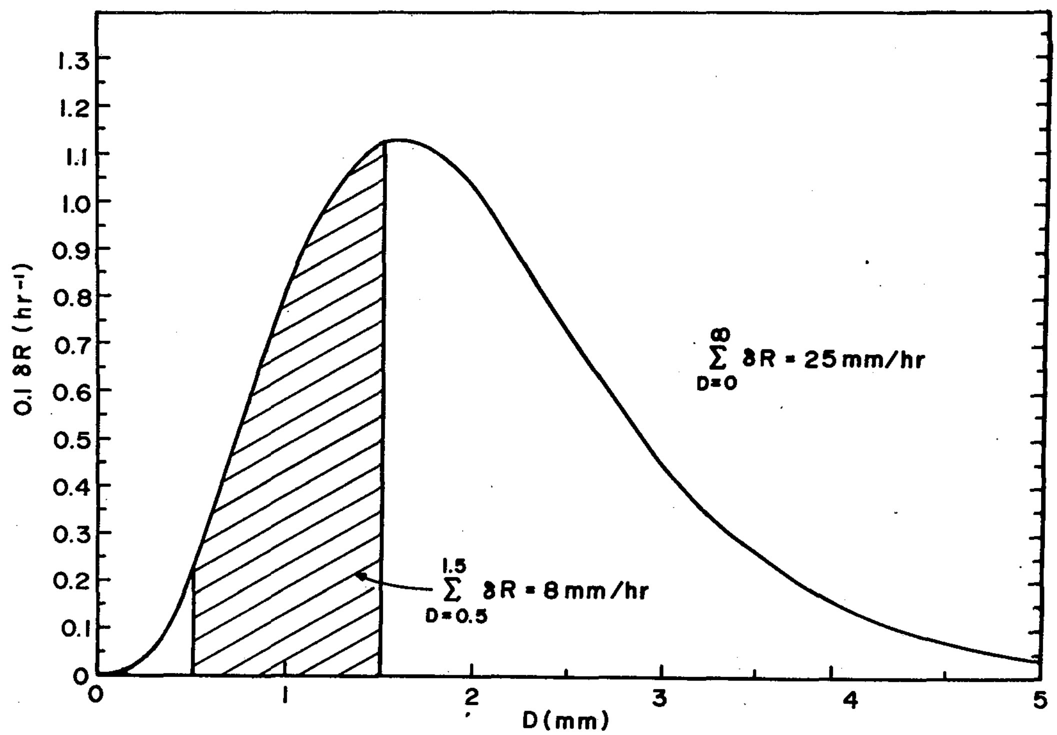

Figure 3. - Contribution to the rainfall rate by drops of different sizes in the distribution $N = 10^{-5} e^{-2.2D} \delta D mm^{-4}$. The shaded area illustrates the part contributing to rain at the ground at 400 seconds, as determined from figure 2.

Figure 4 has been prepared from tabulated values of δR and from figure 2, to show how the distribution of raindrop fall speeds influences the size of raindrops and rainfall rate at the ground as a function of time.

It is obvious from figures 1 and 2 that gravitational sorting is most marked when S is small compared to H, i.e., when the duration at the ground of any given size is short compared to the duration of all precipitation from within S. A semiquantitative criterion for gravity-sorting effectiveness is illustrated by figure 5. The ratio of the vertical depth h of precipitation at the time precipitation begins at the ground to the depth S at the start of the problem, is a stretching factor SF. When SF is very large, the distribution of raindrops arriving at the ground becomes very narrow. It is readily shown that the stretching factor is

$$SF = \frac{h}{S} = \frac{H}{S}\left[1 - \frac{V_{min}}{V_{max}}\right] + 1. \qquad (7)$$

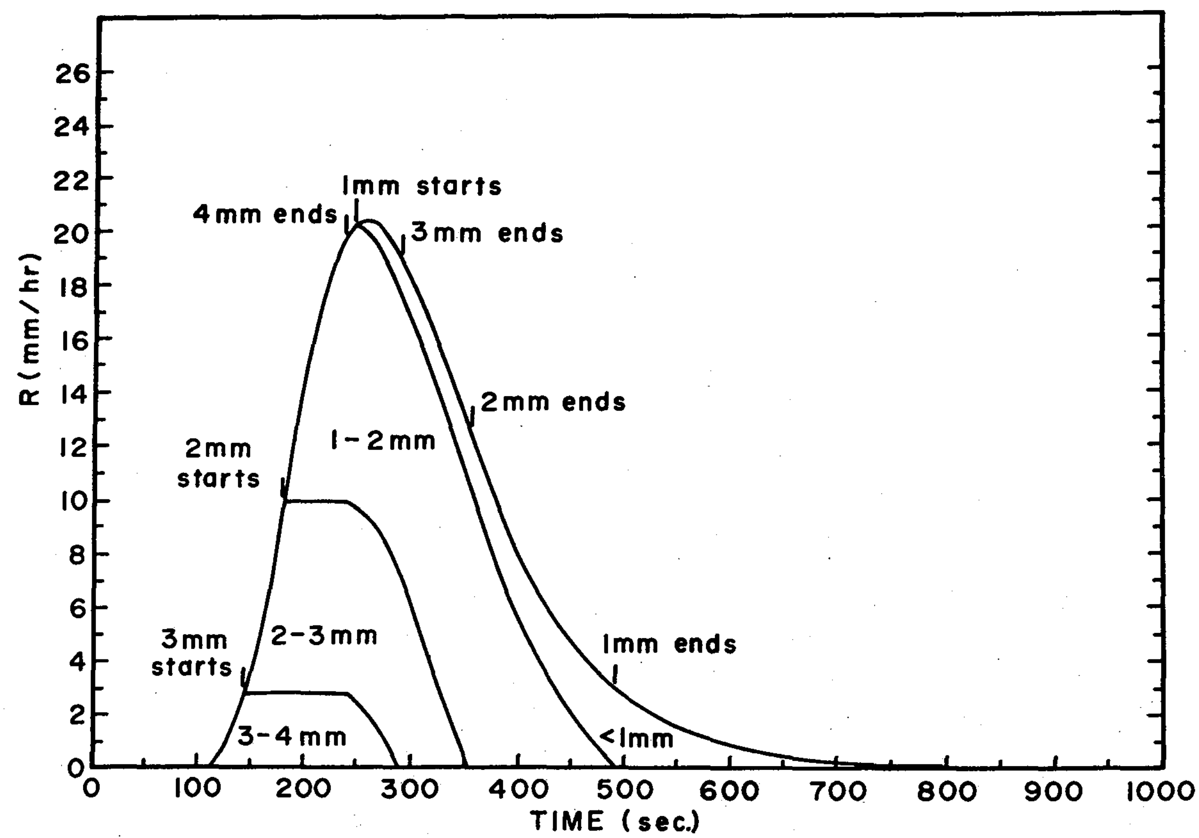

Figure 4. - Composition of rain at the ground as a function of time, due to gravitational sorting of a distribution of 0-4 mm. drops initially spread through a depth between 1 and 2 km.

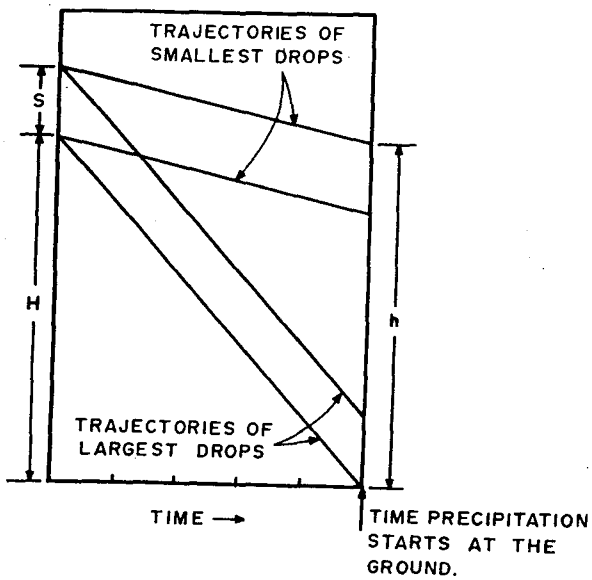

Figure 5. - Geometry of the stretching factor h/S.

When $V_{min} \sim 0$, i.e., the smallest drops are very small, (6) reduces to SF = H/S + 1. When the difference between V_{max} and V_{min} is relatively small, as in snow, H/S must be relatively large for gravity to produce appreciable sorting of particle sizes.

REFERENCES

1. Atlas, D., "Drop Size History During a Shower," Journal of Meteorology, vol. 10, No. 4, August 1953, pp. 291-295.

2. Marshall, J. S. and Palmer, W. McK., "The Distribution of Raindrops with Size," Journal of Meteorology, vol. 5, No. 4, August 1948, pp. 165-166.

3. Spilhaus, A., "Raindrop Size, Shape and Falling Speed," Journal of Meteorology, vol. 5, No. 3, June 1948, pp. 108-110.

DISTRIBUTION WITH HEIGHT OF THE RADAR ECHO COVERAGE AND ITS METEOROLOGICAL SIGNIFICANCE[1]

ABSTRACT

The radar echo coverage has been calculated on several days of two stormy periods in central Oklahoma and compared with the distributions of echo intensity near the earth's surface. The shape of the height distribution of coverage varies slowly on a given day, reflecting diurnal processes and others with periods of several hours or more. The observations indicate that the vertical profiles representing echo coverage and the areal extent of precipitation water at different heights reflect the intensity of convection. In addition, the data indicate that marked infra-diurnal changes of the fractional area covered by precipitation are not attended by marked changes in the character of the weather, as shown by the distribution of echo intensities. Applications of the data are noted.

1. INTRODUCTION

Empirical and theoretical studies [1, 2] indicate that the height-profile of precipitation averaged over horizontal area and time shows a maximum aloft whose elevation increases with the strength of the vertical air currents. For example, a study based on the model circulation illustrated in figure 1 shows profiles where the height of the maximum precipitation content rises from 1.5 km. to above 3 km. when the maximum updraft increases from 2.5 to 10 m./sec. (figure 2). In addition to its theoretical interest as an index of the intensity of convection, the average height-profile of precipitation water content has relevance for different topics represented, for example, by satellite-earth communications, precipitation avoidance by aircraft, and measurement of areal rainfall by radar, the last because the radar beam surveys precipitation at greater heights at greater ranges.

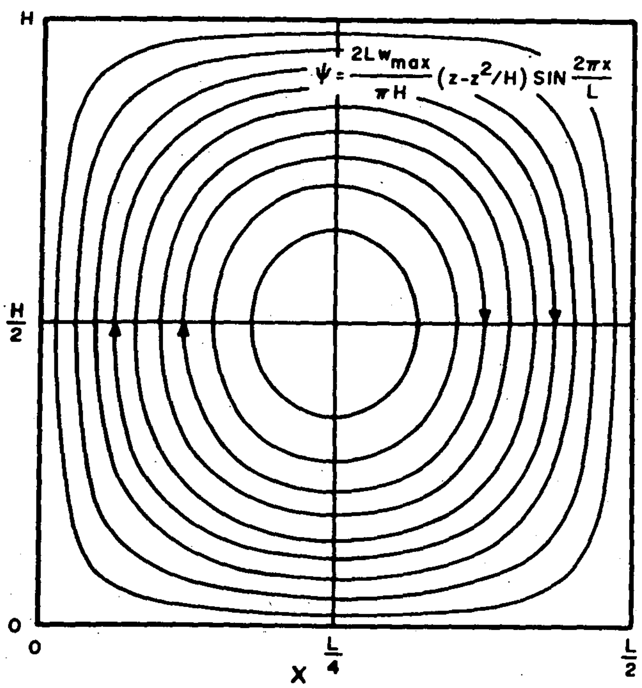

Figure 1. - Model circulation treated in [2].

[1]This note is a slightly revised version of that first presented at the 12th Conference on Radar Meteorology held at Norman, Oklahoma, Oct. 17-20, 1966, and printed in the Proceedings of that Conference.

A parameter closely related to the water content is the echo coverage. Figure 3 shows that the height-profile of echo coverage should be a less sensitive indicator of updraft velocities than the water content profile. However, the coverage index can be acquired with less instrumentation.

2. EMPIRICAL DATA

The NSSL radar data collections have only recently been refined to provide three-dimensional reflectivity data at short intervals. During 1964 and 1965, the areal distribution of reflectivity was measured during selected storms at 0° elevation angle of the antenna, and echo coverage data corresponding to areas with reflectivity factor $Z_e \geq 10$ mm^6/m^3 was collected at higher elevation angles. The coverage at various elevation angles has been converted to the coverage at various heights within a 100 mile radius of NSSL as described in [3].

The data for two storm periods selected for continuity of echoes and radar observations are presented here. The weather situations on

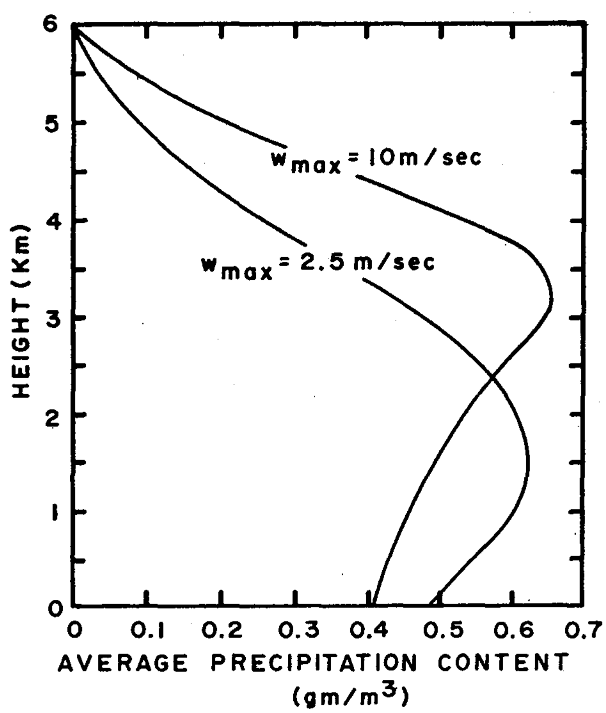

Figure 2. - Average precipitation content at different heights in the saturated circulation of figure 1, averaged over 5000 seconds. Weak and strong circulations last 3240 and 810 seconds, respectively.

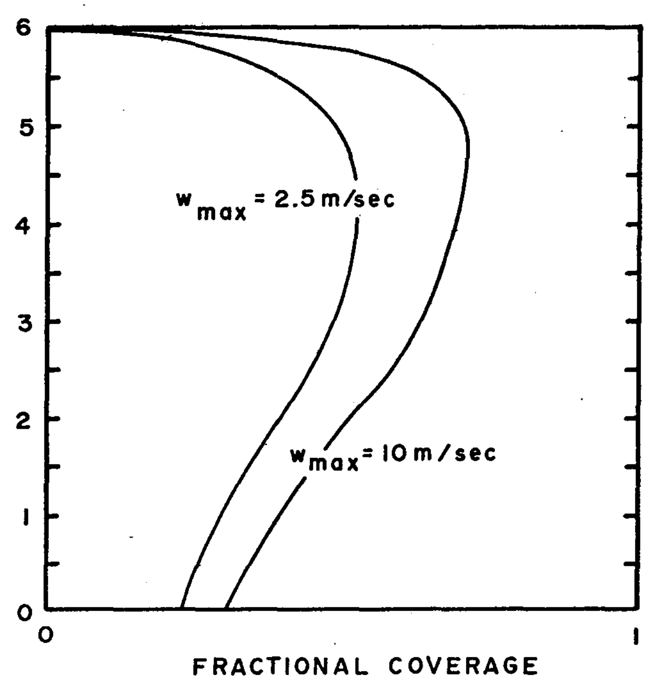

Figure 3. - Height profile of average echo coverage for the cases presented by figures 1 and 2. The coverage is based on the extent of precipitation >.01 gm./m.^{3}, corresponding to Z >10 mm^6/m.^{3}, approximately.

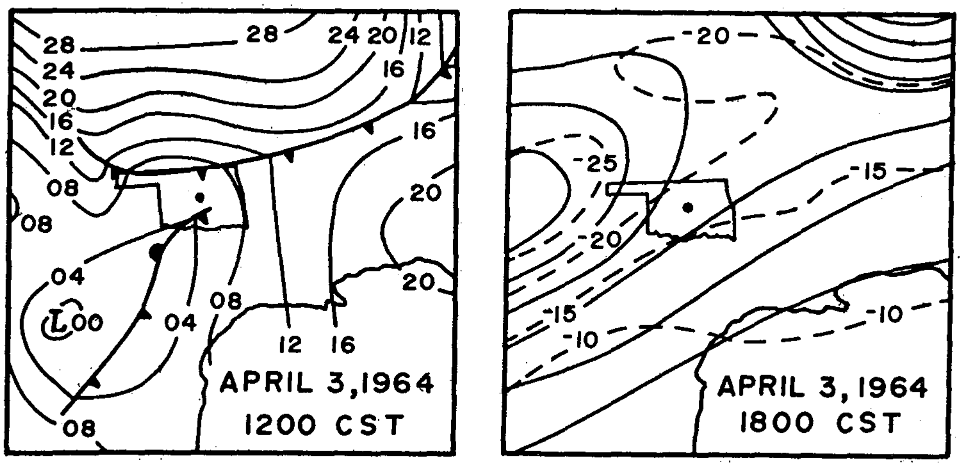

Figure 4a (left) Surface isobars and fronts, 1200 CST, 3 April 1964.

Figure 4b (right) 500-mb. contours and isotherms, 1800 CST, 3 April 1964.

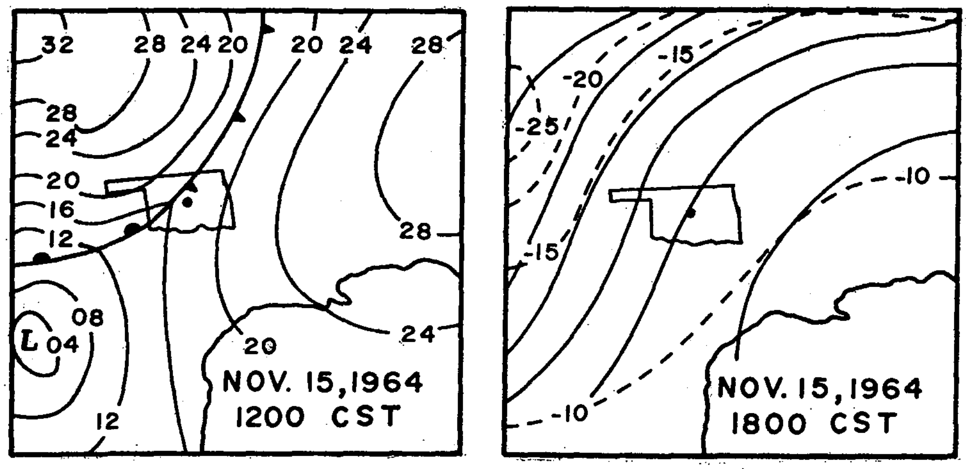

Figure 5a (left) Surface isobars and fronts, 1200 CST, 15 Nov. 1964.

Figure 5b (right) 500-mb. contours and isotherms, 1800 CST, 15 Nov. 1964.

April 3 and Nov. 15, 1964, are illustrated by figures 4 and 5, and soundings are shown in figure 6.

Although the wet-bulb potential temperature declined with height on both occasions, the atmosphere during April 3-4 was much more unstable, with sensible temperature 5°C colder at 500 mb. The low level dryness shown by the April 3rd sounding was replaced by surfacing dewpoints of 18°C within 2 hours after the sounding.

Figures 7 and 8 show the echo coverage within 100 miles of NSSL for selected periods, with radar observations indicated by marks along the time axis. Storm Data [4], lists extensive thunderstorm and tornado activity during the afternoon of April 3rd (see [5], also), and less frequent and intense activity during the early morning of April 4th. Only mild thunderstorm activity was noted on Nov. 14th and 15th.

<u>Storm Data</u> can reference only that activity which is observed and reported and may not be a comprehensive guide in an area like Oklahoma with large sections sparsely populated. Therefore, the distributions of echo intensity at 0° elevation angle are also presented in figures 7 and 8. Roughly, when the intensity distribution is broad, or when a relatively large number of strong echoes are observed, the updrafts are expected to be comparatively strong.

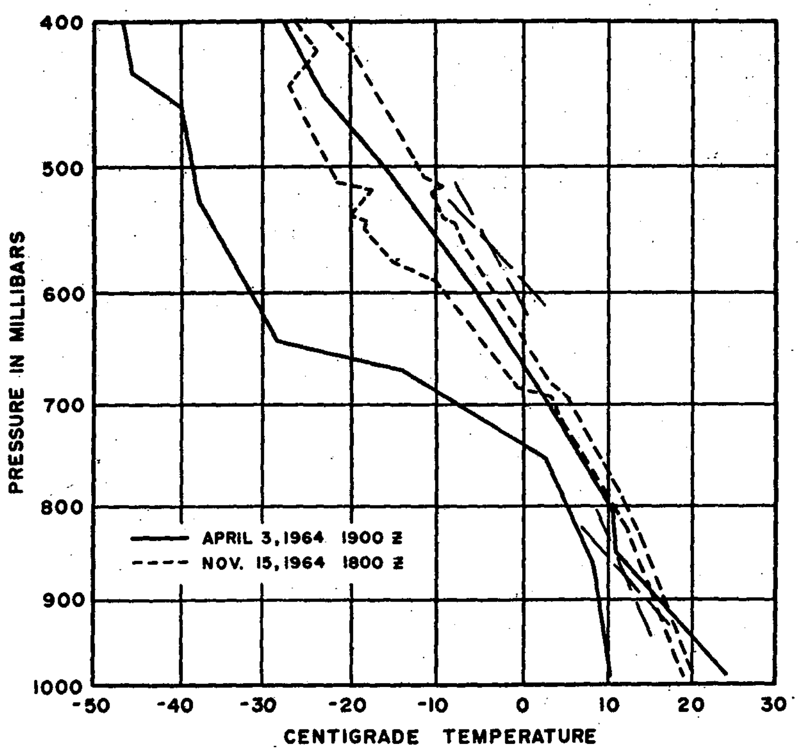

Figure 6. - Soundings at Tinker AFB, near Oklahoma City, 3 April and 15 November 1964.

3. CONCLUSIONS

Figures 7 and 8 show that the coverage had a maximum aloft which was higher during the April period with the more severe storms, and highest (20,000 ft.) during the afternoon of April 3 when storms were most severe and strongest updrafts were expected. Inferences from the cited earlier work are thus supported. Note also that the echo coverage distribution based on 100-mile PPI displays was a slowly varying parameter, reflecting principally diurnal or other processes acting longer than several hours. The data for April 3 show a strong semidiurnal rhythm which seems to characterize severe Oklahoma storms and which demands refined empirical description and improved explanation. Diurnal effects seem weak or absent in the data of Nov. 14 and 15, a time of low sun.

The frequency distribution of intensity in echo areas at 0° elevation angle was irregularly variable over shorter intervals than those characteristic of variations of the coverage profile. However, the long-term trends of the intensity distribution seem to be largely independent of trends in the coverage. In particular, several periods with marked increases and decreases of the coverage (without change of height of the coverage maximum, however) are not attended by correlated changes of the intensity distribution. This suggests that the development and decay of precipitation regimes are marked more by changes in the areal extent of precipitation than by the character thereof. The cellular structure of precipitation is probably controlled by the static stability and vertical distribution of moisture slowly varying over large areas, and its extent is related to diurnal and synoptic processes commensurate with the several-hour intervals typical of the major coverage variations.

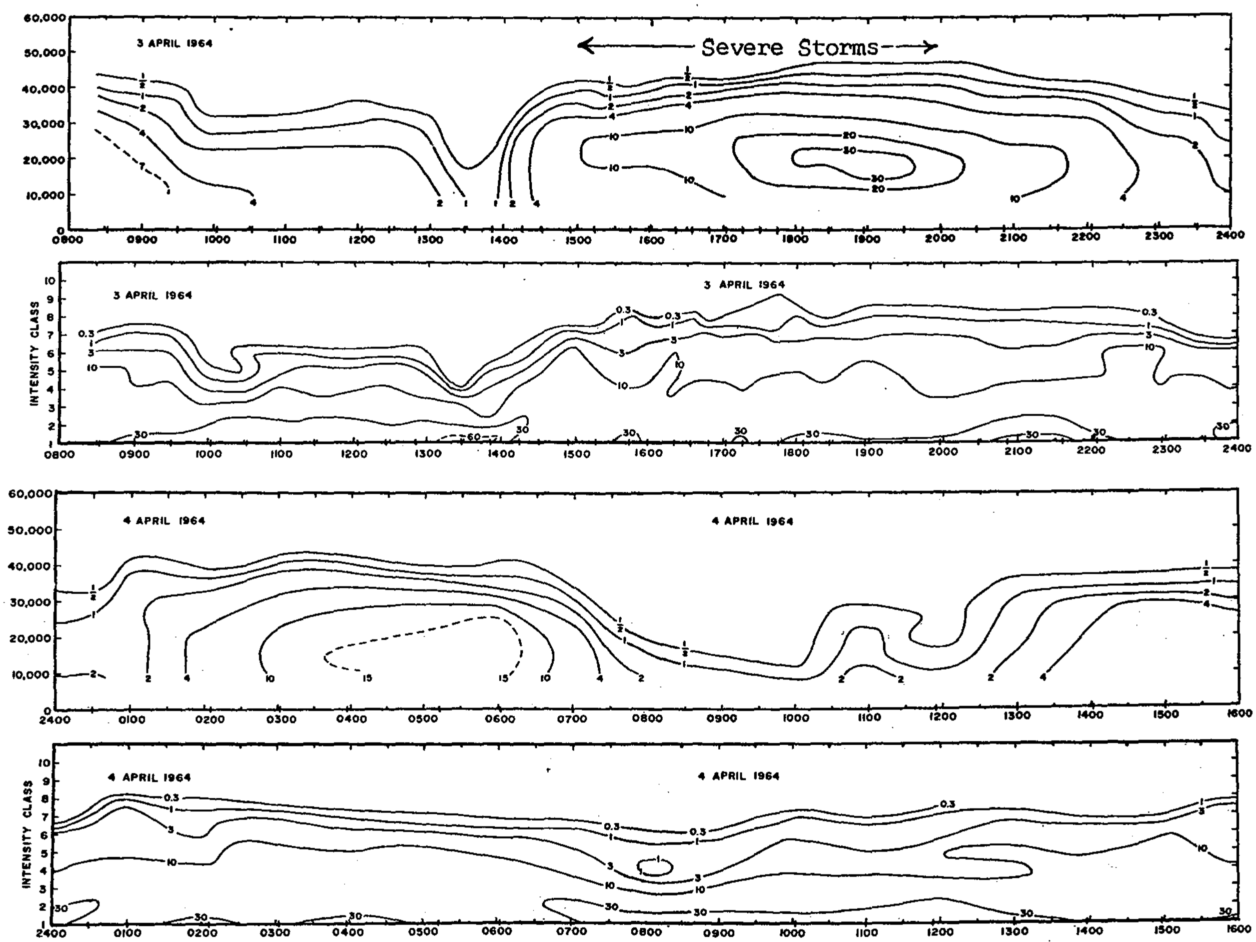

Figure 7. - First and third rows - Percentage of 100-mile radius PPI display at NSSL covered by echoes, plotted against altitude in feet and Central Standard Time, 3-4 April 1964. Note minimum coverage about noon, maximum about sunset. Tornadoes were numerous during the interval marked on April 3rd. Second and fourth rows - Distribution of intensity in echo areas displayed on the 0° elevation PPI, on the same time scale as coverage data. Isopleths indicate the percentage of addresses which contain echo in the intensity classes given on the ordinate.

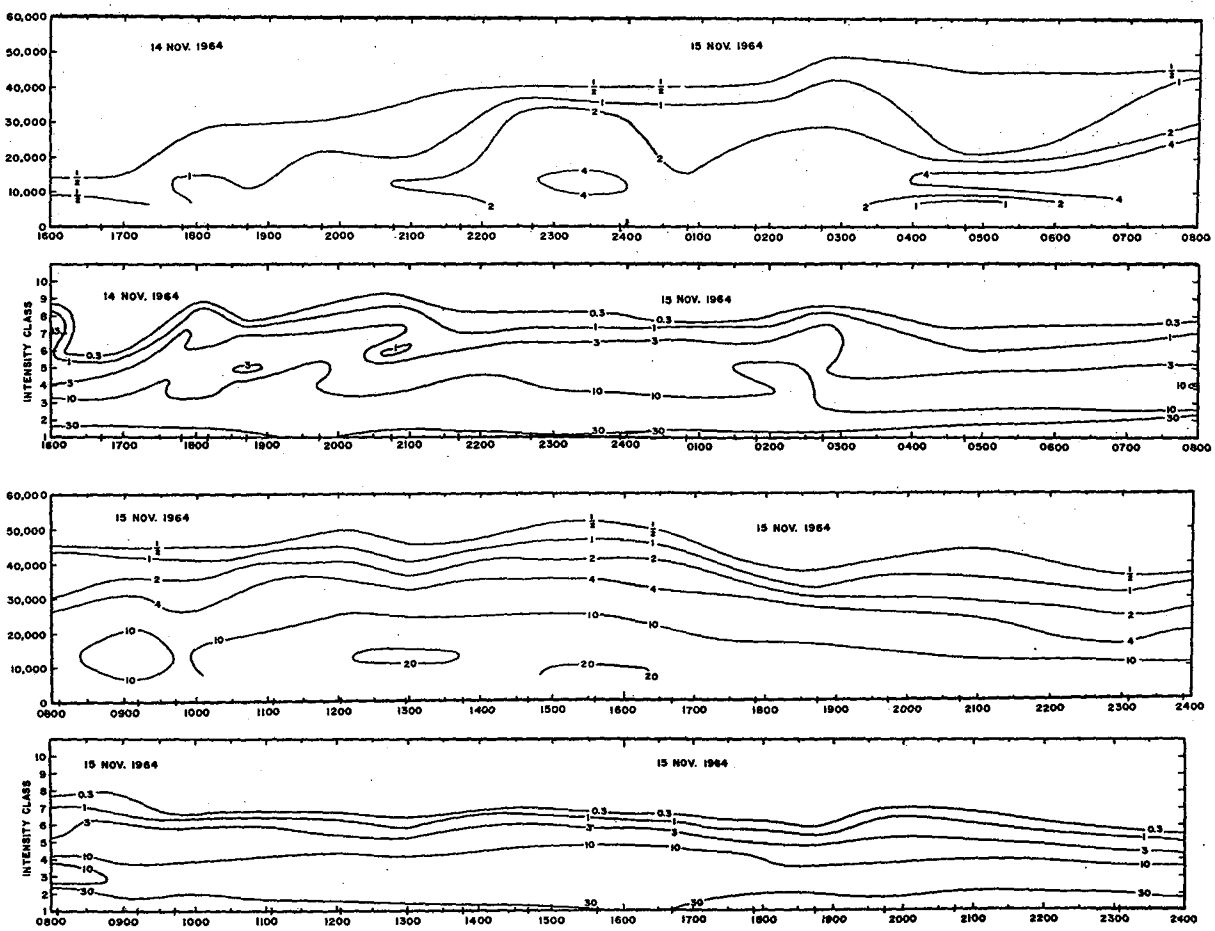

Figure 8. - Echo coverage related to height and time, and echo intensity distribution on 0° elevation PPI as in figure 7. The November period illustrated was characterized by widely distributed showers including some mild thunderstorms.

REFERENCES

1. Hamilton, Paul M., "Vertical Profiles of Total Precipitation in Shower Situations," Quarterly Journal of the Royal Meteorological Society, vol. 92, No. 393, 1966, pp. 346-362.

2. Kessler, E., "Model Circulations with Microphysical Processes," pp. 1-86 in NSSL Technical Memo No. 31, ESSA, U. S. Dept. of Commerce, 1966.

3. Kessler, E. and Russo, J. H., "A Program for the Assembly and Display of Radar-Echo Distributions," Journal of Applied Meteorology, vol. 2, No. 5, 1963, pp. 582-593.

4. U. S. Dept. of Commerce, Weather Bureau, Storm Data, vol. 6, Nos. 4 and 11, 1964.

5. Wilk, K. E., "Motion and Intensity Characteristics of the Severe Thunderstorms of April 3, 1964," pp. 21-29 in NSSL Tech. Memo No. 29, ESSA, U. S. Dept. of Commerce, 1966.

Reprinted from the Monthly Weather Review, Vol. 91, No. 1, January 1963, pp. 13-28. Reference to this article should cite the original publication and not this ESSA Technical Memorandum.

ELEMENTARY THEORY OF ASSOCIATIONS BETWEEN ATMOSPHERIC MOTIONS AND DISTRIBUTIONS OF WATER CONTENT

ABSTRACT

Continuity equations are used to clarify relationships between air motions and distributions of accompanying precipitation. The equations embody simple modeling of condensation and evaporation with the following assumptions: (1) water vapor shares the motion of the air in all respects; (2) condensate shares horizontal air motion, but falls relative to air at a speed that is the same for all the particles comprising precipitation at a particular time and height; (3) the cloud phase is omitted.

After a review of one-dimensional models, the distributions of condensate in two-dimensional model wind fields are discussed with regard to instantaneous evaporation of condensate in unsaturated air and to no evaporation. The most nearly natural cases must lie between these extremes. The methods for obtaining solutions are instructive of basic interactions between air motion and water transport. The steady-state precipitation rate from a saturated horizontally uniform updraft column is shown to equal the sum of the vertically integrated condensation rate and a term that contains the horizontal divergence of wind. The latter term becomes relatively small as the ratio of precipitation fall speeds to updrafts becomes large. A basis for some studies of precipitation mechanisms, the equation $N(V + w) = \text{const.}$, where N is the number of particles comprising precipitation at a particular point in space and time, V is their fall velocity, and w is the updraft, is shown to imply violation of continuity principles unless variations in w are quite small. Continuity equations are applied to radar-observed convective cells (generators) and their precipitation trails, and to radar-observed precipitation pendants (stalactites), and provide bases for estimating the strength, duration, and vertical extent of the associated vertical air currents. The stalactite study also discloses how horizontal variations of precipitation intensity arise during precipitation descent through a saturated turbulent atmosphere.

The continuity equations are powerful tools for illuminating fundamental properties of wind-water relationships. The conclusion discusses attractive paths along which this work should be extended.

1. INTRODUCTION

The study of time-dependent relationships between wind fields and water distributions derives from the belief that knowledge of wind-water relationships is essential for an intelligent approach to the numerous hydro-meteorological problems which hold the increasing direct interest of mankind. Use of wind-water relationships in meteorological analysis should assist the interpretation of radar and satellite observations. Knowledge of the relationships between wind and water fields should assist our consideration of means to modify the weather, since the distributions of water are interwoven with the distributions of latent and sensible heat and the scale, intensity, and shape of convective processes.

This report discusses the application of continuity equations to several interesting problems. Some previously published material (Kessler [4] and [5], and Kessler and Atlas [6]), is briefly reviewed to give coherence to this paper, but the emphasis here is on previously unpublished work.

The principal assumptions have been: (1) Water vapor shares the motion of the air in all respects. (2) Condensate shares the horizontal motion of the air but falls relative to the air at a speed V. V is a negative parameter that may vary with height but that is constant with time at any given height. (This is a great simplification of cloud physics processes - precipitation having a fall velocity V is assumed to form as the result of condensation without a cloud phase. At any particular height, all of the precipitation particles fall at the same speed.) (3) The moisture capacity of the air is a function of height only. (4) The air density is considered locally steady and horizontally uniform.

These premises lead to a continuity equation for M, the density of water substance in all its phases minus the saturation vapor density, viz.,

$$\frac{\partial M}{\partial t}=-u\frac{\partial M}{\partial x}-v\frac{\partial M}{\partial y}-w\left(\frac{\partial M}{\partial z}-G\right)-\frac{\partial}{\partial z}(MV)+Mw\frac{\partial \ln \rho}{\partial z} \qquad (1)$$

where u and v are the winds in the x and y (horizontal) directions, w is the wind in the z (vertical) direction, and ρ is the air density. G is a generation term that denotes the amount of water condensed from a unit volume of saturated air for each unit vertical distance of air travel; $G = -\rho(dQ_s'/dz)$ where Q_s' is the saturation mixing ratio of water vapor in air (for derivation of Eq. (1), see [4] Section 2).[1]

When M is negative, it shares the motion of the air and represents the amount of moisture that must be added to saturate the air; when M is positive, it falls relative to the air at a speed V, and represents the amount of condensate in saturated air. Q plus M is the total water content. These associations between M and V imply instantaneous evap-

[1]When M and G are in mixing ratio units, Eq. (1) is the same except that the last term becomes $-MV(\partial \ln\rho/\partial z)$, and $G = -dQ_s'/dz$. Density units are used in this study because radar reflectivity characteristics, visual appearance, and certain physical effects are best understood in such terms.

oration of condensate in unsaturated air, a fact clearly perceived when one considers that the term $MV = 0$ wherever $M < 0$. The descent of condensate contributes at a rate MV to the addition of M in unsaturated air just beneath, the rate of addition being unaffected by the magnitude of M in the drier air until $M > 0$. Only when $M > 0$ can there be a fallout of water substance.

By treating condensate and vapor separately in two equations, it is practical to study the situation in which precipitation once formed does not evaporate in subsaturated air. This is discussed further in Section 5b below.

2. THE DISTRIBUTION OF M ALONG VERTICALS WHERE THERE IS NO HORIZONTAL ADVECTION

This section summarizes results presented in several other places, and is included here to facilitate understanding of the new results presented in following sections.

A. V + w Everywhere Less than Zero (Motion of Condensate Everywhere Downward)

(1) Steady-state solutions

Omission of compressibility simplifies the discussion without affecting the principal conclusions, and the following expression for the distributions of M in time and height is therefore considered.

$$\frac{\partial M}{\partial t}=-(w+V)\frac{\partial M}{\partial z}-M\frac{\partial V}{\partial z}+wG. \qquad (2)$$

When V is everywhere the same, a condition most closely approached in snow, the third term in Eq. (2) is zero. The steady-state vertical profile of M in a saturated atmosphere is then given by

$$M(z)=M(H)+\int_H^z\left(\frac{wG}{w+V}\right)dz. \qquad (3)$$

This integral has been evaluated exactly for several values of V and a parabolic vertical distribution of updraft w, with $w = 0$ at $z = 0, H$. A typical result with $M(H) = 0$ is shown in the right side of figure 1, taken from [5]. A discussion of the application of (3) to the descent of condensate in saturated downdrafts is given toward the close of Section 7.

When $V = 0$, the steady-state solutions are independent of the shape of the updraft distribution. Eq. (3) then gives, for updrafts, the limiting form of the distribution approached after a

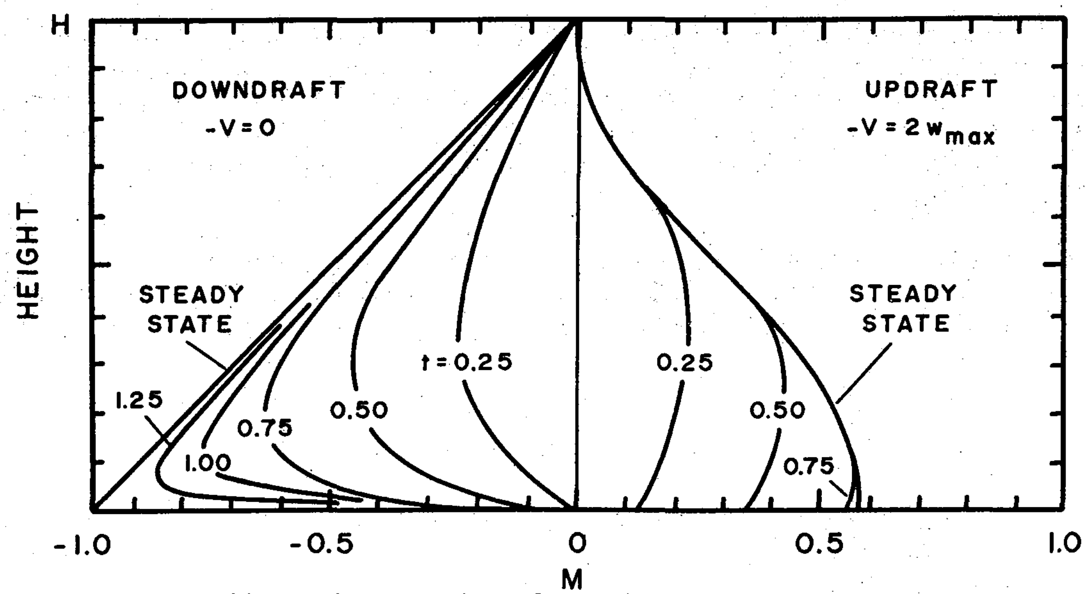

Figure 1. - One-dimensional time-dependent and steady M-distributions in downdrafts (left) and updrafts (right), when G is constant. Values on the abscissa refer to the total water content minus the saturation vapor content in gm./m.^{3} when H = 1 km. and G = 1 gm.m.$^{-3}$km.$^{-1}$ Vertical velocity $w = (4\ w_{max}/H) \times [z - (z^2/H)]$.

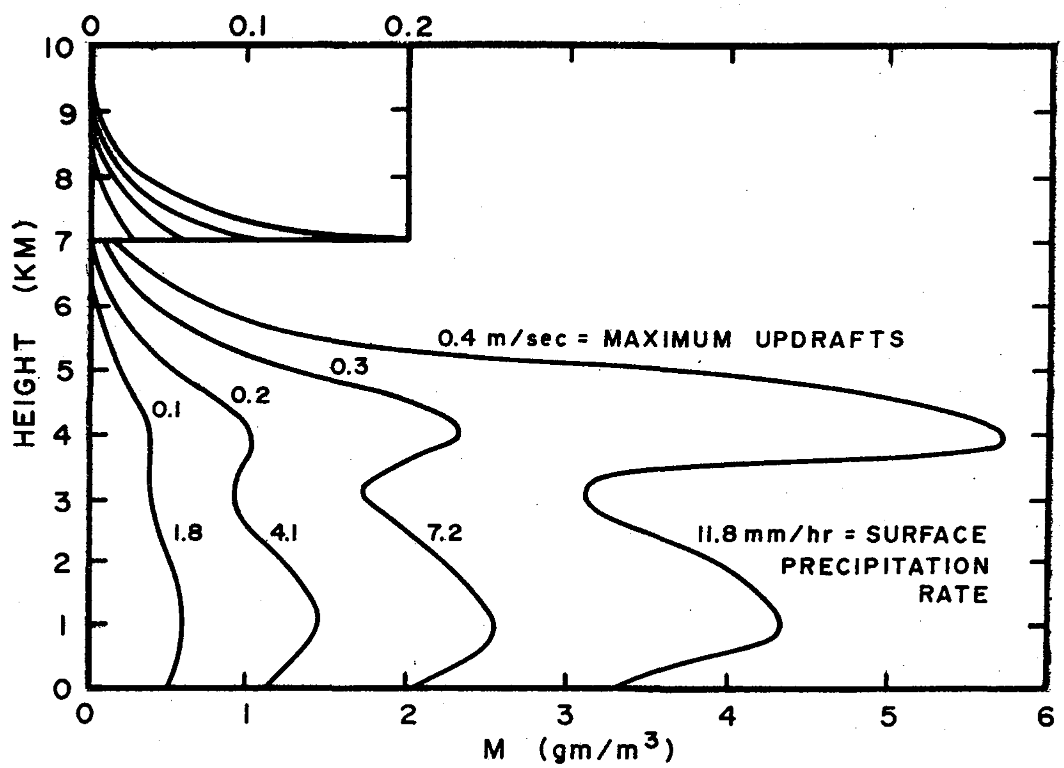

Figure 2. - Theoretical steady-state water-content profiles for various surface snowfall rates near the precipitation center of a winter storm. The maxima occur above layers in which the particles increase their fall speed during descent. The profiles have been calculated using the parameter distributions given in Table 1. (From [6].)

very long time with the unrealistic condition that condensate indefinitely retains negligible falling speed. The application to downdrafts of Eqs. (2) and (3) with V = 0 has a fairly reasonable basis; the solution there represents the distribution of saturation deficit attained after sinking motion has continued for a very long time. This solution for constant G is illustrated in the left side of figure 1.

When V is variable, the third term in (2) must be retained and this equation's steady-state form is then not readily solved analytically. In such cases, finite difference approximations have been used to obtain the solutions. Figure 2 shows computed steady-state profiles of M in the model snowstorm situation indicated by Table 1. These profiles suggest that some of the upper layers observed by radar in winter storms may be due to the kinematic principles discussed here, rather than to the widely discussed generator and trail mechanism (Marshall [10],

Table 1

Abbreviated Tabulation of Model Atmosphere Parameters Used to Compute the Profiles of Figure 2.

Height (km.)	Approximate pressure (mb.)	Relative updraft w	T (°C.)	$Gx10^4$ ($gm./m.^4$)	Particle fall speed (cm./sec.)*
0	1015	0	0	16.8	100
1	900	36	-7	12.3	75
2	795	64	-6	12.0	75
3	700	84	-4	12.6	75
4	615	96	-9	9.7	50
5	540	100	-17	6.4	50
6	470	96	-26	3.9	50
7	410	84	-35	1.9	50
8	355	64	-43	0.8	50
9	310	36	-50	0.4	50
10	265	0	-53	0.3	50

*50 cm./sec. used where T < -8°C.; where temperature increases above -8°C. following the descent of M, the speed is taken as a linear increase with temperature to 100 cm./sec. at 0°C.

for example), which, it is agreed, is the significant factor in most such observations. Since increases of fall velocity are generally associated with increases in particle diameter (to whose sixth power radar is sensitive), a layer of enhanced radar reflectivity is not likely to accompany a layer of enhanced water content that is due to the divergence of precipitation fall velocities. This and several other steady-state variable-V cases have been treated elsewhere (Kessler and Atlas [6]).

(2) Time-dependent solutions

In the steady cases, the vertical distribution of M depicts the individual changes following the descent of M; i.e., $dM/dz = \partial M/\partial z$. When $\partial V/\partial z = 0$, dM/dz is independent of M, and the steady-state profiles provide the key to easy determination of the time-dependent solutions. The packets of M change by an amount $dM = (\partial M/\partial z)dz$ while descending through dz in a time $dt = dz/(V + w)$. The time-dependent solutions when V is invariant can, therefore, be constructed from the steady-state vertical profile of M and the curve showing the height of an M-packet against time. Two sets of results of such calculations based on the initial condition $M \equiv 0$ and the upper boundary condition $M(H) = 0$ are illustrated in figure 1 and are discussed in detail in [4] and [5]. When the fall velocity is a function of height, this method of solving for the time-dependent solutions is inadequate, but it is practical in such cases to use finite difference methods. Many properties of the variable-V solutions can be qualitatively assessed from general considerations supplemented by simple computations.

B. V + w Somewhere Greater than Zero (Motion of Condensate Somewhere Upward)

With V constant and the absolute magnitude of V anywhere less than the associated value of w, there is no steady-state solution valid throughout the depth of the updraft column. However, in this case, where V is everywhere the same, the time-dependent solutions at points where $(V + w) = 0$ are simply $M = M_o + wGt$, and elsewhere can be accurately determined by a procedure only slightly more elaborate than that described above for determining the time-dependent solutions that precede a steady state. (See [5], Sec. 4.)

3. THE STEADY-STATE PRECIPITATION RATE FROM A SATURATED, HORIZONTALLY UNIFORM UPDRAFT COLUMN

The application of continuity considerations shows that the rate of steady precipitation at the ground is not generally equal to the condensation rate in rising air vertically above, even when there is no horizontal advection at the center of an area of widespread updrafts. Equality of steady precipitation and condensation rates is approached as the magnitude of the ratio of precipitation fall speeds to updrafts increases. The results presented here are an extension of Section 5 in [4].

In a steady-state horizontally uniform atmosphere, the horizontal advection terms are zero and the appropriate equation is

$$0=-w\frac{\partial M}{\partial z}-\frac{\partial}{\partial z}(MV)+wG+Mw\frac{\partial \ln \rho}{\partial z}. \tag{4}$$

Integration from the base 0 to the top H of the updraft column gives

$$0=-\int_0^H w\frac{\partial M}{\partial z}dz-MV\Big|_0^H+\int_0^H wGdz+\int_0^H Mw\frac{\partial \ln \rho}{\partial z}dz. \tag{5}$$

The second term on the right of (5) is the precipitation rate at the base of the updraft because at the top $M \geq 0$ and, therefore, $V = 0$ there; the third term is the condensation rate in the vertical column of unit cross section.

The first term on the right is better understood after integration by parts, i.e.,

$$\int_0^H w\frac{\partial M}{\partial z}dz=\int_0^H \frac{\partial}{\partial z}(wM)dz-\int_0^H M\frac{\partial w}{\partial z}dz \tag{6}$$

$$\int_0^H w\frac{\partial M}{\partial z}dz=wM\Big|_0^H-\int_0^H M\frac{\partial w}{\partial z}dz. \tag{7}$$

The first term on the right of Eq. (7) vanishes because $w = 0$ at both $z = 0$ and $z = H$. And the equation of continuity for air implicit in Eq. (1) states that $\partial w/\partial z$ in the second term on the right of (7) is given by

$$\frac{\partial w}{\partial z}=-\left(\frac{\partial u}{\partial x}+\frac{\partial v}{\partial y}+w\frac{\partial \ln \rho}{\partial z}\right). \tag{8}$$

Substitution of Eqs. (8) and (7) into Eq. (5) yields

$$-(MV)_{z=0}=R_{z=0}=\int_0^H wGdz-\int_0^H M\left(\frac{\partial u}{\partial x}+\frac{\partial v}{\partial y}\right)dz. \tag{9}$$

Eq. (9) is a reminder that the horizontal divergence of the wind is implicit even in the one-dimensional forms of Eq. (1). The last term in Eq. (9) may be positive, negative, or zero, and is largely dependent on the ratio of characteristic fall speed to the characteristic updraft.[2] The relative contribution of the last term in Eq. (9) is usually most important in the strong updraft situations where M is increased in greater proportion than w (because the fall speed of precipitation usually increases only a little with a large increase of intensity). From another point of view, note that when V is relatively small and only slowly varying, as in snow, M is relatively quite large near the ground where the divergence is negative, and that the last term in Eq. (9) contributes substantially to the precipitation rate near the center of areas of widespread precipitation. In such cases the precipitation rate significantly exceeds that defined by the condensation term alone. Any excess of precipitation over condensation near an updraft core is, of course, accompanied by a deficit in areas away from the core.

In other cases, particularly where the melting zone, associated with a fivefold increase of particle fall speeds, coincides with the level of no horizontal divergence of the wind, the steady precipitation rate at updraft centers may be somewhat less than the condensation rate there. A physical approach to the results summarized by Eq. (9) is illustrated in figure 5 of [4].

These results should be of some value for relating updraft velocities to observed precipitation rates and radar echo intensities.

4. ASSUMPTIONS IMPLICIT IN THE RELATIONSHIP N(V + w) = CONSTANT

The equation

$$N(V+w)=\text{constant} \quad , \tag{10}$$

where N is the concentration of precipitation particles at various points along a vertical, has been used by several investigators, including the author [3], as a conservation law suited for a study of precipitation models. Some published work concerning precipitation mechanisms rests on one or more implications of this Eq. (10), even where Eq. (10) is not explicitly invoked. Although many important limitations of Eq. (10) and its corollaries have long been recognized, it has not been generally realized that this equation often stands in violation of fundamental principles of continuity.

The conditions under which Eq. (10) is valid can be examined by reference first to

$$\frac{\partial M}{\partial t}=\frac{dM}{dt}-(V+w)\frac{\partial M}{\partial z}, \tag{11}$$

[2]Equation (9) is the same whether the atmosphere is assumed to be compressible or incompressible. However, the distribution of the quantities therein and the magnitude of the integrals vary somewhat with considerations of compressibility. See, for example, figure 1 of [4].

derived immediately from first principles. Eq. (11) states merely that in the absence of horizontal advection, the local change of M is the sum of individual and vertical advective changes. Substitution for $\partial M/\partial t$ from the one-dimensional form of (1) gives

$$\frac{dM}{dt}=wG-M\frac{\partial V}{\partial z}+Mw\frac{\partial \ln \rho}{\partial z}. \tag{12}$$

In (12), let M = Nm, where m is the mass of each particle in a collection of N particles. Then

$$m\frac{dN}{dt}+N\frac{dm}{dt}=wG-mN\frac{\partial V}{\partial z}+mNw\frac{\partial \ln \rho}{\partial z}. \tag{13}$$

Suppose that combination and breakup processes among precipitation particles are weak and that the condensation-evaporation term contributes to the mass of individual particles, but not to their number; i.e., precipitation particles grow or diminish in size, but are neither created nor destroyed. This assumption may be applicable, for example, to the further development of a packet of small hail. Then Eq. (13) can be separated into two equations:

$$m\frac{dN}{dt}=-mN\frac{\partial V}{\partial z}+mNw\frac{\partial \ln \rho}{\partial z} \tag{14}$$

and

$$N\frac{dm}{dt}=wG. \tag{15}$$

The temporal changes of particle concentration along the path of an individual packet are given by

$$\frac{dN}{dt}=\frac{dz}{dt}\times\frac{dN}{dz}=(V+w)\frac{dN}{dz}. \tag{16}$$

Divide (14) by m, substitute (16) into (14), multiply by ∂z, and rearrange terms to obtain

$$\frac{\partial N}{N}=-\frac{\partial V}{V+w}+\left(\frac{w}{V+w}\right)\frac{\partial \rho}{\rho}, \tag{17}$$

which applies along a vertical at any time if the distribution state is steady, but should be restricted to the flow following an individual packet (individual derivatives) when the distributions are unsteady. In the idealized case of descent at constant fall velocity through a constant updraft, the term $\partial V/(V + w)$ in (17) is zero, but there is still a decrease in the number of particles per unit volume because in a compressible atmosphere, effects of horizontal divergence, measured by the third terms in Eqs. (14) and (17), accompany updrafts that are invariant with height. The effect of the third term in (17) must in nature be more or less compensated by the tendency of precipitation fall speeds to decrease as the particles descend into air of increasing density.

Only if w is constant or, at least, everywhere quite small in comparison to V, can the integral of Eq. (17) without the compressibility term be represented by Eq. (10). The assumption that w is constant or everywhere small compared with V is quite similar to the assumption that the horizontal or vertical divergence of the wind is small compared with the vertical divergence of V. This may be clearly understood after consideration of the vertical derivative of Eq. (10);

$$N\left(\frac{\partial V}{\partial z}+\frac{\partial w}{\partial z}\right)+(V+w)\,\frac{\partial N}{\partial z}=0. \tag{18}$$

Eq. (18) contains the term $N(\partial w/\partial z)$, which is properly omitted, since it is practically canceled by effects of horizontal divergence, as shown by the equation of continuity for air. Note that the term $N(\partial w/\partial z)$ has no analog in Eq. (4). Use of Eq. (10) across a layer where w varies implies neglect of horizontal divergence and violation of continuity principles; such use will be associated with important errors unless the magnitude of air speed changes is small.

The inherent similarity of assumptions (1) that steady precipitation and condensation rates are equal and (2) that equations like Eq. (10) can be applied to the study of precipitation, can be understood in terms of this discussion. As fall speed increases relative to w and M, the integral of the horizontal divergence times M in Eq. (9) and the errors associated with Eq. (10) become relatively small, and these assumptions are satisfactory.

Eq. (10) is valid for estimating the change of N accompanying important changes of V which occur over such a short interval that variations of w are negligible, or over larger intervals in which w is everywhere much smaller than V. The application of Eq. (10) is possibly justified in the zone in which snow melts to form rain with an approximately fivefold increase of particle fall speed, especially when the effects of breakup of melting particles can otherwise be included or shown to be small. (See sec. 7B and Table 1 of [4].) Other possible applications are to layers in which updraft speeds are uniform and where N and V can be estimated at at least one height in the layer. In no event, of course, are Eqs. (10) and (18) even crudely sufficient for application over a region where w varies and (V + w) passes through or near zero. They are not applicable, for example, to the study of hail. Where w attains about the same magnitude as V, a more accurate integration of Eq. (18), rather than Eq. (10), must be employed.

It is, at least, of academic interest to note that Eqs. (14) and (15) with boundary and initial conditions, uniquely define m and N at all heights when the masses of the particles are expressed in terms of their fall velocities. The relation $V = -130D^{1/2}$, where V is in m./-sec. and D is in meters (Spilhaus [15]), can be used to give $V = -130(6m/\pi)^{1/6}$(m./sec.), where m is in grams. Use of this relationship with appropriate boundary and initial conditions allows solution of (14) and (15) for m and N where the updrafts are known at every height and time - or, knowledge of m and N along the trajectory of M permits the determination of updraft distributions. Horizontal advection when present simply requires that Eqs. (14), (15), and (17) be applied along the nonvertical trajectory of precipitation descending through the atmosphere. These equations can be viewed as a theory of monodisperse-size-distributed precipitation, applicable in a layer where breakup and combination processes are weak and where fall velocities are everywhere larger, but not necessarily much larger, than the updrafts.

5. TWO-DIMENSIONAL SOLUTIONS

A. Instantaneous Evaporation of Condensate in Subsaturated Air

This section discusses time-dependent distributions of water substance and the methods for deriving them in two model cases where condensate fall speeds are twice the magnitude of maximum updrafts and in two cases where fall speeds are half the maximum updrafts. Two sets of solutions are presented for each updraft-fall speed ratio: one set where there is instantaneous evaporation of condensate in subsaturated air; the other where there is no evaporation of condensate in subsaturated air. The most nearly natural cases must lie between these extremes. The methods for obtaining solutions are instructive of basic interactions between air motions and water transport.

The following equations have been considered in connection with the two-dimensional solutions:

$$\frac{\partial M}{\partial t}=-u\frac{\partial M}{\partial x}-(w+V)\frac{\partial M}{\partial z}-M\frac{\partial V}{\partial z}+wG, \qquad (19)$$

$$w=\frac{4w_{max}}{H}\left[z-\frac{z^2}{H}\right]\cos\frac{2\pi x}{L}, \qquad (20)$$

$$u=\frac{2Lw_{max}}{H}[2z-1]\sin\frac{2\pi x}{L}+f(z), \qquad (21)$$

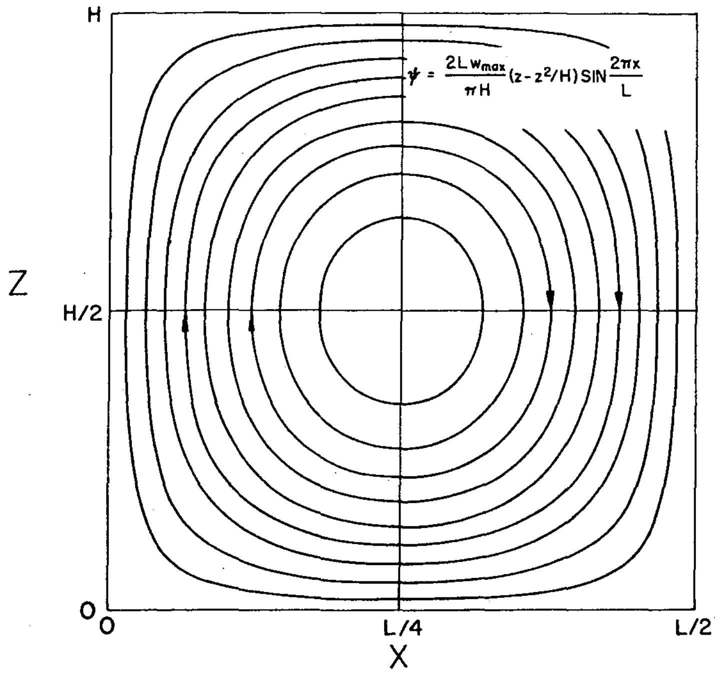

Figure 3. - Streamlines of the wind field corresponding to Eqs. (20), (21), and (22) with f(z) = 0, over the range $0 \le x \le L/2$.

$$\psi = \frac{2Lw_{max}}{\pi H}\left[z - \frac{z^2}{H}\right]\sin\frac{2\pi x}{L} - \int_0^H f(z)dz. \tag{22}$$

Eq. (19) applies to an incompressible atmosphere and Eqs. (20) and (21) satisfy the corresponding continuity condition, viz, $\partial u/\partial x + \partial w/\partial z = 0$. In Eqs. (21) and (22), f(z) is the nondivergent environmental wind. These equations are solved in the layer $0 \le z \le H$, with M specified at z = H. The limits of integration in the horizontal direction are usually chosen so that there is no horizontal wind at these boundaries, for example, $nL/2 \le x \le (n + 1)L/2$, where n is an integer or zero when f(z) = 0. Then the one-dimensional solutions already discussed exist along the verticals at the horizontal limits of the problem area, and no boundary conditions other than the value of M at z = H need be specified at these limits. Other alternatives are both practical and interesting but are not discussed further here.

The wind field described by Eqs. (20), (21), and (22) with f(z) = 0 is shown by figure 3. With V constant for M > 0 and V = 0 wherever M < 0, and with initial condition M = 0, boundary condition M(H) = 0, and G = constant, Eq. (19) has been solved by finite difference methods for the field of M at various times. As noted in the introduction, these assumptions concerning M and V imply the instantaneous evaporation of condensate in any subsaturated air into which it falls. The top rows of figures 4 and

5 show solutions for two relationships between the uniform fall speeds of condensate and the maximum updrafts. Details concerning the method of solution and discussion of these solutions and associated budget parameters are contained in Section 5 of [5].

B. No Evaporation of Condensate in Subsaturated Air

Equation (19) can be solved in a modified way that admits of no evaporation of condensate once formed. Such a method is interesting because in subsaturated air the most nearly natural case must lie between the extremes of no evaporation and instantaneous evaporation of precipitation. The revised method for solving Eq. (19) is based on the following.

Consider two sets of equations, one set for condensate and one for vapor. Each set constitutes a restatement of the same conservation principle expressed by Eq. (19). We have

$$\frac{dM}{dt}=wG, \begin{matrix} M\geq 0 \\ q=0 \\ w>0 \end{matrix} \quad ; \quad (23a) \qquad \frac{dz_M}{dt}=w+V, \quad M>0 \quad ; \quad (23b)$$

$$\frac{dq}{dt}=wG, \quad q<0 \quad ; \quad (24a) \qquad \frac{dz_q}{dt}=w, \quad q<0 \quad ; \quad (24b)$$

where M is now the air's precipitation content, always positive or zero, and q is the vapor density minus the saturation vapor density, zero in saturated air and a negative quantity in unsaturated air. Note that Eq. (23a) is applied only in saturated updrafts (elsewhere $dM/dt = 0$); (23b) is applied to determine the motion of M. Since $q = 0$ in all saturated updrafts, Eqs. (24a) and (24b) are of concern only in following the motion and changes of q in unsaturated air. The term $M\partial V/\partial z$ does not appear in Eq. (23a) because V is assumed constant for condensate. In areas where $M > 0$ and $q < 0$, it is necessary to apply both sets of equations. There is no evaporation when the values of M and q are not added at points where q is negative and M positive.

The two-dimensional solutions have been determined by combining the host of one-dimensional solutions applicable along the trajectories (also streamlines in these cases of steady wind fields) of M and q. Figure 6 illustrates the streamlines for $V/w_{max} = -2$. Note that the streamlines of q are identical with those of the wind field, and that Eqs. (24a) and (24b) can be combined and integrated to yield $q = q_o + G\Delta z$. The solutions for q are thus given by the vertical displacements along air-streamlines; these displacements have been determined by finite-difference and graphical methods. The time-height relationships for M and the steady-state profile of M along each M-streamline have also been determined by combinations of numerical and graphical techniques. The results for M are summarized in figure 7,

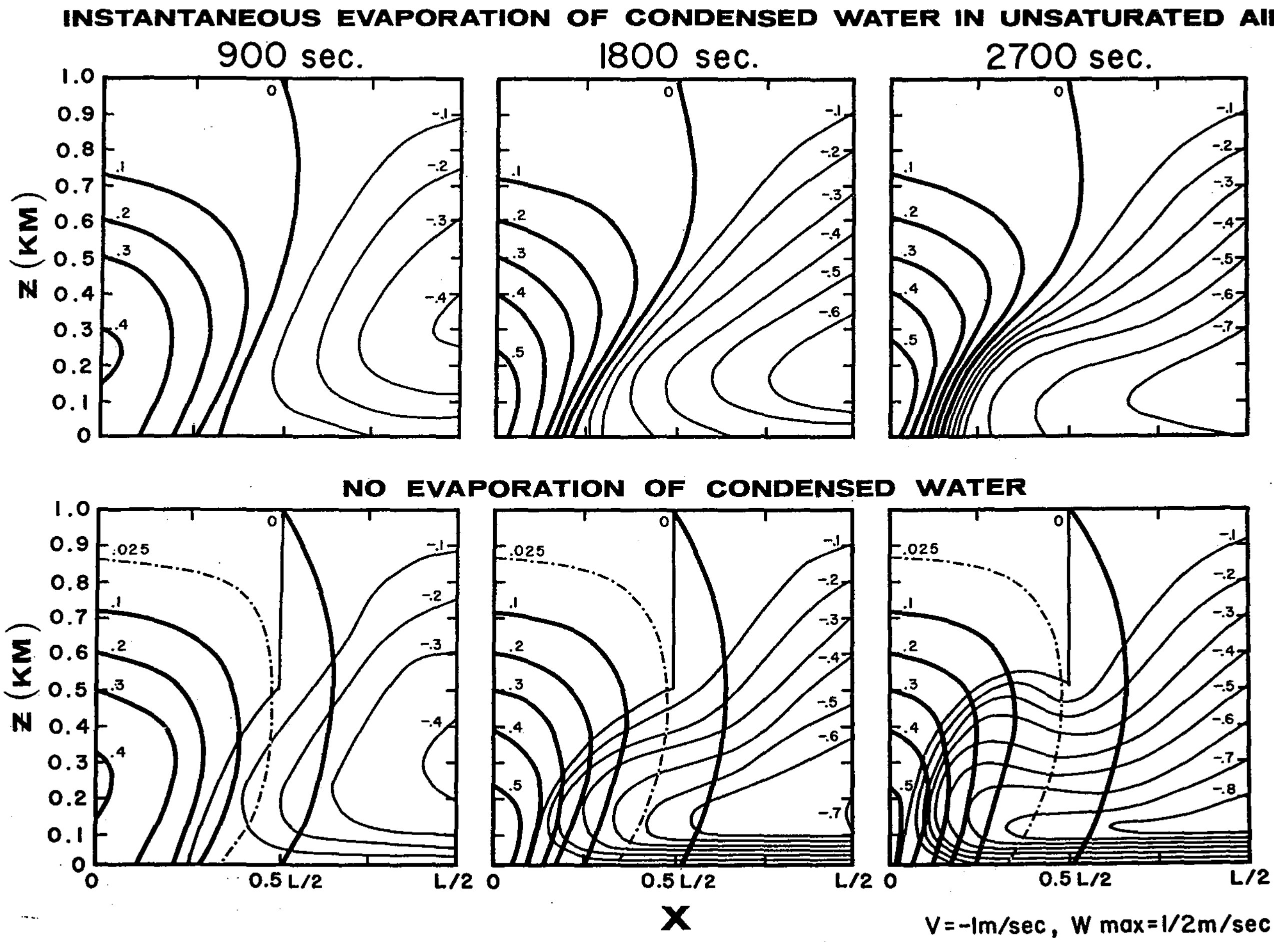

Figure 4. - Analyzed fields of water content based on a steady wind field of shape as shown in figure 3, maximum vertical air speed of 0.5 m./sec., uniform condensate fall speed of 1 m./sec., and lapse of saturation vapor density of 1 gm. m.$^{-3}$ km.$^{-1}$ At time = 0, the atmosphere is everywhere saturated. The heavy lines show the concentration of condensate in gm./m.^{3} and the light lines show the amounts of vapor required to saturate the air. The upper row illustrates the case in which condensate evaporates instantly when it falls into air that has become unsaturated by virtue of its history in the descending branch of the circulation; the lower row illustrates the case in which there is no evaporation of condensate. The time 2700 sec. marks substantial overturning of the air in the circulation cell. Further discussion is in the text.

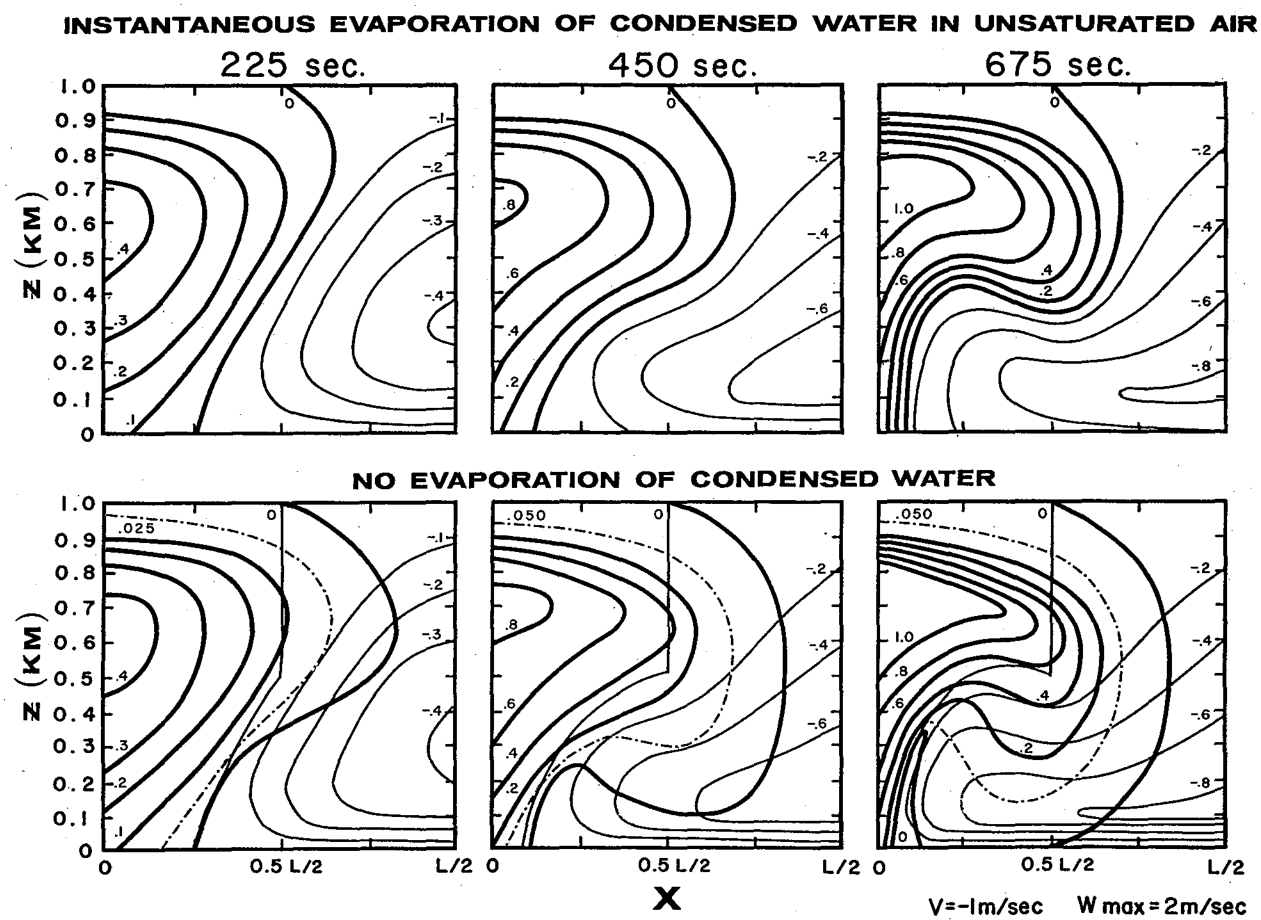

Figure 5. - Same as figure 4, except that w_{max} = 2 m./sec. and the time for substantial overturning of the air is reduced to 675 sec.

which is the principal basis for the graphical development of time dependent solutions in this case.

To obtain the no-evaporation solutions, it is necessary to know the boundary separating air where $q = 0$ from that where $q < 0$; this is defined by the locus of particles that have risen in the updraft part of the cell as much as they had previously descended in the downdraft portion. Figure 6 shows, for three times, this demarcation as determined by finite-difference methods in the interior of the circulation cell and by exact methods on the lower cell boundary. Along the streamlines for condensate, growth of M is assumed to follow the curves of figure 7 only so long as M is in air that is saturated. As soon as M-parcels cross the boundary separating saturated from unsaturated air, i.e., separating air where $q = 0$ from air where $q < 0$, growth of M ceases and the remainder of the M history is due to advection only. The no-evaporation solutions where $V/w_{max} = -2$ are shown in the lower row of figure 4.

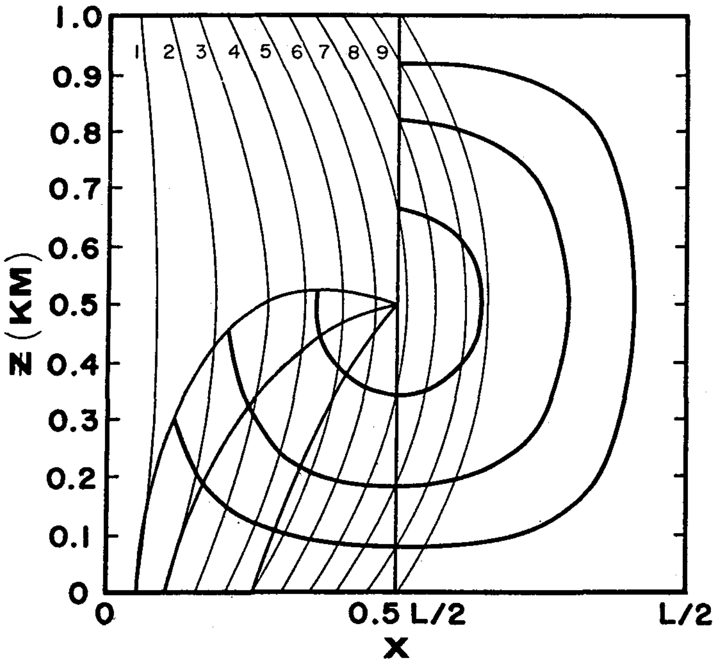

Figure 6. - Streamlines of condensate (light) and of vapor (heavy lines corresponding to those shown in figure 3). The paths of condensate apply to the case $V/w_{max} = -2$. The boundary separating saturated from unsaturated air is shown for times t = 0, 0.45 H/w_{max}, 0.90 H/w_{max}, and 1.35 H/w_{max} by the lines of intermediate weight. Integers on the streamlines of condensate refer to the steady-state solutions shown in figure 7.

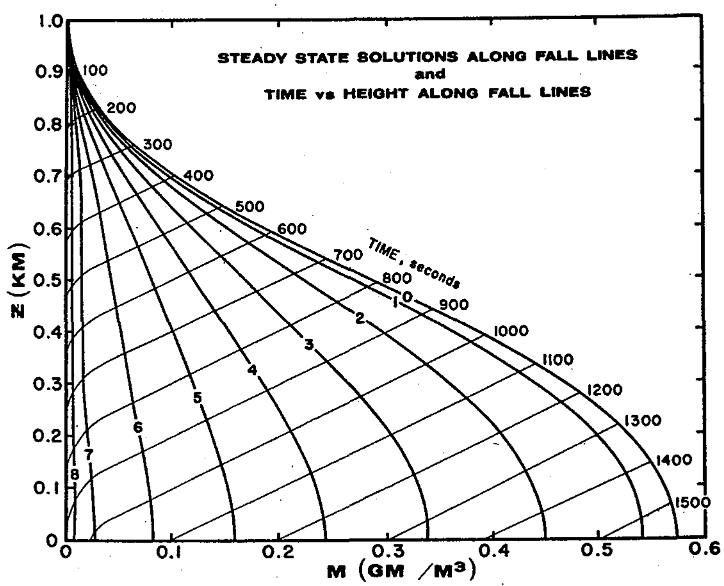

Figure 7. - Diagram used to determine time-dependent distributions of condensate illustrated in lower row of figure 4. The numbered lines descending from the upper left corner are the steady-state M-distributions along the streamlines denoted by corresponding integers in figure 6. The time intervals occupied by M-packets descending from one height to another are given by the lines ascending from the left.

The solutions of the problem where $V/w_{max} = -\frac{1}{2}$ are shown in the lower row of figure 5; these have been obtained in the same manner as described above, but with somewhat greater difficulty, especially where the streamlines of M are loops. (See, for example, [5] figure 7.)

The solutions in upper and lower rows of figures 4 and 5 must differ only where precipitation falls into air which has been rendered unsaturated by the air's prior descent. Other differences between corresponding diagrams, where not attributable to drafting uncertainties, are due to use of a smoothing equation in the program for digital computation of instantaneous evaporation cases. Since large numerical differences between solutions of instantaneous-evaporation and no-evaporation models are confined to small areas in the cases shown, it has not seemed worthwhile to extend to the present study the detailed budget computations discussed in [5].

The solutions shown can be scaled to any distribution of atmospheric parameters which differ by constant factors from those used here, as discussed in [5]. For new scale height $\mathscr{H}$, new generating function $\mathscr{G}$, new vertical air speed $\mathscr{W}_{max}$, and new fall velocity $\mathscr{V}=\mathscr{W}_{max}V/w_{max}$, the new solutions denoted by $\mathscr{M}$ are given by $\mathscr{M}=M\mathscr{G}\mathscr{H}/GH$ which occur at new times $\mathscr{T}=T\mathscr{W}_{max}\mathscr{H}/w_{max}H$. (See Sec. 2 of [5].) The solutions for given G, H, and w_{max} can be applied to any horizontal scale, since the equation of continuity for air requires that stretching of the horizontal scale be associated with an equivalent stretching of the horizontal wind speed, when the vertical air speed is unchanged.

The particular wind and water fields used here have some features demonstrably inconsistent with thermodynamic principles. For example, thermal changes must closely follow moist and dry adiabatic processes in saturated updrafts and unsaturated downdrafts, respectively. Since updrafts and downdrafts have equal intensity in our model wind field, the descending current for a representative conditionally unstable initial lapse rate becomes considerably warmer than the ascending current at corresponding levels, long before the circulation has progressed to the illustrated final stages. Therefore, another model should be considered, say a radially symmetric type, wherein the downdraft area is much more widespread and the downdraft intensities correspondingly more gentle than the updrafts. The solutions in such cases can be produced in just the manner already shown. At the updraft center, the solutions are the same as those already discussed when the vertical velocity distribution is the same as that given by Eq. (20); elsewhere, the principal differences are described in terms of a reduction of the linear extent of the inflow from the descending branch of the circulation, decreased linear extent of the outflow aloft, and somewhat higher precipitation efficiencies in the evaporation cases, since less dry air is interposed between precipitation aloft and the ground.

It is obvious that a higher percentage of the condensate formed in updrafts must reach the ground when updrafts and compensating downdrafts are separated by great distances, and when downdrafts are spread over wider area and are therefore comparatively weak. It is also obvious that for a given circulation in an initially unsaturated atmosphere, more of the water condensed in updrafts will evaporate again before reaching the ground than in the cases illustrated here. Of course, many kinds of circulation can be imagined, and a study incorporating thermodynamic principles quantitatively would be necessary to determine which ones probably occur.

The method of solution by use of streamlines rather than by a rectangular grid is the more inherently accurate and can be modified at the cost of added complexity to take account of various rates of evaporation. For example, the streamline method can be used to study instantaneous evaporation by adding values of $M > 0$ and $q < 0$ algebraically after a short-time interval to define a new field of $M + q$ from which the new locus of $M + q = 0$ can be determined. It seems however, that little would be gained by introduction of complexities of this kind without generalization of the assumptions discussed in the introduction to this study.

6. THE KINEMATIC BASES OF GENERATORS

Generator is the name given to the sources of precipitation streaks (usually snow) observed visually and by radar; like practically all precipitation sources, generators are identified with vertical circulation of air. A history of a generator circulation and the processes affecting it and its associated trail of snow is incorporated in the water content distribution. Generators and trails have been studied extensively by Marshall [10], Atlas [1], and Douglas, Gunn, and Marshall [2]. Weak generators are shown in figure 8. In this section, the application of kinematic theory is shown to provide bases for estimating the lifetime of generators and the strength of their vertical currents from radar and visual observations.

In this investigation, it has been assumed that the generating circulation is given by Eqs. (20), (21), and (22) with $f(z) = 0$; the environmental wind does not vary with height in the generating layer. In figure 9, the wind shear below the generating level has been taken as 5 m. sec.$^{-1}$ km.$^{-1}$ The generating cells are 1 km. deep and G, in Eq. (19), has been taken as 0.7 gm. m.$^{-3}$ km.$^{-1}$, a representative value for winter near the 600-mb. level. Precipitation in the trails falls 1 m./sec., representative of snow, without growth or diffusion. The water density distributions within the cells have been scaled from those illustrated in the upper rows of figures 4 and 5 according to the discussion given in Section 5, and the trails plotted in accordance with the equations that relate fall velocity and wind shear to position relative to the generators, as discussed in the references.

With the given assumptions, all the possible shapes of the M-distributions are implied by the possible range of the ratio V/w_{max}. The ratio $-V/w_{max} = 2$, is given by the patterns at the left of figure 9, and $-V/_{max} = \frac{1}{2}$ is given by the patterns at the right. The labeled water contents are for maximum updrafts of 0.5 and 2 m./sec., respectively. In both cases, the circulation starts at time $t = 0$ and

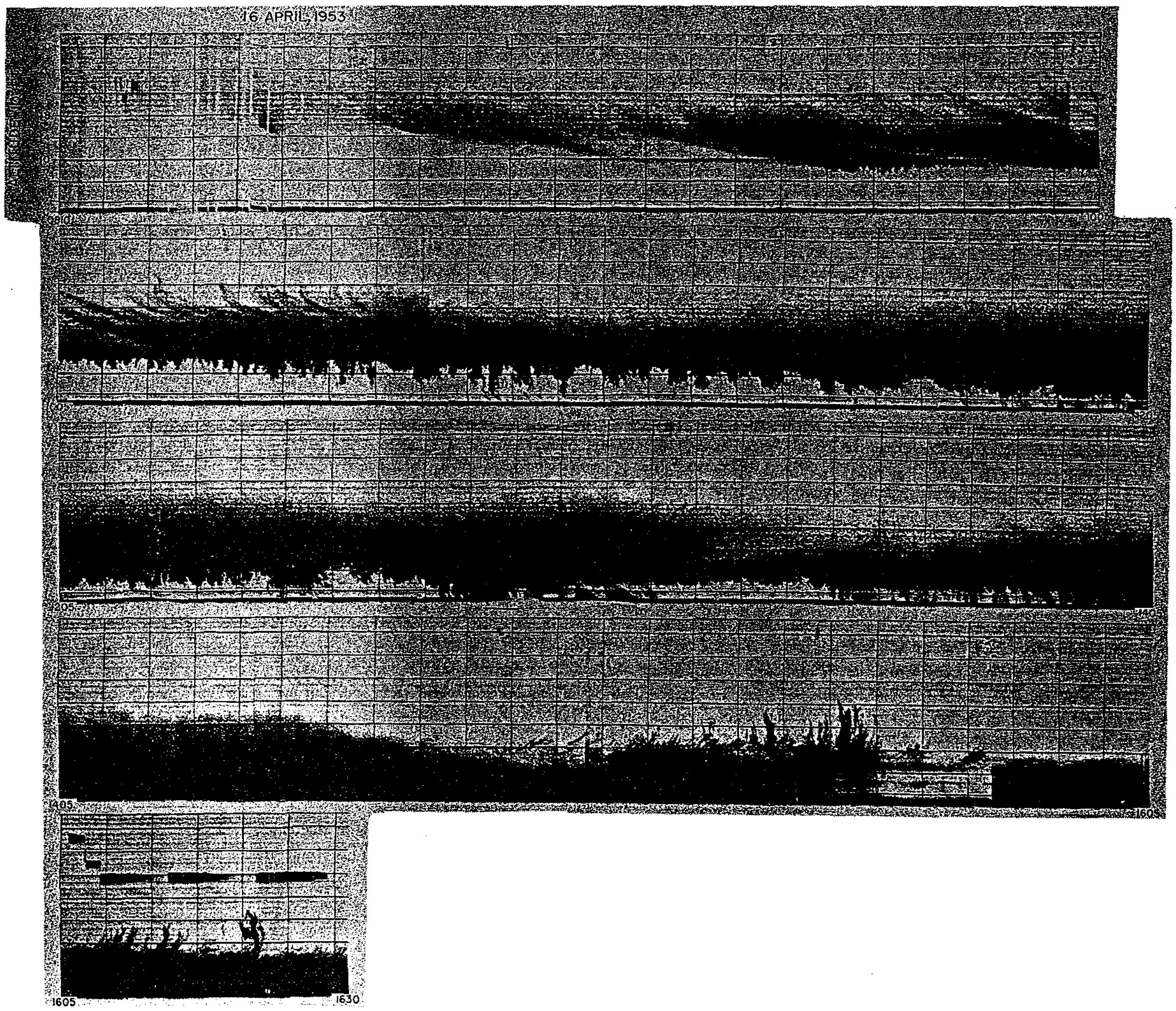

Figure 8. - Photograph of the time-height record made with a 1.25-cm. vertically pointing radar. Vertical lines indicate 5-min. time intervals. Precipitation stalactites are most pronounced in the second row. Weak generators and trails also occur in the second row; trails without detectable generators occur in the first row; and strong generators are in the fourth row.

proceeds until $t = 1.44\ H/w_{max}$ when substantial overturning has occurred,[3] and then ceases. In these models, the precipitation that descends into air that becomes subsaturated in the generator downdrafts evaporates instantly.

Many features of the model distributions in figure 9 are similar to the trails observed visually or by radar. In both model distributions, the maximum value of M is inside the generator during the early, active stages and in or near the generator during most of the period of

[3] $1.44H/w_{max}$ = 48 and 12 min., for left and right patterns, respectively.

simple fallout. Second, water content distributions in the trail of the generator with weak updrafts are constant or slowly varying over the trail length, in good qualitative agreement with observations of many trails. The short trails and large condensed water contents of the model generator on the right are suggestive of many observations that have been subjectively and qualitatively associated with relatively vigorous convection. Third, the lifetimes of the model generators confirm our mostly casual observations that generators seen on radar and cirrus and altocummulus floccules seen visually, are often tracked for tens of miles and as many minutes.

Study not detailed here shows that the most prominent features of the water distribution shapes in the left and right of figure 9 are little different in association with respectively weaker and stronger updrafts. However, where -V and w_{max} are about equal, the shapes of the condensed water distribution are very sensitive to the value of V/w_{max}. This indicates that generator and trail observations might be usefully separated into classes where updrafts are either less than or greater than the terminal falling speeds of the precipitation involved. A uniform long trail such as that illustrated on the left of figure 9 is reasonable only when the fall speed of the precipitation exceeds the updraft; the frequent occurrence of this type of observation indicates the prevalence of convective circulations in snow with vertical speeds rather less than 1 m./sec. The same core-water content distributions and conclusions are valid if the wind field is radially symmetric or if the generator downdrafts are more widely dispersed in a two-dimensional configuration than assumed here.

The solutions suggest inquiry into other quantitative relationships between the possible observable cell and trail parameters and the ratio V/w_{max}. Where the core updraft profile is parabolic with height and precipitation fall velocities are uniform as above, and where the air circulation is steady from $t = 0$ to $t = CH/w_{max}$, the following relationship gives the duration of steady precipitation at the midpoint of the generator base:

$$t_s = \frac{H}{w_{max}} [C-(-K-1)^{-1/2} \tan^{-1} (-K-1)^{-1/2}], \tag{25}$$

where K is equal to V/w_{max} and is less than -1. When there is simple descent in the region below the generator, t_s may be related to the vertical depth D_s of the part of a trail with a steady core intensity by the relation $D_s = t_s V$, and the duration t (of the whole precipitation, releasing circulation) might be empirically related to the total trail depth by the relation $D = tV$.

The numerical value of the steady core-water content at the generator base and in the trail under the same conditions as above is given by

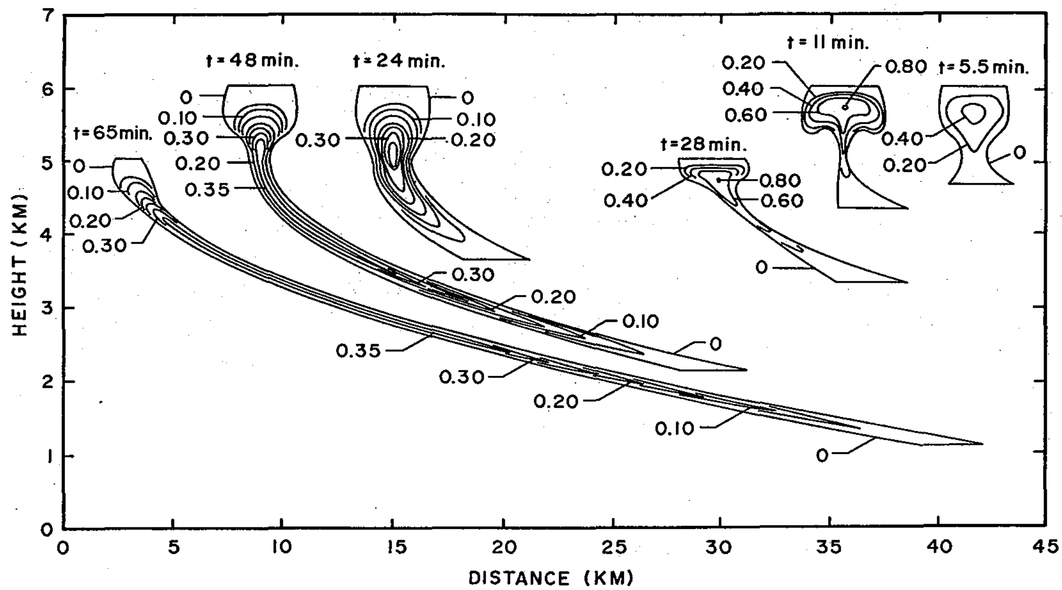

Figure 9. - Model generators and their trails. The fall speed of precipitation is 1 m./sec. and the air circulations are as pictured in figure 3, extended over the interval $-L/2 \leq x \leq L/2$. Maximum updrafts of 0.5 m./sec. apply to the figures on the left, and 2 m./sec. apply to those on the right. The wind shear beneath the generators is 5 m. sec.$^{-1}$ km.$^{-1}$ The condensation function is constant at 0.7 gm. m^{-3} km.$^{-1}$ and isopleths of water content are labeled in gm./m^3. In each triad, the separate pictures can be viewed as different stages in the life of one generator or as three generators in different stages. The middle picture in each set shows the distribution of condensed water at the time the circulating air has overturned and the convective air motion has stopped.

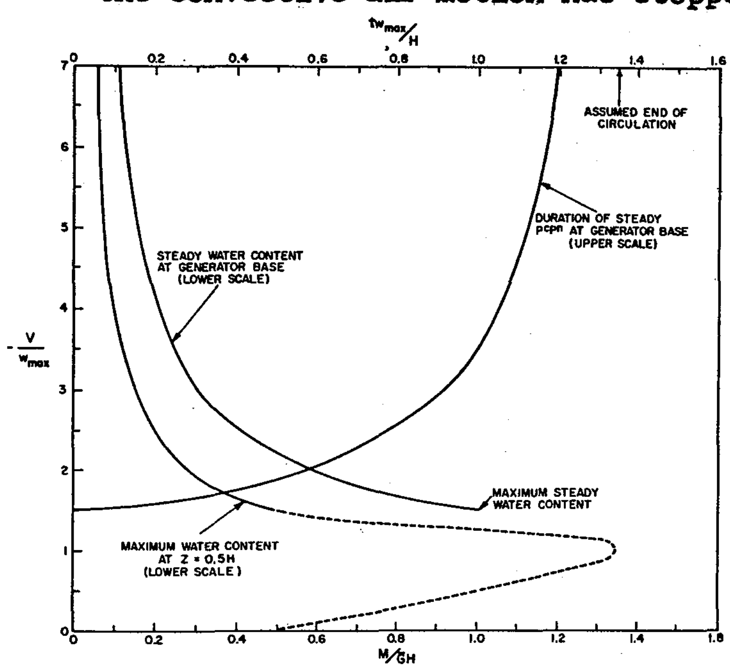

Figure 10. - Parameters of generators and their trails. The duration of steady precipitation and the maximum steady water content at the generator base assume cessation of the circulation at $t = 1.35\ H/w_{max}$.

$$M=\bar{G}HK\,(-K-1)^{-1/2}\,[1-\tan^{-1}(-K-1)^{-1/2}], \tag{26}$$

where $\bar{G}$ is the average value of G in the generator layer.

The maximum steady water content at the generator base for a fixed amount of air overturning occurs when K is such that steady conditions within the generator core are just attained when the air circulation stops. When $K \geq -1$, there is no steady state; the methods used in these cases to compute the time-dependent M-distributions in the updraft cores are discussed in Section 1. These methods have been used to obtain, in figure 10, the dashed part of the curve which shows the maximum water contents at a point midway between base and top of the generator.

7. THE STALACTITE PROBLEM

Stalactites, as observed by vertical-pointing radar, are illustrated in figure 8. The best published discussion of stalactites is probably contained in Douglas, Gunn, and Marshall [2]. These radar-observed phenomena occur when stratiform precipitation descends into a dry air layer, thereby destabilizing it by evaporative cooling. The depth to which overturning of the air then occurs and the extent of the associated downward projections of precipitation (stalactites) appear to be governed by such factors as the initial vertical distributions of temperature and moisture and the precipitation rates. In the stalactite layer, precipitation descends most rapidly in the downdrafts and is slowed or suspended in the updrafts. Moisture descends irregularly, and new convective cells probably arise beneath the old as the precipitation lowers. Stalactites are more pronounced in snow than in rain, in part because evaporation from relatively fast-falling rain is associated with a smaller vertical gradient of the cooling rate than snow is. In this section the application of kinematic theory shows that the stalactite observations may be explained by vertical currents of about 1 m./sec.

Eqs. (19), (20), (21), and (22) describe a model stalactite situation provided that the condition M = constant is applied at z = H and the interior of the circulation cell initially contains dry air. The outstanding feature of this problem is the M-discontinuity that separates descending condensate and the dry air beneath. A proper solution of the instantaneous evaporation case includes accurate delineation of this boundary. However, the digital techniques described in [5] are inadequate in the presence of this discontinuity, and the extension of the computational method used to obtain the solutions shown in the lower rows of figures 4 and 5 is too laborious for hand calculation and has not been programed for a computer.

A simpler problem is defined by the assumption that evaporation is very slight (just enough to start the convective cell and to keep it going!) and that the leading edge of precipitation is therefore given by the locus which connects points descending at speed $(V + w)$ along streamlines of $M > 0$. For the two-dimensional example with $-V = 2w_{max}$, isochrones of the leading edge starting with $t = 0$ at $z = H$ are illustrated in figure 11. An analytical expression for the stalactite length in this no-evaporation case is given by $V(t_u - t_d)$, where t_u and t_d are the times required for condensate to traverse the updraft at $x = 0$ and the downdraft at $x = L/2$, respectively. Where V is constant and the vertical w distribution is parabolic, the stalactite length S is given by

$$S=KH\left[\frac{1}{\mathscr{K}^-}\tan^{-1}\frac{1}{\mathscr{K}^-}-\frac{1}{4\mathscr{K}^+}\ln\frac{2(1+\mathscr{K}^+)-K}{2(1-\mathscr{K}^+)-K}\right] \tag{27}$$

$$K=\frac{V}{w_{max}}<-1,\ \mathscr{K}^-=(-1-K)^{1/2},\text{ and }\mathscr{K}^+=(1-K)^{1/2}.$$

The graph of Eq. (27) is given in figure 12.

A more probable wind structure associated with stalactites consists of a central core of strong downdrafts surrounded by a ring of much weaker updrafts. At some distance from the strong downdraft, the vertical motion is zero. In this case, the stalactite length is deduced from study of precipitation descent in the downdraft core and in the no-draft region considerably removed from the core. The applicable equation, whose plot is also illustrated in figure 12, is the same as Eq. (27), except that the term $(1/\mathscr{K}^-)\tan^{-1}(1/\mathscr{K}^-)$ is replaced by $1/K$.

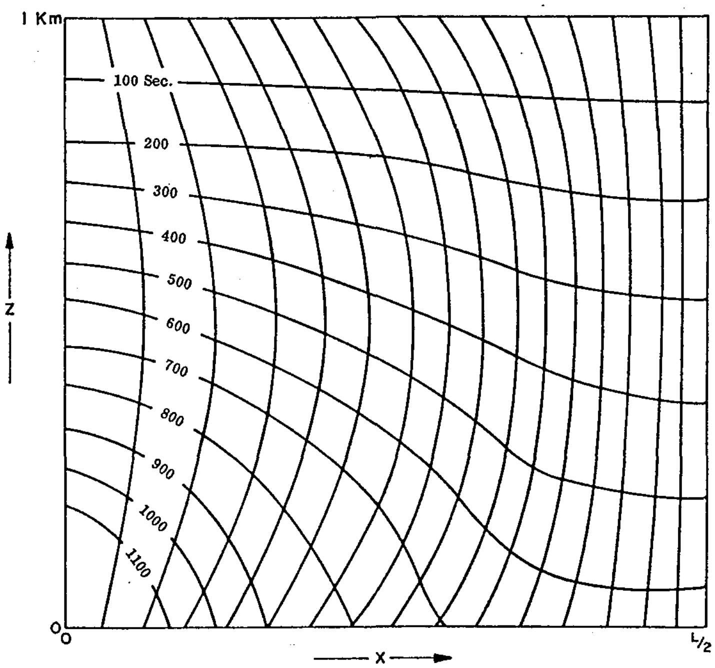

Figure 11. - Horizontally tending lines are isochrones marking the leading edge of nonevaporating precipitation which descends from $z = H$ at $t = 0$. Descent through the wind field where $V/w_{max} = -2$ is along the vertically tending streamlines. Time labels apply if $V = -1$ m./sec., $w_{max} = 0.5$ m./sec., and $H = 1$ km.

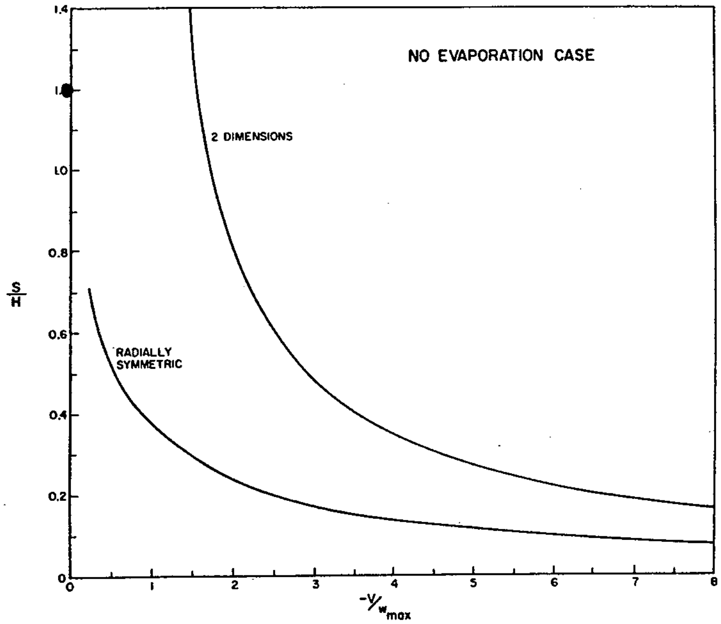

Figure 12. - The ratio of stalactite length S to cell depth H is plotted against $-V/w_{max}$ for cases of no-evaporation in two kinds of wind fields discussed in the text.

The no-evaporation plots in figure 12 represent conservative estimates of stalactite length, in that greater lengths are suggested by an elementary study of evaporative effects, described below. With this conservatism of the present theory in mind, consider V = -1 m./sec. in the radially symmetric case, and note that a circulation cell with maximum downdrafts of 2 m./sec. would give stalactites half the depth of the cell. If updrafts are locally as widespread and as strong as the downdrafts, the maximum stalactite lengths could be as great as the cell depths with maximum vertical currents of only 0.5 m./sec. If the atmospheric circulations in depth are about the same as their horizontal spacing, then the stalactite observations themselves suggest that vertical drafts of about 1 m./sec. are all that is required to explain the observed stalactite lengths. While these analyses of the generator and stalactite mechanisms by no means prove that intense vertical drafts do not exist, they do provide a rational interpretation of the radar observations and of light turbulence observed from aircraft flying near the bases or tops of altostratus layers.

This study of the stalactite mechanism has been extended by consideration of the instantaneous evaporation case as it applies along the special lines x = 0 and x = L/2, where there is no horizontal advection. The simple equations that facilitate solution along these verticals are based on an extension of reasoning discussed in Sections 1 and 2. Consider first the case of instantly evaporating precipitation falling into an unsaturated updraft. The air above the level to which the leading edge of precipitation has descended is saturated and condensation therein causes the growth of precipitation above that leading edge. The vertical distribution of precipitation in the updraft above the precipitation base is, therefore, the same as that previously computed in the one-dimensional updraft case except for the

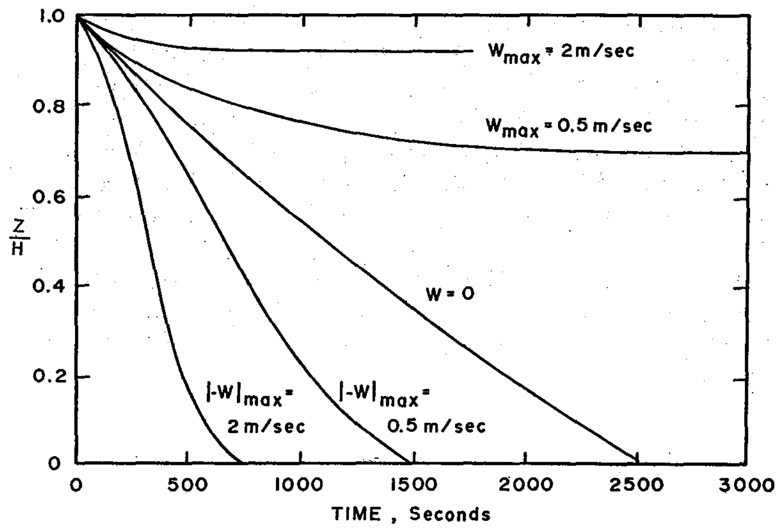

Figure 13. - The time for precipitation falling at 1 m./sec. to descend through a depth H = 1 km. is indicated for two downdrafts (lower curves), two updrafts, and a quiet atmosphere. In each case, precipitation is assumed to evaporate instantly in subsaturated air, the initial distribution of M is $M = -2 + (z/H)(\mathrm{gm./m.}^3)$, and the upper boundary value is $M = 1\ \mathrm{gm./m.}^3$

additive constant in Eq. (3), M(H), the precipitation water content at the upper cell boundary. Eq. (3) also defines condensate distributions in the saturated descending air overtaken by precipitation falling along the line x = 0. The time between the initial state and the final steady state in a small height interval can be calculated from the steady-state final condition, the initial condition, and the wind field. The equation used to determine the time elapsed is a finite-difference formulation of Eq. (1) for the one-dimensional incompressible case, viz.,

$$\frac{M_{z,f}-M_{z,i}}{\Delta t}=-w_z\left[\frac{M_{z+\Delta z,f}-M_{z-\Delta z,i}}{2\Delta z}-G_z\right].-\frac{(VM)_{z+\Delta z,f}-(VM)_{z-\Delta z,i}}{2\Delta z}. \qquad (28)$$

The distributions of all quantities in Eq. (28) except Δt are specified, and it is therefore simple to solve for Δt. Eq. (28) has been solved for Δt in five different vertical air currents where the initial moisture distribution is defined by $M_i = (-2 + z/H)\ \mathrm{gm./m.}^3$, $G = 10^{-3}\ \mathrm{gm./m.}^4$, and $H = 10^3\mathrm{m}$. The results are illustrated in figure 13, where it is seen that the particular assumptions regarding the rate of addition of moisture at z = H and the initial dryness of the air lead to a balance between the vertical advection of dry air and the descent of condensate in the updraft cases. In these updraft cases, therefore, stalactite lengths as measured by the difference in height of the precipitation base at x = 0 and x = L/2 would be indefinitely long. Of course, the cell that gives rise to the stalactite phenomenon does not have an indefinitely persisting circulation. If it did, it would eventually become saturated throughout by a return flow of vapor from its downdraft portion and the portion of the cell in which precipitation is held aloft would become indefinitely smaller with time. Circulations actually decay before such limits are reached.

The foregoing leads to another interesting consideration. The steady precipitation emerging beneath the updrafts of a convective cell imbedded in a saturated atmosphere has a higher intensity, and that emerging from the downdraft side has, due to evaporation in saturated downdrafts, a smaller intensity than the precipitation entering the cell at the top. This indicates how, in a vertical air circulation, stratiform precipitation falling through the circulation is redistributed and emerges with horizontal gradients of intensity. The distributions for a saturated atmosphere are easily computed, and may be useful in interpreting radar records where small convective cells are established within widespread precipitation by microphysical effects, as is often the case, for example, near the level where snow melts to rain (Wexler [16] and Newell [11]).

8. CONCLUSIONS

The continuity equations are powerful tools for illuminating fundamental properties of wind-water relationships. The greatest advances should come as theory and observation are combined, so that each supplements and complements and indicates paths of useful development for the other. Application of kinematic theory to analyses of conventional data with satellite photographs and distributions of radar reflectivity and Doppler velocity should yield improved descriptions of the wind field accompanying precipitation and of the associations of these fields with wind shear, static stability, and other quantities of dynamical significance.

It is important to generalize the theory to account for and evaluate the bulk effects of cloud physics processes. This avenue of study is relevant to the problems of weather modification by such means as artificial seeding. A preliminary discussion of such a generalization is contained in Kessler and Newburg [7].

As dynamical numerical models of the atmosphere become more sophisticated, equations of continuity for cloud and precipitation in more nearly natural forms will be incorporated therein and should reveal how the air motions, water transports, and cloud physics processes interact to determine the scales, shapes, and intensities of convective events. The recent works by Lilly [8], Malkus and Witt [9], Ogura and Phillips [12], Saltzman [13], and Sasaki [14], for example, may provide suitable thermohydrodynamic frameworks for such advanced studies.

ACKNOWLEDGMENTS

The manuscript was reviewed by Dr. Edward Newburg and Mr. George Kern, of TRC, who also contributed via several stimulating discussions. Mr. Albert Chmela, of the Weather Radar Branch, Air Force Cambridge Research Laboratories, determined the solutions illustrated in the lower row of figure 4, and Mr. Paul Duchow, of The Travelers Research Center, Inc., computed those shown in the lower row of figure 5. Mr. Rudolf Loeser, of AFCRL, Mr. Brian Sackett, of TRC, and Mr. Carlos Droescher, of NSSL, drafted the figures.

REFERENCES

1. Atlas, D., "The Radar Measurement of Precipitation Growth," Sc. D. Thesis, Massachusetts Institute of Technology, 1955, (See Appendix).
2. Douglas, R. H., Gunn, K. L. S., and Marshall, J. S., "Pattern in the Vertical of Snow Generation," Journal of Meteorology, vol. 14, No. 2, Apr. 1957, pp. 95-114.
3. Kessler, E. III, "Radar-Synoptic Analysis of an Intense Winter Storm," Geophysical Research Papers, No. 56, U. S. Air Force Cambridge Research Center, Oct. 1957, 218 pp.
4. Kessler, E. III, "Kinematical Relations between Wind and Precipitation Distributions," Journal of Meteorology, vol. 16, No. 6, Dec. 1959, pp. 630-637.
5. Kessler, E. III, "Kinematical Relations between Wind and Precipitation Distributions, II," Journal of Meteorology, vol. 18, No. 4, Aug. 1961, pp. 510-525.
6. Kessler, E. III and Atlas, D., "Model Precipitation Distributions," Aero/Space Engineering, vol. 18, No. 12, Dec. 1959, pp. 36-40.
7. Kessler, E. III and Newburg, E., "Relationships between Tropical Precipitation and Kinematic Cloud Models," First Quarterly Progress Report on Signal Corps Contract DA 36-039 sc 89099, Travelers Research Center, Inc., 1962.
8. Lilly, D. K., "On the Numerical Simulation of Bouyant Convection," Tellus, vol. 14, No. 2, May 1962, pp. 148-172.
9. Malkus, J. S. and Witt, G., "The Evolution of a Convective Element; A Numerical Calculation," in The Atmosphere and the Sea in Motion, Rockefeller Institute Press, New York, 1959, pp. 425-439.
10. Marshall, J. S., "Precipitation Trajectories and Patterns," Journal of Meteorology, vol. 10, No. 1, Feb. 1953, pp. 25-29.
11. Newell, R., "Some Radar Observations of Tropospheric Cellular Convection," Research Report No. 33 by Weather Radar Research, Massachusetts Insitute of Technology, on Contract AF 19(604)-2291, 1959.
12. Ogura, Y. and Phillips, N. A., "Scale Analysis of Deep and Shallow Convection in the Atmosphere," Journal of the Atmospheric Sciences, vol. 19, No. 2, Mar. 1962, pp. 173-179.
13. Saltzman, B., "Finite Amplitude Free Convection as an Initial Value Problem, I," Journal of the Atmospheric Sciences, vol. 19, No. 4, July 1962, pp. 329-341.
14. Sasaki, Y., "Effects of Condensation, Evaporation and Rainfall on the Development of Mesoscale Disturbances: A Numerical Experiment," Scientific Report No. 1, Texas A. and M. College on Contract AF 19(604)-6136, 1960.
15. Spilhaus, A. F., "Raindrop Size, Shape and Falling Speed," Journal of Meteorology, vol. 5, No. 3, June 1948, pp. 108-110.
16. Wexler, R., "Advection and the Melting Layer," Meteorological Radar Studies No. 4, Blue Hill Meteorological Observatory, Harvard University, Contract AF 19(604)-950, 1957, 12 pp.

National Severe Storms Laboratory Technical Memoranda

The NSSL Technical Memoranda, beginning with No. 28, continue the sequence established by the U.S. Weather Bureau National Severe Storms Project, Kansas City, Missouri. Numbers 1-22 were designated NSSP Reports. Numbers 23-27 were NSSL Reports, and 24-27 appeared as subseries of Weather Bureau Technical Notes.

No. 1 National Severe Storms Project Objectives and Basic Design. Staff, NSSP. March 1961.

No. 2 The Development of Aircraft Investigations of Squall Lines from 1956 1960. B.B. Goddard.

No. 3 Instability Lines and Their Environments as Shown by Aircraft Soundings and Quasi-Horizontal Traverses. D. T. Williams. February 1962.

No. 4 On the Mechanics of the Tornado. J. R. Fulks. February 1962.

No. 5 A Summary of Field Operations and Data Collection by the National Severe Storms Project in Spring 1961. J. T. Lee. March 1962.

No. 6 Index to the NSSP Surface Network. T. Fujita. April 1962.

No. 7 The Vertical Structure of Three Dry Lines as Revealed by Aircraft Traverses. E. L. McGuire. April 1962.

No. 8 Radar Observations of a Tornado Thunderstorm in Vertical Section. Ralph J. Donaldson, Jr., April 1962.

No. 9 Dynamics of Severe Convective Storms. Chester W. Newton. July 1962.

No. 10 Some Measured Characteristics of Severe Storm Turbulence. Roy Steiner and Richard H. Rhyne. July 1962.

No. 11 A Study of the Kinematic Properties of Certain Small-Scale Systems. D. T. Williams. October 1962.

No. 12 Analysis of the Severe Weather Factor in Automatic Control of Air Route Traffic. W. Boynton Beckwith. December 1962.

No. 13 500-Kc./Sec. Sferics Studies in Severe Storms. Douglas A. Kohl and John E. Miller. April 1963.

No. 14 Field Operations of the National Severe Storms Project in Spring 1962. L. D. Sanders. May 1963.

No. 15 Penetrations of Thunderstorms by an Aircraft Flying at Supersonic Speeds. G.P. Roys. Radar Photographs and Gust Loads in Three Storms of 1961 Rough Rider. Paul W.J. Schumacher. May 1963.

No. 16 Analysis of Selected Aircraft Data from NSSP Operations, 1962. T. Fujita. May 1963.

No. 17 Analysis Methods for Small-Scale Surface Network Data. D.T. Williams. August 1963.

No. 18 The Thunderstorm Wake of May 4, 1961. D.T.Williams. August 1963.

No. 19 Measurements by Aircraft of Condensed Water in Great Plains Thunderstorms. George P. Roys and Edwin Kessler. July 1966.

No. 20 Field Operations of the National Severe Storms Project in Spring 1963. J.T. Lee, L. D. Sanders, and D.T. Williams. January 1964.

No. 21 On the Motion and Predictability of Convective Systems as Related to the Upper Winds in a Case of Small Turning of Wind with Height. James C. Fankhauser. January 1964.

No. 22 Movement and Development Patterns of Convective Storms and Forecasting the Probability of Storm Passage at a Given Location. Chester W. Newton and James C. Fankhauser. January 1964.

No. 23 Purposes and Programs of the National Severe Storms Laboratory, Norman, Oklahoma. Edwin Kessler. December 1964.

No. 24 Papers on Weather Radar, Atmospheric Turbulence, Sferics, and Data Processing. August 1965.

No. 25 A Comparison of Kinematically Computed Precipitation with Observed Convective Rainfall. James C. Fankhauser. September 1965.

No. 26 Probing Air Motion by Doppler Analysis of Radar Clear Air Returns. Roger M. Lhermitte. May 1966.

No. 27 Statistical Properties of Radar Echo Patterns and the Radar Echo Process. Larry Armijo. May 1966. The Role of the Kutta-Joukowski Force in Cloud Systems with Circulation. J. L. Goldman. May 1966.

No. 28 Movement and Predictability of Radar Echoes. James Warren Wilson. November 1966.

No. 29 Notes on Thunderstorm Motions, Heights, and Circulations. T.W. Harrold, W. T. Roach, and Kenneth E. Wilk. November 1966.

No. 30 Turbulence in Clear Air Near Thunderstorms. Anne Burns, Terence W. Harrold, Jack Burnham, and Clifford S. Spavins. December 1966.

No. 31 Study of a Left-Moving Thunderstorm of 23 April 1964. George R. Hammond. April 1967.

No. 32 Thunderstorm Circulations and Turbulence from Aircraft and Radar Data. James C. Fankhauser and J. T. Lee. April 1967.